

Response to Referee #1:

We thank the reviewer for constructive comments and suggestions. We have revised our manuscript according to his comments and suggestions. In the following we would like to reply the comments point by point.

General Comments:

This manuscript developed a Hg module in a nested atmospheric model, by considering the emissions, chemistry and deposition. The authors have evaluated the modeling of total gaseous mercury (TGM), oxidized mercury, wet and dry deposition of Hg. At last, the nested model was used to study the outflow of Hg from China (mainland?). This work may be potentially important, however, I have several serious concerns with the novelty and methodology of this study. There are many mercury models and it's not clear whether the model developed in the paper is more advanced than other models. For example, Br chemistry has been considered in other models (Amos et al., 2012), but not in the present model. Treatment of the re-emissions from land and ocean is a very weak aspect. In addition, there is a lack of detailed methodology in the model, in particular for some key chemical and deposition processes, making it hard to judge if the model is advanced or not. At last, as a major weakness, the diurnal variations and vertical trends are not evaluated, leaving it questionable whether the model captures the key chemical processes of Hg. In general, the present paper doesn't provide enough novelty to get published by GMD.

Response: Thanks the reviewer to state that our work may be potentially important. We agree that lack of enough model description and some potential key processes of Hg chemistry made the reviewer hard to judge if the model is advanced or not. We have done our best to plug into these processes and modules to improve the model. This study is tried to develop an online global nested Hg transport model with flexible horizontal resolution, but focus on the region of China and made better model performance. We afford a new online nested method to improve model performance in regional scale. Compared to traditional multi-scale modeling approach (using a

global model to provide initial and boundary conditions to a regional model) (Seigneur et al., 2001), online nested method with the same physical and chemical parameterizations among global and nested domains could avoid uncertainties induced by different boundary conditions. Compared to offline nested method used in the GEOS-Chem model (Zhang et al., 2012), online nested method can provide boundary conditions with higher time resolution from the global domain to the nested domain. Typically, the time resolution of boundary condition in offline and online nested model is 3 hour (or 1 hour) and 10 minute (or 5 minute), respectively. Besides, as stated in the introduction, little model validation has been conducted over East Asia (especially China) in previous global modeling studies due to lack of observational data. We have made great efforts to collect various Hg observations from literatures (especially published in Chinese journals) and conducted comprehensive model evaluation over East Asia in this study. Finally, the global impacts of the primary anthropogenic emissions from the world's largest single emitter, China, have been investigated for the first time. In the revised manuscript, we revised the introduction (Section 1) to highlight the major improvement (namely online nested simulation) of our Hg model.

We made the major revisions for this paper to get published by GMD following comments of the reviewer and the editor. The responses to the serious concerns with model methodology used in our model as raised by the reviewer are as follows.

1/ Br chemistry

Large uncertainties in atmospheric chemistry of Hg is one of the fundamental limitations of current models. The primary gaseous oxidants of Hg(0) in current models include O₃, OH, H₂O₂ and reactive halogen species (e.g. Br, Cl, I, Br₂, Cl₂, BrO, ClO, IO, etc.). Lei et al. (2013) demonstrated that adding Br chemistry has little impact on overall global TGM patterns based on sensitivity experiments using the CAM-Chem Hg model. Wang et al. (2014) also pointed out that Br is less important than O₃ and OH as oxidants for Hg(0) in Hg simulation over China with high oxidation capacity. Besides, several latest Hg modeling studies (Simone et al., 2014; Gencarelli et al., 2014) still used O₃-OH oxidation mechanism alone in their models.

It seems that at the current level of understanding the O₃-OH oxidation mechanism is still sufficient for Hg simulation. However, the importance of Br atoms in gas phase reaction of Hg has been identified by several studies (Holmes et al., 2006, 2010), and these reactions are believed to be essential in Polar region and marine boundary layer. We accept the advice of the reviewer and add Br chemistry for gas oxidation of Hg, to provide the option of using Br oxidation mechanism and address the impact of Br chemistry in our model.

As shown by Table R1, we add five Br chemical reactions in the gas phase (Seigneur and Lohman, 2008) in addition to the O₃-OH oxidation mechanism to test how the Br oxidation reactions affect the Hg distributions. Similar to the treatment of Holmes et al. (2006, 2010), the five reactions are treated as a single reaction, with an effective Hg(0) first-order rate constant that is a function of the individual reaction rates and the concentrations of Br, BrO and OH based on the assumption that Br, BrO and OH concentrations don't change by their reactions with Hg. This is also the same with the implementation described in CAMx (2014). The effective first-order rate constant is calculated as follows:

$$k_{eff} = \frac{k_1[Br](k_3[Br]+k_4[OH])}{k_2+k_3[Br]+k_4[OH]} + k_5[BrO] \quad s^{-1}$$

Table R1. Bromine reactions added in the model (T is the temperature in degrees Kelvin, and P is the pressure in atmospheres).

NO.	Reaction	Rates
BR1	Hg(0)(g)+Br(g)→HgBr(g)	$k_1 = 3.6 \times 10^{-13} P \left(\frac{T}{298}\right)^{-1.86} \text{ cm}^3 \text{ molec}^{-1} \text{ s}^{-1}$
BR2	HgBr(g)→Hg(0)(g)	$k_2 = 3.9 \times 10^9 \exp\left(\frac{-8537}{T}\right) \text{ s}^{-1}$
BR3	HgBr(g)+Br(g)→HgBr ₂ (g)	$k_3 = 2.5 \times 10^{-10} \left(\frac{T}{298}\right)^{-0.57} \text{ cm}^3 \text{ molec}^{-1} \text{ s}^{-1}$
BR4	HgBr(g)+OH(g)→HgBrOH(g)	$k_4 = 2.5 \times 10^{-10} \left(\frac{T}{298}\right)^{-0.57} \text{ cm}^3 \text{ molec}^{-1} \text{ s}^{-1}$
BR5	Hg(0)(g)+BrO(g)→Hg(II)(g)	$k_5 = 1.0 \times 10^{-15} \text{ cm}^3 \text{ molec}^{-1} \text{ s}^{-1}$

In the GNAQPMS-Hg model, Br and BrO are not explicitly simulated. Therefore, we specify typical vertical profiles of Br and BrO concentrations over land and ocean, with higher values over ocean (2.9×10^{-8} and 2.9×10^{-7} ppm for Br and BrO) than over land (5.0×10^{-9} and 5.0×10^{-8} ppm for Br and BrO). During the night, the concentrations

of Br and BrO are assumed to be zero, considering that the photolysis of Br₂ is the primary source for these radicals.

Figure R1 shows the difference of surface TGM concentrations resulting from introducing Br reactions. Decrease in TGM concentrations is found in the whole globe. This is because additional Br chemistry transforms more Hg(0) into Hg(II), which subsequently enhances the deposition of Hg(II), leading to the reduction of TGM concentrations. Larger TGM reduction is found in the Northern Hemisphere than in the Southern Hemisphere. In general, the change in TGM concentration is less than 0.2 ng m⁻³ in most areas which indicates that introducing Br chemistry seems to have little impact on overall TGM magnitudes and patterns. These results are similar to Lei et al. (2013) which test the impact of Br chemistry using the CAM-Chem-Hg model. Although adding the Br chemistry does not significantly change the TGM pattern, but it may affect the gaseous Hg partitioning between Hg(0) and Hg(II), and hence may affect the global Hg deposition patterns. More in-depth tests and analysis are needed to address these impacts in the future.

In the revised manuscript, the description of Br oxidation mechanism and its impact on global Hg concentrations is given in Section 2.2.2 in the text and Section S1.1 in the supplement.

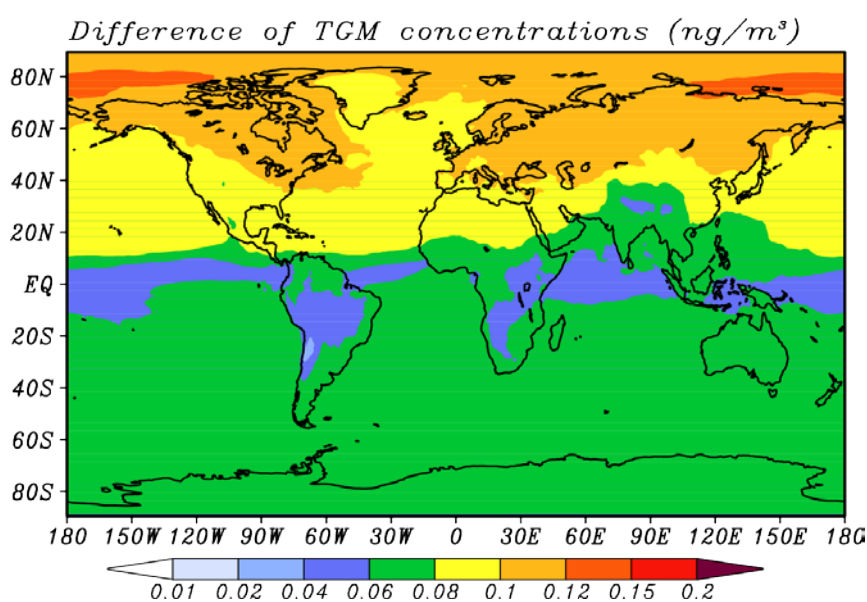


Figure R1. Change in surface TGM concentrations (ng m⁻³) by introducing bromine chemistry (positive value means the TGM concentrations decrease after added bromine chemistry).

2/ Hg reemission

In the present model, the treatments of Hg reemissions from land and ocean mainly follow the method used by Jung et al. (2009). Besides, global and regional total emission amounts are prescribed according to estimates in previous studies (Selin et al., 2007, 2008; Mason, 2009; Soerensen et al., 2010). This can make sure the global and regional total reemissions from land and ocean are generally reasonable. As show in Figure S6 in the supplement, the spatial patterns of the reemissions from land and ocean are similar with previous modeling studies. Certainly, we also agree with the reviewer that treatment of the reemissions from land and ocean is a weak aspect in the present work. In the future, parameterizations of air-sea and air-land Hg dynamic exchange will be included in the model to better resolve Hg reemissions.

3/ Lack of detailed model methodology

Detailed description concerning Hg chemistry and deposition parameterizations used in our model has been given in the revised manuscript (Section S1-2 in the supplement). Specially, latest advances in Hg chemistry modeling (e.g. gas-particle partitioning of Hg(II), Br chemistry) have also been included and tested in our model in the revised manuscript (Section 2.2.2-2.2.3 in the text and Section S1 in the supplement).

4/ Evaluation of diurnal and vertical variation

Considering that no public observational data is available, we didn't conduct quantitative evaluation of Hg diurnal and vertical variation in this study. Instead, we shown the diurnal variation of simulated TGM concentrations in three mountainous sites (Mt. Lulin, Mt. Leigong and Mt. Changbai) in China and the vertical variation of simulated TGM concentrations over the North Pacific Ocean in the revised manuscript. The above simulated results were qualitatively compared to previous studies to confirm the model capability in simulating diurnal and vertical variation of Hg concentrations. Detailed comparisons and analyses are given in Section S4.2 (Figs. S12-13) in the supplement in the revised manuscript.

Specific comments:

Introduction:

The major Hg chemistry and mechanisms are not well described (e.g. gas particle partitioning). The authors need to explain what they have improved in the modeling of Hg in the present work. Otherwise, there is no novelty.

Response: The major Hg chemistry and mechanisms are described in Section 2.2-2.4. Figure 1 and Table 1 also give the detailed Hg chemical reactions in gas and aqueous phase included in our model. The descriptions of Br chemistry and gas-particle partitioning of Hg(II) were also added to Section 2.2 in the revised manuscript. In the first version of our model, we mainly follow previous studies to treat Hg chemistry and mechanisms. Our focus in this study is the online nested simulation and comprehensive model evaluation in China and also the global impact of Chinese anthropogenic Hg emissions. To our point of view, the improvement in the modeling of Hg in the present work is the online nested capacity of our model. Online nested simulation has two advantages at least. Firstly, it can increase model resolution in the targeted region which could potentially improve the model performance. Secondly, the global and nested simulations use the same physical and chemical parameterizations which could avoid uncertainties induced by different boundary conditions. Therefore, we think the present work is a useful attempt and important. In the revised manuscript, we revised the introduction (Section 1) to highlight the major improvement (namely online nested simulation) of our Hg model.

2.2 Mercury chemistry

1/ the effects of temperature and relative humidity on Hg chemistry are not well explained.

Response: The reaction rate constants provided in Table 1 are for temperatures in the range of 20 to 25⁰C. No temperature dependence information is available. The effect of relative humidity on Hg chemistry is not taken into account in our model. This treatment is in line with most Hg models. An annotation was added to Table 1 in the

revised manuscript.

2/ the treatment of the gas-particle partitioning of Hg (II) is not clear.

Response: In the revised manuscript, detailed description of the Hg(II) gas-particle partitioning mechanism included in the model is given in Section S1.2 in the supplement. And model sensitivity experiments were conducted to test the effects of this mechanism on global Hg concentrations and deposition. Detailed comparisons and analyses are shown in Section 2.2.3 in the text and Figs. S2-3 in the supplement.

Mercury deposition:

1/ the method description is not clear. Detailed equations and parameterizations for dry and wet deposition are needed, otherwise it is hard to judge if the model is rigorous or not.

Response: The dry and wet deposition schemes used in our model are similar to the implementation described in the ECHMERIT (Jung et al., 2009) and CAMx (CAMx, 2014) models. The detailed descriptions of the dry and wet deposition schemes used in the model are shown below and also added to Section S2 in the supplement.

Dry deposition:

In the model, dry deposition is treated as a first-order removal mechanism. The deposition flux of a pollutant to the surface is the product of a characteristic deposition velocity and its concentration in the surface layer. Deposition velocities are derived from models that account for the reactivity, solubility, and diffusivity of gases, the sizes of particles, local meteorological conditions, and season-dependent surface characteristics. Dry deposition parameterizations of gases and aerosols are based on the work of Wesely (1989) and Slinn and Slinn (1980), respectively.

For gases, deposition velocity V_d is calculated from three primary resistances r (s m^{-1}) in series as described below.

$$V_d = \frac{1}{r_a + r_b + r_s}$$

The aerodynamic resistance r_a represents bulk transport through the lowest model

layer by turbulent diffusion. The quasi-laminar sub-layer resistance r_b represents molecular diffusion through the thin layer of air directly in contact with the particular surface to which material is being deposited. The surface resistance r_c depends upon the physical and chemical properties of the surface.

For particles, surface deposition occurs via diffusion, impaction, and gravitational settling. Particle size is the dominant variable controlling these processes. Particle deposition velocity for a given aerosol size is calculated using the following resistance equation.

$$V_d = V_{sed} + \frac{1}{r_a + r_b + r_a r_b v_{sed}}$$

V_{sed} is the gravitational settling (or sedimentation) velocity which is dependent on aerosol size and density.

The detail formulations of how to calculate r_a , r_b , r_s and V_{sed} for gases and aerosols can be found in Wesely (1989) and Slinn and Slinn (1980) or the user's guide of the CAMx model (CAMx, 2014).

In the GNAQPMS-Hg model, dry deposition of Hg(0), Hg(II) and Hg(P) are all accounted for by adaption the parameterizations described above. Several physical properties (e.g. Henry's law constant, molecular weight, surface reactivity) of the Hg species are specified in order to calculate their deposition velocities. The Henry's Law constant for Hg(0) is set to be 0.11 M atm⁻¹ (Lin and Pehkonen, 1999) with a temperature factor of -4970 K (Clever et al., 1985), and the surface reactivity is set to zero. Hg(II) represents HgCl₂ and Hg(OH)₂. Its Henry's Law constant is assumed to be the same as HNO₃ because they have similar solubility (Bullock and Brehme, 2002). Like HNO₃, Hg(II) has a strong tendency to stick to surfaces and its dry deposition occurs readily, so the surface resistance for Hg(II) in the dry deposition scheme is set to zero. The Hg(P) dry deposition velocity is set equal to that for sulfate, similar to that applied in the CMAQ-Hg and STEM-Hg model (Bullock and Brehme, 2002; Pan et al., 2008).

Wet deposition:

In the model, wet deposition of the chemical species are calculated using an approach with medium complexity. In-cloud and below-cloud scavenging are included. The basic formulation implemented in the model is a scavenging approach in which the local rate of concentration change $\frac{\partial c}{\partial t}$ within or below a precipitating cloud depends on a scavenging coefficient Λ :

$$\frac{\partial c}{\partial t} = -\Lambda c$$

The scavenging coefficient is estimated differently for gases and particles, based on relationships described by Seinfeld and Pandis (1998). For gases, two components are calculated: 1) direct diffusive uptake of ambient gases into falling precipitation; and 2) accretion of cloud droplets that contain dissolved gases. For particles, there are also two components: 1) impaction of ambient particles into falling precipitation with an efficiency that is dependent upon particle size; and (2) accretion of cloud droplets that contain particle mass. Overall, the scavenging coefficient depends on an assumed scavenging efficiency, the total rainfall intensity (large-scale and convective precipitation), cloud water content and species solubility according to Henry's law, a mean cloud or rain droplet radius and rain droplet falling velocity. The large-scale and convective precipitation are not distinguished in this method. For species with low solubility (with a Henry's law constant of less than 100 M atm^{-1}), no wet deposition is calculated. More detail description of how to calculate the scavenging coefficients for gases and particles can be found in Seinfeld and Pandis (1998) or the user's guide of the CAMx model (CAMx, 2014). The physical properties (e.g. Henry's Law constant, surface reactivity, molecular diffusivity) of Hg species used in the wet deposition module are the same as those in the dry deposition module.

2/ it seems all precipitations are treated in the same manner, without distinguishing the large-scale and convective precipitation.

Response: Yes. In this model version, we do not distinguish the large-scale and convective precipitation in the wet deposition process. We consider the in-cloud and

below-cloud scavenging of Hg and use different treatment for gaseous and particulate pollutants. The approach is similar to the implementation described in the ECHMERIT (Jung et al., 2009) and CAMx model.

3/ for wet deposition, the release of Hg (P) when water freezes to ice is not considered.

Response: Yes. We will try to consider this process by following the work of Holmes et al.(2010) and Amos et al. (2012) in the future work.

Mercury emissions:

1/ how is the emissions from biomass burning, geogenic emissions, land and ocean specified for Hg(0), Hg(II), and Hg(P)?

Response: Following previous modeling studies (Jung et al., 2009; Holmes et al., 2010), all Hg emissions from natural sources (e.g. biomass burning, geogenic emissions, land and ocean) are treated as Hg(0) in our model. This information has been added to Section 2.4 in the revised manuscript.

2/ neglecting the seasonality of Hg emissions from anthropogenic sources is a weakness of the present work.

Response: Seasonality of anthropogenic Hg emissions is important in model simulation. Unfortunately, global anthropogenic Hg emissions from AMAP and EDGAR which have been widely used in Hg modeling all have no seasonal variation. Therefore, it is very hard to obtain information about the seasonality of Hg anthropogenic emissions.

3/a major weakness in this section is the treatment of Hg reemissions from land and ocean. The total emissions from land and ocean are not justified by any observations, and the method used in spatial allocation is not convincing. I don't see any relationship between the biogenic CO emission and the Hg reemission.

Response: The treatments of Hg reemissions from land and ocean mainly follow the

method used by Jung et al. (2009). Besides, global and regional total emission amounts are prescribed according to estimates in previous studies (Selin et al., 2007, 2008; Mason, 2009; Soerensen et al., 2010). This can make sure the global and regional total reemissions from land and ocean are generally reasonable. Reemissions are somehow relevant to biological activity (e.g. vegetation) so we used biogenic CO emissions as temporal and spatial surrogates. This method was also used by the ECHMERIT model (Jung et al., 2009). Certainly, reemissions are also relevant to deposition pattern, soil and water Hg content and environmental elements (e.g. solar radiation, wind speed). So the method of spatial allocation used in this study might induce some uncertainties, but we think the general spatial patterns are reasonable as show in Figure S6 in the supplement. In future work, parameterizations of air-sea and air-land Hg dynamic exchange will be included in the model to better resolve Hg reemissions.

Model setup

1/ some information are missed in this section (e.g. what is the time step in the model calculation? what is the vertical coordinate used in the model?)

Response: The time step in the model calculation (including emission, advection, diffusion, chemistry and deposition) is 600 s. The meteorology input frequency is 6h in the global domain but 3h in the nested domain. These information have been added to Section 2.5 in the revised manuscript.

The description of the vertical coordinate used in the model has been given in Section 2.5 in the manuscript. That is “Vertically, the model uses 20 terrain-following layers from the surface to 20 km a.s.l., with a decreasing resolution with height. Roughly, the lowest 14-18 layers are in the troposphere and the remaining layers are in the stratosphere.”.

2/ a coarse-resolution inventory (0.5 degree for AMAP, and 0.5 degree when using GEIA inventory for an interpolation) does not match the resolution in the model (0.3 degree).

Response: Thanks for the comments. We used a mass-conservative interpolation method to remap the emission inventory to match the model grid in the global and nested domains. Firstly, we divide the emissions in a $0.5^{\circ}\times 0.5^{\circ}$ grid into 2500 small grid with resolution of $0.01^{\circ}\times 0.01^{\circ}$. Then every $0.01^{\circ}\times 0.01^{\circ}$ grids are match to the $1^{\circ}\times 1^{\circ}$ and $0.33^{\circ}\times 0.33^{\circ}$ grids based on their central latitudes and longitudes. This method make sure the total emissions in the global and nested domains are the same.

Model evaluation

Line 17, Page 6960: the time periods of the measurements do not match with those of the simulations. Dismatch of the time periods when comparing the model with the observations is a major weakness. In particular, there is a large bias when comparing modelled annual mean Hg concentrations with daily measurements by cruise. Unfortunately, the authors only attribute model-observation discrepancies to this mismatch, without making any efforts to assess this influence.

Response: We agree that mismatch of the time periods when comparing the model with the observations might be a weakness of the present work. However, as stated in the manuscript, only Europe and North America have routine monitoring networks for atmospheric Hg concentrations and deposition. Actually, observations of wet deposition and precipitation in Europe and North America are from EMEP and MDN respectively, and the time periods are exactly the same with the simulation results. In contrast, no public Hg observation datasets are available in East Asia. So we have no choice but to use observations (collected from literatures) with mismatched time periods over East Asia.

All observations of Hg concentrations at land sites used in this study are averaged over time periods larger than 1 year. Analyses of long-term measurements show that trends in mean TGM during the last decade are small (of order $1\%a^{-1}$) or negligible at most background sites in the Northern Hemisphere (Temme et al., 2007; Wangberg et al., 2007). Therefore, the influences of the mismatch of time periods between model results and Hg concentration observations would not be large. Similar observational datasets (as shown in Table S2-S4 in the supplements) are also used by previous

modeling studies (Selin et al., 2007, 2008; Holmes et al., 2010).

Observations from ship cruises are just used for initial comparison of simulated results over ocean following previous studies (Selin et al., 2007, 2008; Holmes et al., 2010). These observations are not used for quantitative model evaluation and not including in the calculation of statistical parameters of model performance.

Annual dry and wet deposition measurements in East Asia (Table S5 in the supplement) are all obtained from literatures. Considering that dry and wet deposition fluxes are affected by environmental factors (e.g. precipitation) and they might differ from one year to another, so the influence of the mismatched time periods would be relatively larger. Again, no observations of Hg deposition are available at present. So we have no better choice.

Overall, we think the influence of the mismatch of the time periods between model results and observations is relatively large for dry and wet deposition comparisons in East Asia but relatively small for other comparisons. By saying “It should be noted that the time periods of the measurements do not all match with those of the simulation, and this difference may partially explain any model–observation discrepancies.”, we just want to remind the readers that this is one of the factors causing the model-observation discrepancies. Quantitative assessments of the influence are difficult and outside the scope of this study.

The above explanation is given to Section S4.1 of the supplement in the revised manuscript.

Total gaseous mercury (TGM)

1/ Fig. 3: scatter plots by region are needed to evaluate the model performance when comparing model with observations.

Response: Scatter plots by region between simulated and observed surface TGM have been given in Figure 10 (a) in the manuscript.

2/ a major weakness in this section is that the reasons for the discrepancies are not well explained. There are uncertainties in emissions, chemistry, and deposition.

Without discussion on these sources of errors using enough sensitivity tests, it is hard to judge if the treatments of these processes in the model are rigorous or not.

Response: Thanks for the comments. In the revised manuscript, several model sensitivity experiments have been conducted to better understand the effects of Hg chemistry and emissions on the global patterns of Hg concentrations and deposition and the sources of model errors. The Br oxidation mechanism and related model tests are given in Section 2.2.2 in the text and Section S1.1 in the supplement. The mechanism of gas-particle partitioning of Hg(II) and related model tests are given in Section 2.2.3 in the text and Section S1.2 in the supplement. The new anthropogenic emissions in South Africa and related model tests are given in Section S3 in the supplement.

3/ the modeled TGM over the Pacific is 1.4-1.6 ng/m³, compared to the observed 2.6-3.0 ng/m³. However, this large discrepancies have not been explained.

Response: As stated in Section 3.3, these discrepancies can be attribute to the inability of current models to reproduce the air–sea exchange of Hg reasonably. More specifically, this is due to upwelling mercury from the sub-surface ocean, possibly reflecting the legacy of past anthropogenic emissions (Holmes et al., 2010), and has been partially demonstrated by Soerensen et al. (2012). This process will be implemented in a future model version. The detailed explanation has been added to Section 3.3 in the revised manuscript.

4/ Fig. 5: in East Asia, as a most important source region, the model doesn't capture the low concentrations in summer and overestimates the TGM concentrations in autumn, and these discrepancies are not explained. As a result, it seems that the model doesn't capture the key processes governing the chemistry and deposition of Hg.

Response: Thanks for the comments. In Fig. 5, the comparisons of monthly variation of TGM were shown as regional average. Specifically, there are three sites in East Asia, including Mt. Lulin and Mt. Leigong in China and Chuncheon in Korea. The

site by site comparisons are shown in Fig. R2 to find the sources of model discrepancies. The TGM monthly variation in three sites are all reasonably reproduced by the model. However, significant model overestimation can be found in Chuncheon which might be due to uncertainties in local anthropogenic Hg emissions (Kim et al., 2012). And TGM in Mt. Leigong in Winter is relatively underestimated. Model performance in Mt. Lulin is the best. Therefore, the model overestimates TGM concentrations in summer and autumn in East Asia, as shown by Fig. 5, mainly due to model discrepancies in Chuncheon. Besides, from Fig. R2, we can see that nested simulation can well improve model performance in simulated TGM monthly variation in East Asia (especially in Chuncheon). In the revised manuscript, the above explanation is added to Section 3.3 in the text and Fig. R2 is added to the supplement.

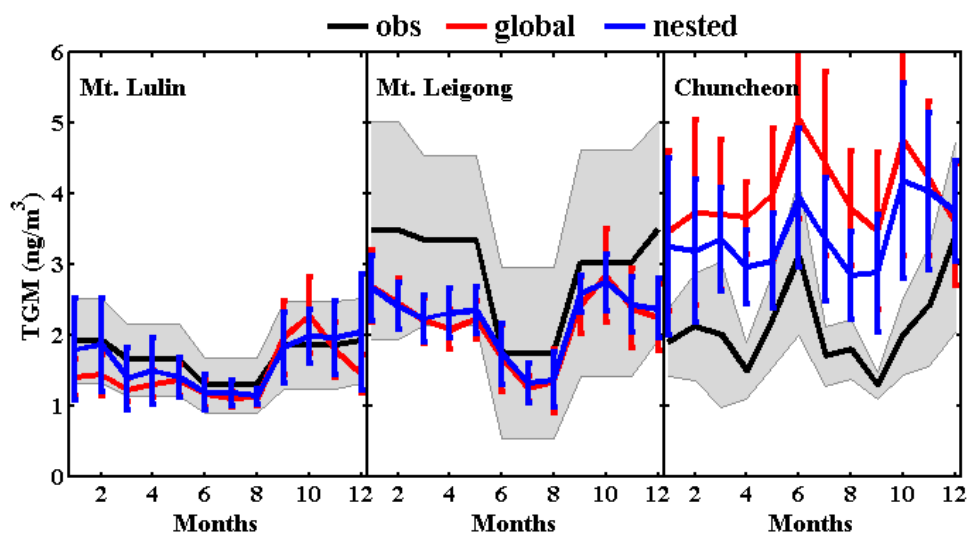


Figure R2. Mean seasonal variation of TGM in Mt. Lulin and Mt. Leigong in China, and Chuncheon in Korea. Shaded areas and vertical bars show one standard deviation for observations and for model results.

Oxidized mercury

Line 5, Page 6963: the authors don't provide convincing explanation for the overestimation of the oxidized mercury concentrations. As a result, it seems that the model fails to simulate the key processes governing the chemistry and deposition of Hg.

Response: As stated in the manuscript, we attributed the overestimation of the oxidized mercury concentrations to excessive oxidation of Hg(0) by relatively high

concentrations of simulated OH and O₃ and uncertainties concerning Hg chemical speciation in emission inventories. We think these are the leading factors. Of course, uncertainties of Hg chemistry (e.g. gas-particle partitioning of RGM, in-plume reduction of RGM) and deposition processes in the present model should also contribute to this discrepancy. These factors have been further considered in the revised manuscript.

Dry deposition

Line 13, Page 8: the authors attribute the model overestimation to Hg(II) and Hg(P) emissions. However, a discrepancy of 98 v.s. 648 pg m⁻³ is out of the uncertainty range of emissions. It seems that the model fails to simulate the key processes governing the chemistry and deposition of Hg.

Response: We agree that many factors including model emission, chemistry, deposition, horizontal resolution should contribute to this overestimation. We believe that uncertainties of emission magnitude and speciation would be one of the major factors. As can be seen from Figure S4 in the supplement and Figure 9 in the text, Hg emission and dry deposition share a similar spatial distribution with high values in the central and east coast of Japan. Especially, the largest emission and deposition are found in the Tokyo area. Therefore, we can see that dry deposition have high relation to emission. The emission magnitude is possibly overestimated in the Tokyo area due to the fact that population density is used as surrogate to map the emission. Besides, emission speciation for Hg(0), Hg(II) and Hg(P) should also be important because dry deposition in the Tokyo area is mainly contributed by Hg(II) deposition. Finally, missing model mechanism to deal with fast in-plume reduction of Hg(II) would be another major factor. Previous studies showed that fast in-plume reduction of Hg(II) happened when Hg was emitted from large point sources and this process caused rapid decrease in Hg(II) near large point sources (Vijayaraghavan et al., 2008; Amos et al., 2012; Zhang et al., 2012). These factors are all considered in Section 3.6 in the revised manuscript.

3.7.1 East Asia vs. North America and Europe

1/ Line 5, Page 6966: I suggest that the authors give some estimates of the Hg emissions from 2000-2010 to support their first explanation.

Response: Thanks for the suggestion. Wu et al. (2006) estimated that anthropogenic emissions in China increased at averaged annual rate of 2.9% during the period 1995-2003. Liang et al. (2013) pointed out that Hg emissions in China had increased by 164% during 1992-2007. These studies can support our first explanation. These references have been added to Section 3.7.1 in the revised manuscript.

2/ Line 6, Page 6966: I suggest that the authors compare the model-observations discrepancy over East Asia between the global and nested model to support their second explanation.

Response: The comparison of model performance over East Asia between the global and nested simulations has been done and shown in Table 3 and Figure 11 in the manuscript. The results are consistent with the second explanation.

3/ Line 6, Page 6966: there is no evidences showing that the emission uncertainty in East Asia is larger than that in North America and Europe.

Response: Uncertainties of emission inventory are mainly origin from the activity data and emission factor. These fundamental data in developing countries (e.g. China) are not as adequate and accurate as those in North America and Europe. Study by Muntean et al. (2014) has shown that uncertainties of Hg emissions in “Non Annex I” (developing) countries are larger than those in OECD90 and EIT countries. Besides, Large underestimations in Hg anthropogenic emissions over East Asia have been demonstrated in several previous studies (Jaffe et al., 2005; Pan et al., 2007; Song et al., 2015). Based on the above reasons, we believe that the emission uncertainty in East Asia is larger than that in North America and Europe.

4/ In general, it should be careful when comparing the different model performance among different regions. The miss of some chemical processes in the model should

also explain the poor model performance over East Asia. Insufficient explanation of the discrepancy causes the model to be very uncertain.

Response: We agree with the reviewer. The missing of some chemical and physical processes such as gas-particle partitioning of Hg(II), in-plume reduction of Hg(II), dynamic land reemission in the present model should also explain the poor model performance over East Asia. These explanations have been also added to Section 3.7.1 in the revised manuscript.

3.7.2 Global vs. nested simulations

The authors state that the emission, chemistry and deposition are self-consistent between the global and nested simulation. However, from Figure 7 and Figure 9, the regional TOTAL wet and dry deposition seem to be very different between the two simulations. I am not sure if this is only due to the smooth effect of mapping. I suggest that: 1/ the authors remove the smooth effect in these maps by showing the original model resolution;

Response: By stated self-consistent we just want to express that the total emissions, the physical and chemical parameterizations (including advection, diffusion, dry and wet deposition, chemistry) used in the global and nested simulation are the same. Actually, as stated in the manuscript (Section 3.7.2), Hg dry deposition amounts decrease notably in the coastal regions while wet deposition amounts increase in mountain regions of southeast China in the nested simulation. This resulting in model performance improvement in the nested simulation and will also resulting in different total dry and wet deposition between the global and nested simulation. The study of Zhang et al. (2012) using GEOS-Chem model also show similar results. We don't think the regional total deposition will keep the same in the global and nested simulations. Following the reviewer's advice, we have used gridfill shaded figures which can remove the smooth effect to replace the original Figure 7 and Figure 9 in the revised manuscript.

2/ there should be maps showing the absolute and relative differences between the two simulations;

Response: We agree with the reviewer. The dry and wet deposition in the global simulation are interpolated to match the model grids and compared to the results in the nested simulation. The differences of dry and wet deposition between the two simulations are shown in Figure R3. Figure R3 is also added to the supplement in the revised manuscript.

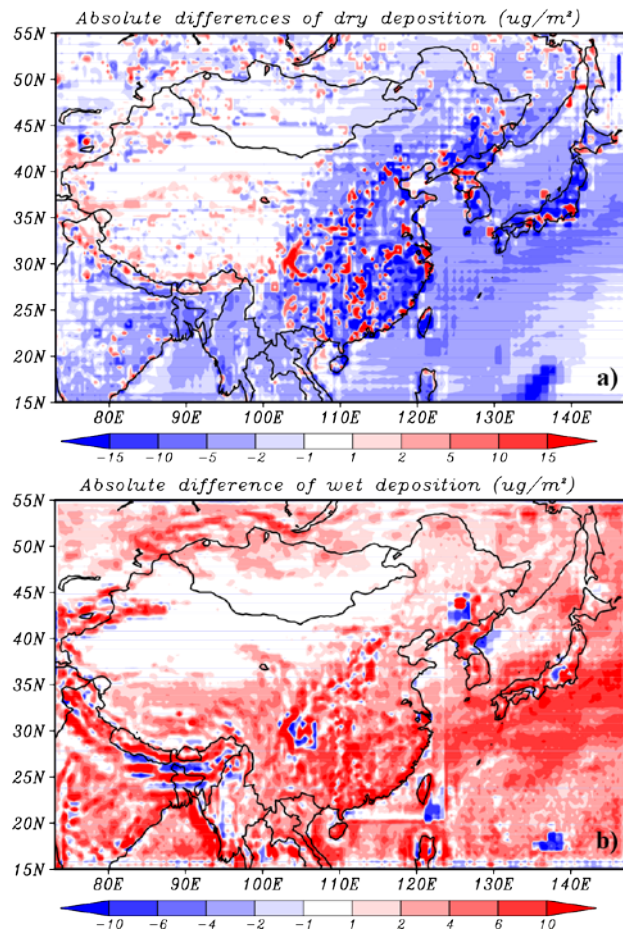


Figure R3. Absolute differences of annual dry and wet deposition over East Asia between the global and nested simulations (Nested-Global).

3/ there should be a detailed comparison of Hg budgets between the two simulations. Then, the author should provide enough evidences to substantiate that the two simulations are really self-consistent.

Response: Hg budgets over East Asia in the global and nested domains are shown in Table R2. Hg emissions in the two simulations keep exactly the same. TGM burden in

the two simulations are close with a difference percentage of 7%. However, as expected, dry and wet deposition in the two simulations are strikingly different. The dry deposition in the nested simulation is lower than that in the global simulation. This might be caused by different land use and land cover used in some model grids in the two simulations which will change the calculated dry deposition velocities of Hg. On the contrary, wet deposition in the nested simulation are much larger than that in the global simulation. This is mainly caused by different meteorological input in the two simulations. As stated in Section 3.7.2, more frequent orographic and convective precipitation occur in the southwest China in the nested simulation which resulted in elevated wet deposition of Hg. Table R2 is added to the supplement in the revised manuscript.

Table R2. Hg budgets over East Asia (15-55°N, 75-145°E) in the global and nested simulations (Unit: Mg yr⁻¹).

	global domain	nested domain	nested/global
Total Sources	1461	1461	1.00
anthropogenic	979	979	1.00
land	269	269	1.00
ocean	213	213	1.00
Total Sinks	824	843	1.02
Wet deposition	182	278	1.53
Dry deposition	642	565	0.88
TGM burden	548	512	0.93

Impacts of Chinese primary anthropogenic sources

1/ the authors state that 30% of surface Hg concentrations was contributed by China's primary anthropogenic sources. Then, what sources and which regions contributes to the remaining 70%? If the contribution of Hg reemissions is large, only accounting for the impact of China's primary anthropogenic sources would have very limited significance.

Response: In this study, we just focus on the impacts of Chinese primary anthropogenic sources due to the fact that emission control measures can only be implemented on primary anthropogenic sources in most cases. Except Chinese

primary anthropogenic sources, other local sources including natural emissions (from soil, vegetation and water), biomass burning emissions and reemissions of previous deposited Hg, and long-range transport should contribute to the remaining 70% of surface Hg concentrations in China. Quantitative assessment of the contribution of different sources and regions to the surface Hg concentrations in China is out of the scope of this study. Actually, in-depth analysis of the source apportionment of Hg concentrations and deposition over China has been conducted by Wang et al. (2014) by using the GEOS-Chem model. And the effects of Hg reemissions have also been discussed in the end of Section 4 in the manuscript.

2/ change "Hg concentrations" to "surface Hg concentrations" at any place if necessary.

Response: We have changed “Hg concentrations” to “surface Hg concentrations” in the revised manuscript.

3/ the trans-Pacific transport of Hg is not validated by any observations (e.g. the time series at Okinawa).

Response: Actually, model evaluation of Hg concentrations and deposition in East Asia (including China, Japan, Korea) and North America have been shown in the manuscript. This to some extent validated the trans-Pacific transport of Hg. Note that Hg observations in Okinawa are not publicly available. Therefore, we do not conduct model comparisons in this site.

References:

- Amos, H. M., Jacob, D. J., Holmes, C. D., Fisher, J. A., Wang, Q., Yantosca, R. M., Corbitt, E. S., Galarneau, E., Rutter, A. P., Gustin, M. S., Steffen, A., Schauer, J. J., Graydon, J. A., Louis, V. L. St., Talbot, R. W., Edgerton, E. S., Zhang, Y., and Sunderland, E. M.: Gas-particle partitioning of atmospheric Hg(II) and its effect on global mercury deposition, *Atmos. Chem. Phys.*, 12, 591-603, doi:10.5194/acp-12-591-2012, 2012.
- Bullock, O. R., and Brehme, K. A.: Atmospheric mercury simulation using the CMAQ model: formulation description and analysis of wet deposition results, *Atmos. Environ.*, 36, 2135-2146, doi:10.1016/s1352-2310(02)00220-0, 2002.
- CAMx: CAMx, user's guide, version 6.1, Environ International Corporation, California, 2014.
- Clever, H. L., Johnson, S. A., and Derrick, M. E.: The solubility of mercury and some sparingly soluble mercury salts in water and aqueous-electrolyte solutions, *J. Phys. Chem. Ref. Data*, 14, 631-681, 1985.
- Lin, C. J., and Pehkonen, S. O.: The chemistry of atmospheric mercury: a review, *Atmos. Environ.*, 33, 2067-2079, doi:10.1016/s1352-2310(98)00387-2, 1999.
- Gencarelli, C. N., De Simone, F., Hedgecock, I. M., Sprovieri, F., and Pirrone, N.: Development and application of a regional-scale atmospheric mercury model based on WRF/Chem: a Mediterranean area investigation, *Environmental Science and Pollution Research*, 21, 4095–4109, 2014.
- Holmes, C. D., D. J. Jacob and X. Yang: Global lifetime of elemental mercury against oxidation by atomic bromine in the free troposphere. *Geophysical Research Letters* 33(20): L20808, 2006.
- Holmes, C. D., Jacob, D. J., Corbitt, E. S., Mao, J., Yang, X., Talbot, R., and Slemr, F.: Global atmospheric model for mercury including oxidation by bromine atoms, *Atmos. Chem. Phys.*, 10, 12037-12057, doi:10.5194/acp-10-12037-2010, 2010.
- Jaffe, D., Prestbo, E., Swartzendruber, P., Weiss-Penzias, P., Kato, S., Takami, A., Hatakeyama, S., and Kajii, Y.: Export of atmospheric mercury from Asia, *Atmos. Environ.*, 39, 3029-3038, doi:10.1016/j.atmosenv.2005.01.030, 2005.
- Jung, G., Hedgecock, I. M., and Pirrone, N.: ECHMERIT V1.0-a new global fully coupled mercury-chemistry and transport model, *Geosci. Model Dev.*, 2, 175-195, 2009.
- Kim, S. H., Han, Y. J., Holsen, T. M., and Yi, S. M.: Atmospheric particulate mercury: Concentrations and size distributions, *Atmos. Environ.*, 61, 94-102, 2012.
- Lei, H., Liang, X., Wuebbles, D. J., and Tao, Z.: Model analyses of atmospheric mercury: present air quality and effects of transpacific transport on the United States, *Atmos. Chem. Phys.*, 13, 10807-10825, doi:10.5194/acp-13-10807-2013, 2013.
- Liang, S., Xu, M., Liu, Z., Suh, S. and Zhang T.: Socioeconomic Drivers of Mercury Emissions in China from 1992 to 2007, *Environ. Sci. Technol.*, 47(7): 3234-3240, 2013.
- Mason, R.: Mercury emissions from natural processes and their importance in the global mercury cycle, in: *Mercury Fate and Transport in the Global Atmosphere*, edited by: Mason, R., and Pirrone, N., Springer, USA, 173-191, 2009.
- Muntean, M., G. Janssens-Maenhout, S. Song, N. E. Selin, J. G. J. Olivier, D. Guizzardi, R. Maas and F. Dentener (2014). Trend analysis from 1970 to 2008 and model evaluation of EDGARv4 global gridded anthropogenic mercury emissions. *Science of The Total Environment* 494–495(0): 337-350.

- Pan, L., Chai, T., Carmichael, G. R., Tang, Y., Streets, D., Woo, J.-H., Friedli, H. R., and Radke, L. F.: Top-down estimate of mercury emissions in China using four-dimensional variational data assimilation, *Atmos. Environ.*, 41, 2804-2819, doi:<http://dx.doi.org/10.1016/j.atmosenv.2006.11.048>, 2007.
- Pan, L., Carmichael, G. R., Adhikary, B., Tang, Y., Streets, D., Woo, J.-H., Friedli, H. R., and Radke, L. F.: A regional analysis of the fate and transport of mercury in East Asia and an assessment of major uncertainties, *Atmos. Environ.*, 42, 1144-1159, doi:10.1016/j.atmosenv.2007.10.045, 2008.
- Seigneur, C., Karamchandani, P., Lohman, K., Vijayaraghavan, K., and Shia, R. L.: Multiscale modeling of the atmospheric fate and transport of mercury, *J. Geophys. Res.-Atmos.*, 106, 27795-27809, doi:10.1029/2000jd000273, 2001.
- Seigneur, C. and K. Lohman.: Effect of bromine chemistry on the atmospheric mercury cycle. *J. Geophys. Res.*, 113, D23309, doi:10.1029/2008JD010262, 2008.
- Seinfeld, C. P. and Pandis, S. N.: *Atmospheric Chemistry and Physics, From Air Pollution to Climate Change*, 1998.
- Selin, N. E., Jacob, D. J., Park, R. J., Yantosca, R. M., Strode, S., Jaegle, L., and Jaffe, D.: Chemical cycling and deposition of atmospheric mercury: Global constraints from observations, *J. Geophys. Res.-Atmos.*, 112, D02308, doi:10.1029/2006jd007450, 2007.
- Selin, N. E., Jacob, D. J., Yantosca, R. M., Strode, S., Jaegle, L., and Sunderland, E. M.: Global 3-D land-ocean-atmosphere model for mercury: Present-day versus preindustrial cycles and anthropogenic enrichment factors for deposition, *Global Biogeochem. Cy.*, 22, Gb3099, doi:10.1029/2008gb003282, 2008.
- Simone, D. F., C. N. Gencarelli, I. M. Hedgecock and N. Pirrone (2014). Global atmospheric cycle of mercury: a model study on the impact of oxidation mechanisms. *Environmental Science and Pollution Research* 21(6): 4110-4123.
- Slinn, S.A. and W.G.N. Slinn. Predictions for particle deposition on natural waters. *Atmos. Environ.*, 24, 1013-1016, 1980.
- Soerensen, A. L., Sunderland, E. M., Holmes, C. D., Jacob, D. J., Yantosca, R. M., Skov, H., Christensen, J. H., Strode, S. A., and Mason, R. P.: An improved global model for air-sea exchange of mercury: High concentrations over the North Atlantic, *Environ. Sci. Technol.*, 44, 8574-8580, doi:10.1021/es102032g, 2010.
- Soerensen, A. L., Jacob, D. J., Streets, D., Witt, M., Ebinghaus, R., Mason, R. P., Andersson, M. and Sunderland E. M.: Multi-decadal decline of mercury in the North Atlantic atmosphere explained by changing subsurface seawater concentrations, *Geophys. Res. Lett.* 39: Art #L21810, 2012.
- Song, S., Selin, N. E., Soerensen, A. L., Angot, H., Artz, R., Brooks, S., Brunke, E.-G., Conley, G., Dommergue, A., Ebinghaus, R., Holsen, T. M., Jaffe, D. A., Kang, S., Kelley, P., Luke, W. T., Magand, O., Marumoto, K., Pfaffhuber, K. A., Ren, X., Sheu, G.-R., Slemr, F., Warneke, T., Weigelt, A., Weiss-Penzias, P., Wip, D. C., and Zhang, Q.: Top-down constraints on atmospheric mercury emissions and implications for global biogeochemical cycling, *Atmos. Chem. Phys.*, 15, 7103-7125, doi:10.5194/acp-15-7103-2015, 2015.
- Temme, C., Blanchard, P., Steffen, A., Banic, C., Beauchamp, S., Poissant, L., Tordon, R., and Wiens, B.: Trend, seasonal and multivariate analysis study of total gaseous mercury data from the Canadian atmospheric mercury measurement network (CAMNet), *Atmos. Environ.*, 41,

- 5423–5441, doi:10.1016/j.atmosenv.2007.02.021, 2007.
- Vijayaraghavan, K., P. Karamchandani, C. Seigneur, R. Balmori, and S.-Y. Chen: Plume-in-grid modeling of atmospheric mercury, *J. Geophys. Res.*, 113, D24305, doi:10.1029/2008JD010580, 2008.
- Wang, L., S. Wang, L. Zhang, Y. Wang, Y. Zhang, C. Nielsen, M. B. McElroy and J. Hao (2014). Source apportionment of atmospheric mercury pollution in China using the GEOS-Chem model. *Environmental Pollution* 190(0): 166-175.
- Wangberg, I., Munthe, J., Berg, T., Ebinghaus, R., Kock, H. H., Temme, C., Bieber, E., Spain, T. G., and Stolk, A.: Trends in air concentration and deposition of mercury in the coastal environment of the North Sea Area, *Atmos. Environ.*, 41, 2612–2619, doi:10.1016/j.atmosenv.2006.11.024, 2007.
- Wesely, M. L.: Parameterization of surface resistances to gaseous dry deposition in regional-scale numerical models, *Atmos. Environ.*, 23, 1293-1304, doi:http://dx.doi.org/10.1016/0004-6981(89)90153-4, 1989.
- Wu, Y., S. Wang, D. G. Streets, J. Hao, M. Chan and J. Jiang (2006). Trends in anthropogenic mercury emissions in China from 1995 to 2003. *Environmental Science & Technology* 40(17): 5312-5318.
- Zhang, Y., Jaegle, L., van Donkelaar, A., Martin, R. V., Holmes, C. D., Amos, H. M., Wang, Q., Talbot, R., Artz, R., Brooks, S., Luke, W., Holsen, T. M., Felton, D., Miller, E. K., Perry, K. D., Schmeltz, D., Steffen, A., Tordon, R., Weiss-Penzias, P., and Zsolway, R.: Nested-grid simulation of mercury over North America, *Atmos. Chem. Phys.*, 12, 6095-6111, doi:10.5194/acp-12-6095-2012, 2012.

Response to Referee #2:

We thank the reviewer for constructive comments and suggestions. We have revised our manuscript according to his comments and suggestions. In the following we would like to reply the comments point by point.

1 General Comments

The manuscript describes the addition of a Hg module to a global chemical transport model, with a focus on the impact of emissions from China. The model performs similarly to most of the other models already described in the literature.

The model lacks a bi-directional exchange flux at the land-atmosphere and ocean-atmosphere interfaces, the model does not contain the option to use a Bromine based oxidation mechanism for Hg oxidation, even in the Arctic, and the comparison between model and observations has been performed using mismatched years. The authors themselves point out that this inconsistency is a weakness in their study. The authors have also used an emission database that is known to be flawed, but have not attempted to rectify this. The dry deposition to wet deposition ratio is out of line with other studies apart from one GEOS-Chem study quoted by the authors, Selin et al. (2007), which was revised a year later, Selin et al. (2008), more recent GEOS-Chem simulations also suggest more equal dry and wet deposition fluxes (Amos et al., 2012; Zhang et al., 2012). There does not seem to be any major improvement over previous Hg models in this manuscript, and in fact a number of important processes are less well described than in other models, I do not think there is much reason to publish this article in GMD.

Response: Thanks very much for the comments. From our perspective, the present work is unique or important in the following aspects. Firstly, online nested Hg simulation with flexible horizontal resolution was developed and evaluated in this study. Compared to traditional multi-scale modeling approach (using a global model to provide initial and boundary conditions to a regional model) (Seigneur et al., 2001), online nested method use the same physical and chemical parameterizations in the global and nested domains which could avoid uncertainties induced by different

boundary conditions. Compared to offline nested method used in the GEOS-Chem model (Zhang et al., 2012), online nested method can provide boundary conditions with higher time resolution from the global domain to the nested domain. Typically, the time resolution of boundary condition in offline and online nested model is 3 hour (or 1 hour) and 10 minute (or 5 minute), respectively. Therefore, online nested simulation would potentially improve model performance in regional scale. Secondly, as stated in the introduction, little model validation has been conducted over East Asia (especially China) in previous global modeling studies due to lack of observational data. We have made great efforts to collect various Hg observations from literatures (especially published in Chinese journals) and conducted comprehensive model evaluation over East Asia in this study. Finally, the global impacts of the primary anthropogenic emissions from the world's largest single emitter, China, have been assessed for the first time in this study. In the revised manuscript, we revised the introduction to highlight the major improvement (namely online nested simulation) of our Hg model. We hope the reviewer and the editor to reconsider this paper to get published by GMD.

The responses to the general comments with model methodology used in our model as raised by the reviewer are as follows.

1) bi-directional exchange flux at the land-atmosphere and ocean-atmosphere interfaces

In the present model, the treatments of Hg reemissions from land and ocean mainly follow the method used by Jung et al. (2009). Besides, global and regional total emission amounts are prescribed according to estimates in previous studies (Selin et al., 2007, 2008; Mason, 2009; Soerensen et al., 2010). This can make sure the global and regional total reemissions from land and ocean are generally reasonable. As show in Figure S6 in the supplement, the spatial patterns of the reemissions from land and ocean are similar with previous modeling studies. Certainly, we also agree with the reviewer that lack of a bi-directional exchange flux at the land-atmosphere and ocean-atmosphere interfaces is a weak aspect in the present work. In the future, parameterizations of air-sea and air-land Hg dynamic exchange will be included in the

model to better resolve Hg reemissions.

2) Bromine based oxidation mechanism for Hg oxidation

Large uncertainties in atmospheric chemistry of Hg is one of the fundamental limitations of current models. The primary gaseous oxidants of Hg(0) in current models include O₃, OH, H₂O₂ and reactive halogen species (e.g. Br, Cl, I, Br₂, Cl₂, BrO, ClO, IO, etc.). Lei et al. (2013) demonstrated that adding Br chemistry has little impact on overall global TGM patterns based on sensitivity experiments using the CAM-Chem Hg model. Wang et al. (2014) also pointed out that Br is less important than O₃ and OH as oxidants for Hg(0) in Hg simulation over China with high oxidation capacity. Besides, several latest Hg modeling studies (Simone et al., 2014; Gencarelli et al., 2014) still used O₃-OH oxidation mechanism alone in their models. It seems that at the current level of understanding the O₃-OH oxidation mechanism is still sufficient for Hg simulation. However, the importance of Br atoms in gas phase reaction of Hg has been identified by several studies (Holmes et al., 2006, 2010), and these reactions are believed to be essential in Polar region and marine boundary layer. We accept the advice of the reviewer and add Br chemistry for gas oxidation of Hg, to provide the option of using Br oxidation mechanism and address the impact of Br chemistry in our model. Detailed results are given in Section 2.2.1 in this response document.

3) Mismatch of the time periods between simulation results and observations

Detailed explanations concerning the influence of the mismatch of the time periods between model results and observations are given in the responses to the specific comments (Section 2.3.1). Overall, we think the influence of the mismatch of the time periods may be relatively large for dry and wet deposition comparisons over East Asia but relatively small for other comparisons. However, no public dataset of Hg observations over East Asia is available at present. So we have no better choice.

4) Flawed emission database

We used the AMAP 2000 inventory (Pacyna et al., 2006) because it was used by the HTAP multi-model experiment for Hg (Pirrone and Keating, 2010) and also widely used by many other published modeling studies (Selin et al., 2008; Jung et al.,

2009; Lei et al., 2013). We are very sorry that we do not know the emissions in South Africa are wrong in the AMAP 2000 inventory when we started the present work in 2010. We have replaced the Hg emissions in South Africa using the AMAP 2010 inventory and rerun the model to test the impacts of updating the emissions. The emissions update results in significantly decreasing of local Hg emissions and concentrations over South Africa. More detailed analyses are given in Section 2.2.3 in this response document.

5) dry deposition to wet deposition ratio

Dry and wet deposition account for 78 and 22 % of total deposition in the simulation results, respectively. This ratio is different with the results presented by Selin et al. (2008) and Amos et al. (2012). But it is comparable with the results of Selin et al., (2007). Actually, a more latest modeling study using the CAM-Chem-Hg model (Lei et al., 2013) also gave a similar ratio. Dry and wet deposition contribute 70% and 30% to total deposition in their results. These differences might be caused by different Hg chemistry and deposition parameterizations and also meteorological inputs used in different models.

2 More Specific comments

2.1 Introduction

The Minamata convention has its own website <http://www.mercuryconvention.org/>. Rather than the HTAP report, (Pirrone and Keating, 2010), the most recent Technical Background report to the Global Mercury Assessment might be more appropriate, AMAP/UNEP (2013). The GEOS-Chem reference is out of date there are a number of more up to date publications, with various improvements on Selin et al. (2007). The same is true of CMAQ-Hg, and ECHMERIT (De Simone et al., 2014). The global model used by Environment Canada (GRAHM, see Dastoor and Durnford (2013) and references) is not included in the list, neither is WRF/Chem-Hg (Gencarelli et al., 2014). Zhang et al. (2012) is probably the most recent article looking at local/long-distance sources of Hg to the US, perhaps it should be cited earlier.

Response: Thanks for the suggestions. The references in the introduction (Section 1) have been updated according to the advices of the reviewer.

2.2 Model Description

2.2.1 Mercury Chemistry

All the Hg(II) produced by the reactions between Hg and O₃ and OH is assumed to be in the gas phase, this is not in line with most other models and will have a major impact on deposition flux fields in many regions. The authors should justify this, or ideally rerun the model splitting the oxidation products between the gas and aerosol phases to have an idea of how important this is. Indeed (Amos et al., 2012) partition the products between gas and particulate phase as a function of temperature and PM_{2.5}. The lack of a Br oxidation mechanism is a serious shortcoming, as it is known that Br oxidises Hg, and therefore is significant not only in the Arctic but also in the MBL, and the difference in the concentration fields and deposition flux fields should using this mechanism should have been evaluated.

Response: Following the advices of the reviewer, we have added the mechanisms of the gas-particle partitioning of Hg(II) and Br oxidation in the model, and assessed the effects of these processes on global Hg concentrations and deposition in the revised manuscript.

1) Gas-particle partitioning of Hg(II)

In the revised manuscript, detailed description of the Hg(II) gas-particle partitioning mechanism included in the model is given in Section S1.2 in the supplement. And model sensitivity experiments were conducted to test the effects of this mechanism on global Hg concentrations and deposition. Detailed comparisons and analyses are shown in Section 2.2.3 in the text and Figs. S2-3 in the supplement.

2) Br oxidation

We have added Br chemistry for gas oxidation of Hg and test the impacts on Hg concentrations. As shown by Table R1, we add five Br chemical reactions in the gas phase (Seigneur and Lohman, 2008) in addition to the O₃-OH oxidation mechanism to test how the Br oxidation reactions affect the Hg distributions. Similar to the

treatment of Holmes et al. (2006, 2010), the five reactions are treated as a single reaction, with an effective Hg(0) first-order rate constant that is a function of the individual reaction rates and the concentrations of Br, BrO and OH based on the assumption that Br, BrO and OH concentrations don't change by their reactions with Hg. This is also the same with the implementation described in CAMx (2014). The effective first-order rate constant is calculated as follows:

$$k_{eff} = \frac{k_1[Br](k_3[Br]+k_4[OH])}{k_2+k_3[Br]+k_4[OH]} + k_5[BrO] \quad s^{-1}$$

Table R1. Bromine reactions added in the model (T is the temperature in degrees Kelvin, and P is the pressure in atmospheres).

NO.	Reaction	Rates
BR1	Hg(0)(g)+Br(g)→HgBr(g)	$k_1 = 3.6 \times 10^{-13} P \left(\frac{T}{298}\right)^{-1.86} \text{ cm}^3 \text{ molec}^{-1} \text{ s}^{-1}$
BR2	HgBr(g)→Hg(0)(g)	$k_2 = 3.9 \times 10^9 \exp\left(\frac{-8537}{T}\right) \text{ s}^{-1}$
BR3	HgBr(g)+Br(g)→HgBr ₂ (g)	$k_3 = 2.5 \times 10^{-10} \left(\frac{T}{298}\right)^{-0.57} \text{ cm}^3 \text{ molec}^{-1} \text{ s}^{-1}$
BR4	HgBr(g)+OH(g)→HgBrOH(g)	$k_4 = 2.5 \times 10^{-10} \left(\frac{T}{298}\right)^{-0.57} \text{ cm}^3 \text{ molec}^{-1} \text{ s}^{-1}$
BR5	Hg(0)(g)+BrO(g)→Hg(II)(g)	$k_5 = 1.0 \times 10^{-15} \text{ cm}^3 \text{ molec}^{-1} \text{ s}^{-1}$

In the GNAQPMS-Hg model, Br and BrO are not explicitly simulated. Therefore, we specify typical vertical profiles of Br and BrO concentrations over land and ocean, with higher values over ocean (2.9×10^{-8} and 2.9×10^{-7} ppm for Br and BrO) than over land (5.0×10^{-9} and 5.0×10^{-8} ppm for Br and BrO). During the night, the concentrations of Br and BrO are assumed to be zero, considering that the photolysis of Br₂ is the primary source for these radicals.

Figure R1 shows the difference of surface TGM concentrations resulting from introducing Br reactions. Decrease in TGM concentrations is found in the whole globe. This is because additional Br chemistry transforms more Hg(0) into Hg(II), which subsequently enhances the deposition of Hg(II), leading to the reduction of TGM concentrations. Larger TGM reduction is found in the Northern Hemisphere than in the Southern Hemisphere. In general, the change in TGM concentration is less than 0.2 ng m^{-3} in most areas which indicates that introducing Br chemistry seems to have little impact on overall TGM magnitudes and patterns. These results are similar

to Lei et al. (2013) which test the impact of Br chemistry using the CAM-Chem-Hg model. Although adding the Br chemistry does not significantly change the TGM pattern, but it may affect the gaseous Hg partitioning between Hg(0) and Hg(II), and hence may affect the global Hg deposition patterns. More in-depth tests and analysis are needed to address these impacts in the future.

In the revised manuscript, the description of Br oxidation mechanism and its impact on global Hg concentrations is given in Section 2.2.2 in the text and Section S1.1 in the supplement.

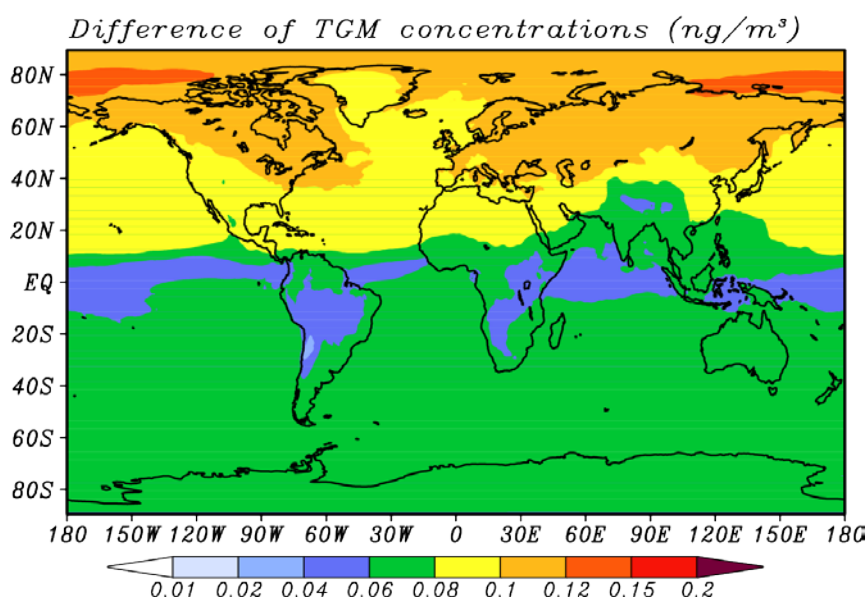


Figure R1. Change in surface TGM concentrations (ng m⁻³) by introducing bromine chemistry (positive value means the TGM concentration decreases after added bromine chemistry).

2.2.2 Mercury Deposition

Pirrone and Keating (2010) is not an appropriate reference for this comment, the authors should cite the individual publications describing the results from the different Hg models.

Response: “Both dry and wet removal pathways are equally significant to the total deposition of mercury.” is one of the main findings stated in Section 4.3.2 (Page 108) in the HTAP report (Pirrone and Keating, 2010). So we think Pirrone and Keating (2010) should be an appropriate reference here.

2.2.3 Mercury Emissions

The authors have ignored the latest anthropogenic emission inventories, AMAP/UNEP (2013); Rafaj et al. (2013); Muntean et al. (2014). The authors increase the Asian emissions in the inventory following Selin et al. (2008), however they do not reduce the South African emissions which are known to be wrong (AMAP/UNEP, 2008), nor do they include artisanal mining, which Selin et al. (2008) did, giving totals for different regions. The authors later state that high TGM concentrations are found downwind of mining areas in South Africa without pointing out that is where the Hg emission inventory was very wrong. The 2005 emission inventory revised the Hg emissions from gold production down by two orders of magnitude (150 Mg). As the 2000 and 2005 inventories are on the same grid, perhaps it would have been possible to substitute the 2000 data with the 2005 data relatively easily? The use of biogenic CO emissions from oceans and land should be justified. I would have thought that this led to an overestimate of emissions particularly in the Southern Ocean where wind speeds and productivity are high. The expression “Additionally, ocean emissions are adjusted” does not provide enough detailed information to assess the author’s methodology.

Response: We have always pay close attention to the development of anthropogenic Hg emission inventory and we aware that global emission inventories with base years of 2005 and 2010 are available from AMAP (AMAP/UNEP, 2013) and EDGAR (Muntean et al., 2014).

We started the present work in 2010. We used the AMAP 2000 inventory (Pacyna et al., 2006) because it was used by the HTAP multi-model experiment for Hg (Pirrone and Keating, 2010) and also widely used by many other published modeling studies (Selin et al., 2008; Jung et al., 2009; Lei et al., 2013). We are very sorry that we do not know the emissions in South Africa are wrong in the AMAP 2000 inventory. As shown by Figure R2, we replaced the anthropogenic Hg emissions in South Africa by using the AMAP 2010 inventory and assessed this emission update on the simulated results. The emission amounts in South Africa decrease by about a factor of 4 (from 259 Mg to 64 Mg). After updating the emissions, the surface Hg concentrations in South Africa decrease by up to 1 ng m^{-3} , but have little changes

elsewhere (the differences of concentrations are smaller than 0.01 ng m^{-3} in most areas) as shown by Figure R3. The simulated TGM concentrations at Cape Point decrease from 1.77 ng m^{-3} to 1.23 ng m^{-3} , more close to the observed values. The above results (including Figures R2 and R3) are added to Section S3 in the supplement. And corresponding explanations are also given in Section 2.4 and 3.3 in the revised manuscript to remind the readers that the anthropogenic emissions over South Africa are flawed.

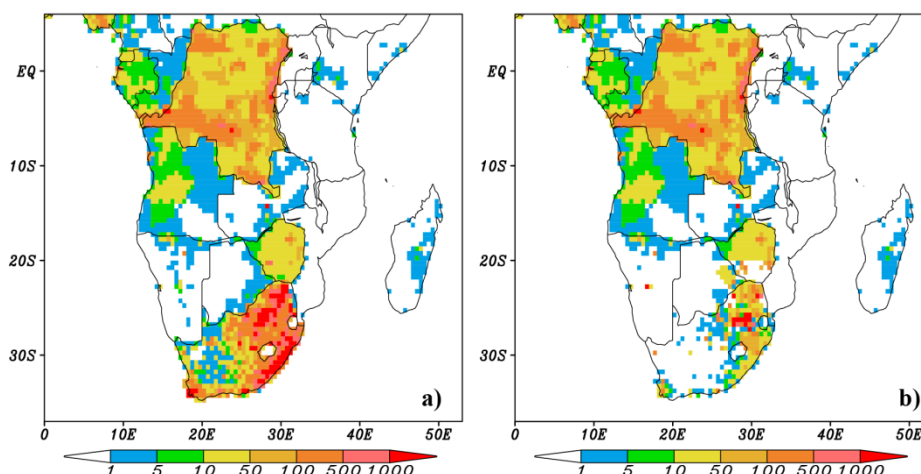


Figure R2. Annual anthropogenic Hg emissions (kg/grid) in South Africa, a) the AMAP 2000 inventory and b) the AMAP 2010 inventory in South Africa (16-34°E, 36-20°S) + the AMAP 2000 inventory elsewhere.

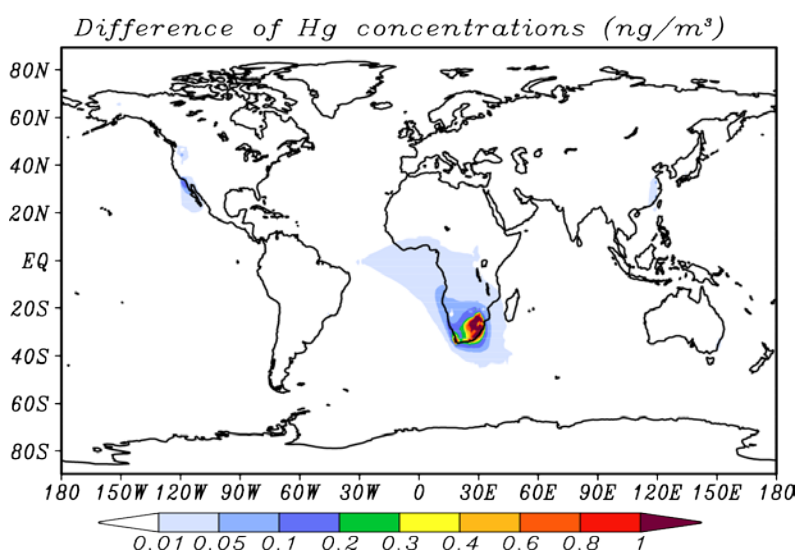


Figure R3. Difference of global surface Hg concentrations after updating the anthropogenic emissions in South Africa by using the AMAP 2010 inventory.

As stated in the manuscript, Hg reemissions from land and ocean are not only

mapped according to biogenic CO emissions, but also constrained by global and regional total emission amounts prescribed according to estimates in previous studies (Selin et al., 2007, 2008; Mason, 2009; Soerensen et al., 2010). This can make sure the global and regional total amounts and patterns of land and ocean reemissions are generally reasonable. Reemissions are somehow relevant to biological activity (e.g. vegetation) so we used biogenic CO emissions as temporal and spatial surrogates. This method was also used by the ECHMERIT model (Jung et al., 2009). Certainly, reemissions are also relevant to deposition pattern, soil and water Hg content and environmental elements (e.g. solar radiation, wind speed). So the method of spatial allocation used in this study might induced some uncertainties, but we think the general spatial patterns are reasonable as show in Figure S6 in the supplement. In future work, parameterizations of air-sea and air-land Hg dynamic exchange will be included in the model to better resolve Hg reemissions.

As stated above, global and regional total ocean emissions are prescribed in the simulation. Although the ocean emissions are mapped according to biogenic CO emissions, the regional total amounts over different sea areas are determined based on previous studies (Strode et al., 2007; Selin et al., 2008; Soerensen et al., 2010). Through this adjustment, the spatial and temporal variation of Hg ocean emissions could be better characterized.

2.2.4 Model setup

Twenty vertical layers does not seem very many. Why use NO_x emissions from 1983 to 1990? The latest version of MOZART is version 4, why use v2.4?

Response: Yes. To save computation time, we used a medium vertical resolution with 20 layers from the surface to 20 km in the present model. We think this resolution is enough for Hg simulation and it is higher than many other Hg models (e.g. Jung et al., 2009).

Online parameterization of lightning NO_x emissions was not included in the present model. Instead, we used the lightning NO_x emissions averaged from 1983 to 1990 from Price et al. (1997).

Yes, the latest version of MOZART is version 4. We just used MOZART outputs of O₃, NO_x, CO as initial and top boundary conditions in our simulations. This dataset has been also used in many of our other studies (Li et al., 2009; 2011) and shown good model performances. Besides, as shown in Figure S11, the O₃ seasonal cycle in 900, 500, 250 hPa were well reproduced. Therefore, we think the dataset from MOZART-v2.4 is sufficient.

2.3 Model evaluation

2.3.1 Observational data

There is a coordinated global Hg monitoring network <http://gmos.eu/>, see also http://www.geo-tasks.org/geoss_portfolio/health_gmos.php. The temporal mismatch between the observations and the modelling period all but renders any comparison between simulations and measurements invalid. I fail to see how the authors imagine they can publish this.

Response: Thanks for the reminder. We knew that there is a coordinated global Hg monitoring network (Global Mercury Observation System, GMOS) established in the end of 2010. However, observations from GMOS are still not available publicly at this moment. We hope the observations from GMOS will open to the public in the near future.

We recognize that the mismatch of the time periods when comparing the model with the observations is a weakness of the present work. However, as stated in the manuscript, only Europe and North America have routine monitoring networks for atmospheric Hg concentrations and deposition. Actually, observations of wet deposition and precipitation in Europe and North America are from EMEP and MDN respectively, and the time periods are exactly the same with the simulation results. In contrast, no public Hg observation datasets are available in East Asia. So we have no choice but to use observations (collected from literatures) with mismatched time periods over East Asia.

All observations of Hg concentrations at land sites used in this study are averaged over time periods larger than 1 year. Analyses of long-term measurements show that

trends in mean TGM during the last decade are small (of order $1\%a^{-1}$) or negligible at most background sites in the Northern Hemisphere (Temme et al., 2007; Wangberg et al., 2007). Therefore, the influences of the mismatch of time periods between model results and Hg concentration observations would not be large. Similar observational datasets (as shown in Table S2-S4 in the supplements) are also used by previous modeling studies (Selin et al., 2007, 2008; Holmes et al., 2010).

Observations from ship cruises are just used for initial comparison of simulated results over ocean following previous studies (Selin et al., 2007, 2008; Holmes et al., 2010). These observations are not used for quantitative model evaluation and not including in the calculation of statistical parameters of model performance.

Annual dry and wet deposition measurements in East Asia (Table S5 in the supplement) are all obtained from literatures. Considering that dry and wet deposition fluxes are affected by environmental factors (e.g. precipitation) and they might differ from one year to another, so the influence of the mismatched time periods would be relatively larger. Again, no observations of Hg deposition are available at present. So we have no better choice.

Overall, we think the influence of the mismatch of the time periods between model results and observations is relatively large for dry and wet deposition comparisons in East Asia but relatively small for other comparisons. Therefore, we don't think the model comparison results presented in this study are invalid. Quantitative assessments of the influence are difficult and outside the scope of this study.

The above explanation is given to Section S4.1 of the supplement in the revised manuscript.

2.3.2 Global mercury budget

The total atmospheric burden of Hg is very, very high, compare Mason et al. (2012), so high in fact that it is almost certainly wrong. Quoting a recent study using GEOS-Chem, Horowitz et al. (2014), "Our simulated present-day atmospheric reservoir of 5800Mg is slightly higher than the observational range (4600 - 5600 Mg), but this could be accommodated by uncertainty in Hg re-emission from soils."

The ratio between dry and wet deposition seems to me to be improbable. Are the authors sure they don't have a problem in their wet deposition scheme, are convective and synoptic precipitation included? Have they checked the WRF output with precipitation observations? Of course it could be the dry deposition that it over-estimated but this dry/wet ratio is quite different from most modelling studies and needs to be investigated. The article quoted as corroboration of the dry/wet ratio, Selin et al. (2007), was improved upon Selin et al. (2008) and the dry to wet deposition ratio revised.

Response: Thanks for very detailed comments and instructions. We have carefully checked the major Hg processes (e.g. chemistry, dry and wet deposition) in the simulation and found initial condition is the main factor to cause the high atmospheric burden of Hg. In the previous model run, initial surface concentrations of Hg(0) in the Northern and Southern Hemispheres were set to be 1.6 and 1.2 ng m⁻³ and they decrease gradually with altitude. This initial condition equals to an atmospheric Hg burden of about 9105 Mg and resulted in an annual averaged simulated atmospheric Hg burden of about 8679 Mg after 4 years model run. We rerun the model using clean initial condition of Hg(0) and get an atmospheric Hg burden of 5546 Mg after 4 years model run. Besides, these model experiments also demonstrated that the model initial condition has little impacts on the global Hg concentrations and deposition with 3 years model spin up time. The atmospheric burden of 5546 Mg is close to those results reported by Selin et al. (2007, 2008), Mason et al. (2012) and Horowitz et al. (2014). Table 2, Figure 2, and the analyses in Section 3.2 in the original manuscript are revised according to this new atmospheric Hg burden.

Dry and wet deposition account for 78 and 22 % of total deposition in the simulation results, respectively. This ratio is different with the results presented by Selin et al. (2008) and Amos et al. (2012). But it is comparable with the results of Selin et al., (2007). Actually, a more latest modeling study using the CAM-Chem-Hg model (Lei et al., 2013) also gave a similar ratio. Dry and wet deposition contribute 70% and 30% to total deposition in their results. These differences might be caused by different Hg chemistry and deposition parameterizations and also meteorological

inputs used in different models.

Figure R4 compares the WRF precipitation output with those from GPCP and NCEP reanalysis datasets. We can see that WRF can well reproduce the global distribution of precipitation. However, it seems to overestimate precipitations in regions near the equator but underestimate them in the Northwest Pacific, the North Atlantic and ocean south of 30°S. Considering large uncertainties in precipitation simulation in current models, these biases would be well acceptable. Finally, convective and synoptic precipitations are all included in our model. However, we do not distinguish the convective and synoptic precipitation in the wet deposition process, instead we just used total precipitation (convective+synoptic). The approach to treat Hg wet deposition is similar to the implementation described in ECHMERIT (Jung et al., 2009) and CAMx model. More detailed description of the wet deposition parameterization used in the model is given in Section S2.2 of the supplement in the revised manuscript.

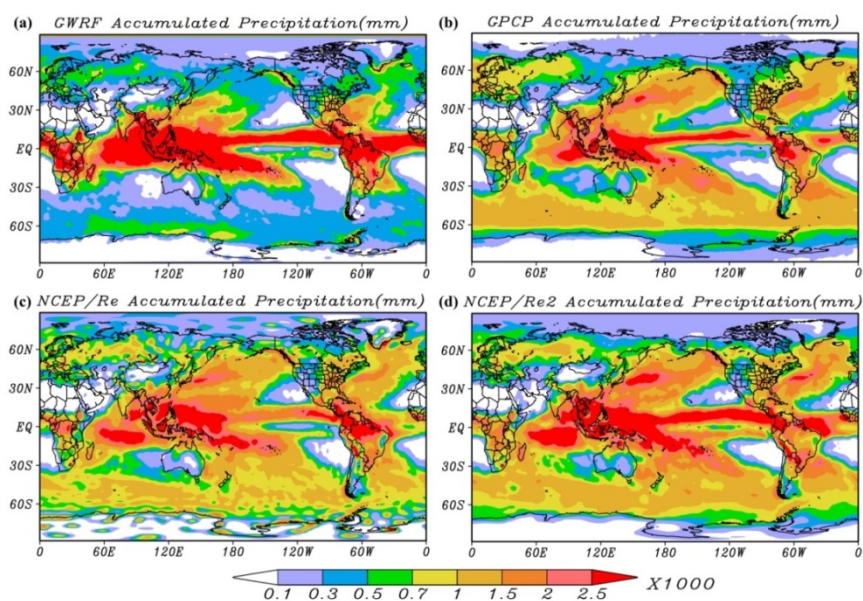


Figure R4. Global spatial distribution of accumulated precipitation simulated by WRF (a), and obtained from the GPCP (Global Precipitation Climatology Project) (b), NCEP reanalysis 1 (c) and NCEP reanalysis 2 (d) datasets in 2001.

2.3.3 Total gaseous mercury

This comment, “High surface TGM concentrations are found in or downwind of areas with intensive mercury-relative mining (e.g. Western USA, Southern Africa),” is

very odd. Looking at the emissions inventory for 2000, higher emissions in the Western US, compared to the Eastern US for example, are not apparent, and it is not clear what "intensive mercury-relative mining" might be. The emissions from South Africa are an error in the inventory, which the authors should be aware of. Why there should be such high TGM concentrations in Alaska is not clear either, the emissions database would not seem to indicate that there would be. And it seems unlikely that forest fires would cause such high concentrations over a whole year. Perhaps the authors should check their emissions interpolation routines. On the underestimate of the inter-hemispheric gradient, the articles cited are not the most recent and certainly in the authors model linking Hg emissions to CO emissions from the ocean will contribute to this problem. The authors finish this section mentioning the problem with the emission inventory, so why did they use it (or not change the South African emissions as they did with the Asian emissions), and why make the earlier comment about high concentrations downwind of mining errors if they know this is caused by erroneously high emissions?

Response: Thanks for very detailed comments and instructions. It is true that in the anthropogenic emission inventory (Figure S4 (a) in the supplement), higher emissions in the Western US compared to the Eastern US are not apparent. However, as shown in Figure S5 (b) in the supplement, high geogenic emissions are found in Western US and Alaska. As stated in the manuscript (Section 2.4), the geogenic emissions represent mobilization of Hg by degassing from geological reservoirs and they are distributed according to the locations of Hg mines as an indicator of Hg deposits. The spatial distribution of geogenic emissions is consistent with those used in the GEOS-Chem model (Selin et al., 2007, 2008). Therefore, high TGM concentrations found in the Western US and Alaska are consistent with Hg emissions and are reasonable.

On the underestimation of the inter-hemispheric gradient, we agree that linking Hg emissions to biogenic CO emissions from the ocean might possibly contribute to this bias. Besides, we think there are two other major reasons causing this discrepancy. Firstly, the inability of present model to reproduce the air–sea exchange of Hg

reasonably as stated in the manuscript. More specifically, this is due to upwelling mercury from the sub-surface ocean, possibly reflecting the legacy of past anthropogenic emissions (Holmes et al., 2010). This process will be implemented in a future model version. Secondly, simulated TGM concentrations in East Asia and Europe were underestimated, and the NMBs were -32% and -8%, respectively. These explanations are added to Section 3.3 in the revised manuscript.

Thanks the reviewer to remind us that the anthropogenic emissions over South Africa are an error in the AMAP 2000 inventory. we have replaced the anthropogenic Hg emissions over South Africa by using the AMAP 2010 inventory and assessed this emission update on the simulated results. Detailed analyses have given in Section 2.2.3 in this response document. And corresponding explanations are given in Section 2.4 and 3.3 in the revised manuscript to remind the readers that the anthropogenic emissions over South Africa are flawed.

2.3.4 Oxidized mercury

The bias reported in Table 3 for North America and Europe requires at least a comment.

Response: Thanks for the reminder. The explanation has been given in Section 3.4 in the manuscript. As follows “This discrepancy may partially be attributed to excessive oxidation of Hg(0) by relatively high concentrations of OH and O₃ (especially over the ocean) and uncertainties concerning Hg chemical speciation in emission inventories”.

2.3.5 Wet deposition

It would have been useful to see a global map of wet deposition to compare the distribution to previous model results. There appears to be a discontinuity in figures 7c and d (roughly 20N, 120E).

Response: The global map of simulated Hg wet deposition is given in Figure R5. It can be see that the spatial pattern is related to precipitation, Hg emissions and oxidized Hg concentrations. Large wet deposition are found over East Asia, southeast

America, and regions near the equator. This global pattern is generally reasonable compared to previous modeling studies (Holmes et al., 2010; Chen et al., 2014).

Yes, there is a discontinuity in figures 7c and d. This is caused by the two-way nesting simulation of WRF. Actually, we set three nesting domains (global, East Asia and the east part of China) in the WRF simulation, but we just used the uppermost two domains in the Hg simulation to save computation time. The discontinuity lies just on the boundaries of the innermost domain (e.g. 21N, 123E). We have checked this discontinuity in precipitation fields by compared two WRF simulations with two-way nesting option on and off, and found no big differences between these two simulations. Therefore, this discontinuity will not affect our Hg modeling results.

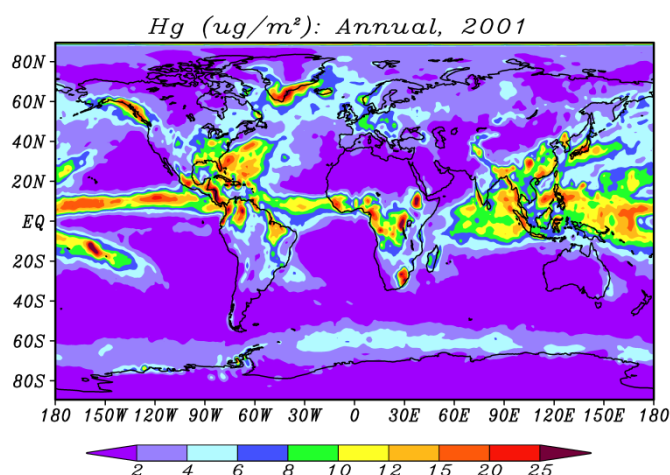


Figure R5. Simulated global annual Hg wet deposition in 2001.

2.3.6 Dry deposition

The authors refer to observations, whereas dry deposition is not measured (unfortunately) but is inferred or calculated from bulk, throughfall and wet deposition measurements.

Response: We agree with the reviewer. The following explanation as “It should be noted that data (Table S5 in the supplement) used to evaluate model simulation of dry deposition is not directly measured, but is inferred or estimated based on measurements of total Hg in through fall and rainwater, wet deposition and atmospheric concentrations.” has been added to Section 3.6 in the revised manuscript to remind the readers.

2.3.7 Model performance and comparison

The authors state that the model performs better for Europe and North America than for Asia. This is patently not true in the case of oxidized Hg. Also in this section the problem of comparing simulations from one year with observations from another comes up again. This makes very little sense. If the measurements, particularly in China were made relatively recently, and data from North America and Europe are available up until the present, what sense is there simulating 2001? Especially when it is known that the anthropogenic emissions database for that year is flawed. The 2005 emissions inventory has been available since 2008 and the 2010 inventory has been available since last year. It strikes me as a bizarre choice and scientifically speaking, inept and inappropriate.

Response: As illustrated in Table 3, the values of three statistical parameters (R, NMB, RMSE) for TGM and wet deposition are all better in North America and Europe than in East Asia. For oxidized Hg, the situation is more complicated. Two of the statistical parameters (R and RMSE) are much better in North America and Europe than in East Asia. However, lower NMB is found in East Asia. This is because the model overestimated oxidized Hg in some sites but underestimated them in the other sites and therefore resulted in low model bias. The larger RMSE found in East Asia could support this explanation. Therefore, we stated that the model performed generally better for Europe and North America than for Asia.

Detailed explanation concerning the influence of the mismatch of the time periods between model results and observations has been given in the above response (Section 2.3.1). We think the influence of the mismatch of the time periods may be relatively large for dry and wet deposition comparisons over East Asia but relatively small for other comparisons. However, no dataset of Hg deposition observations over East Asia is available at present. So we have no better choice. All observations of Hg deposition over East Asia (Table S5 in the supplement) are obtained from literatures. Every site has its own time periods. They range from year 1999 to 2009. If we change the base year of the model simulation, it is still hard to match the time periods of all these observations.

we have replaced the anthropogenic Hg emissions over South Africa by using the AMAP 2010 inventory and assessed this emission update on the simulated results. Detailed analyses have given in Section 2.2.3 in this response document. And corresponding explanations are given in Section 2.4 and 3.3 in the revised manuscript to remind the readers that the anthropogenic emissions over South Africa are flawed.

2.4 Conclusions

Unfortunately the model is unconvincing, the results are as well, therefore it is difficult to be sure that the conclusions drawn here are valid.

Response: In the above responses, we have provided detailed information and explanations to answer the doubts raised by the reviewer concerning our model methodology and results. Besides, following the advices of the reviewer, we have introduced latest advances in Hg chemistry (e.g. Br chemistry, gas-particle partitioning of Hg(II)) into our model to assess their impacts on Hg simulated results presented in this study. Overall, we believe the present modeling results are generally reasonable and comparable to previous Hg modeling studies based on our comprehensive model evaluation, although there still have model uncertainties needing further investigation. The conclusions drawn here are strictly based on the modeling results and analyses presented in this study and we insist that they are generally valid.

References:

- AMAP/UNEP: Technical Background Report for the Global Mercury Assessment 2013, Tech. rep., Arctic Monitoring and Assessment Programme AMAP and United Nations Environment Programme (UNEP) Chemicals Branch, <http://www.unep.org/hazardoussubstances/Mercury/Informationmaterials/ReportsandPublications/tabid/3593/Default.aspx>, 2013.
- Amos, H. M., Jacob, D. J., Holmes, C. D., Fisher, J. A., Wang, Q., Yantosca, R. M., Corbitt, E. S., Galarneau, E., Rutter, A. P., Gustin, M. S., Steffen, A., Schauer, J. J., Graydon, J. A., Louis, V. L. St., Talbot, R. W., Edgerton, E. S., Zhang, Y., and Sunderland, E. M.: Gas-particle partitioning of atmospheric Hg(II) and its effect on global mercury deposition, *Atmos. Chem. Phys.*, 12, 591-603, doi:10.5194/acp-12-591-2012, 2012.
- CAMx: CAMx, user's guide, version 6.1, Environ International Corporation, California, 2014.
- Chen, L., Wang, H. H., Liu, J. F., Tong, Y. D., Ou, L. B., Zhang, W., Hu, D., Chen, C., and Wang,

- X. J.: Intercontinental transport and deposition patterns of atmospheric mercury from anthropogenic emissions, *Atmos. Chem. Phys.*, 14, 10163-10176, doi:10.5194/acp-14-10163-2014, 2014.
- Gencarelli, C. N., De Simone, F., Hedgecock, I. M., Sprovieri, F., and Pirrone, N.: Development and application of a regional-scale atmospheric mercury model based on WRF/Chem: a Mediterranean area investigation, *Environmental Science and Pollution Research*, 21, 4095–4109, 2014.
- Holmes, C. D., D. J. Jacob and X. Yang (2006). Global lifetime of elemental mercury against oxidation by atomic bromine in the free troposphere. *Geophysical Research Letters* 33(20): L20808.
- Holmes, C. D., Jacob, D. J., Corbitt, E. S., Mao, J., Yang, X., Talbot, R., and Slemr, F.: Global atmospheric model for mercury including oxidation by bromine atoms, *Atmos. Chem. Phys.*, 10, 12037-12057, doi:10.5194/acp-10-12037-2010, 2010.
- Horowitz, H. M., Jacob, D. J., Amos, H. M., Streets, D. G., and Sunderland, E. M.: Historical Mercury Releases from Commercial Products: Global Environmental Implications, *Environ. Sci. Technol.*, 48, 10 242–10 250, 2014.
- Jung, G., Hedgecock, I. M., and Pirrone, N.: ECHMERIT V1.0-a new global fully coupled mercury-chemistry and transport model, *Geosci. Model Dev.*, 2, 175-195, 2009.
- Lei, H., Liang, X., Wuebbles, D. J., and Tao, Z.: Model analyses of atmospheric mercury: present air quality and effects of transpacific transport on the United States, *Atmos. Chem. Phys.*, 13, 10807-10825, doi:10.5194/acp-13-10807-2013, 2013.
- Li, J., Z. Wang, H. Akimoto, J. Tang and I. Uno (2009). Modeling of the impacts of China's anthropogenic pollutants on the surface ozone summer maximum on the northern Tibetan Plateau. *Geophysical Research Letters* 36.
- Li, J., Z. Wang, X. Wang, K. Yamaji, M. Takigawa, Y. Kanaya, P. Pochanart, Y. Liu, H. Irie, B. Hu, H. Tanimoto and H. Akimoto (2011). Impacts of aerosols on summertime tropospheric photolysis frequencies and photochemistry over Central Eastern China. *Atmospheric Environment* 45(10): 1817-1829.
- Mason, R.: Mercury emissions from natural processes and their importance in the global mercury cycle, in: *Mercury Fate and Transport in the Global Atmosphere*, edited by: Mason, R., and Pirrone, N., Springer, USA, 173-191, 2009.
- Mason, R. P., Choi, A. L., Fitzgerald, W. F., Hammerschmidt, C. R., Lamborg, C. H., Soerensen, A. L., and Sunderland, E. M.: Mercury biogeochemical cycling in the ocean and policy implications, *Environmental Research*, 119, 101 – 117, 2012.
- Muntean, M., G. Janssens-Maenhout, S. Song, N. E. Selin, J. G. J. Olivier, D. Guizzardi, R. Maas and F. Dentener (2014). Trend analysis from 1970 to 2008 and model evaluation of EDGARv4 global gridded anthropogenic mercury emissions. *Science of The Total Environment* 494–495(0): 337-350.
- Pacyna, E. G., Pacyna, J. M., Steenhuisen, F., and Wilson, S.: Global anthropogenic mercury emission inventory for 2000, *Atmos. Environ.*, 40, 4048-4063, doi:http://dx.doi.org/10.1016/j.atmosenv.2006.03.041, 2006.
- Pirrone, N., and Keating, T.: *Hemispheric Transport of Air Pollution 2010 Part B: Mercury*, United Nations, New York and Geneva, 210 pp., 2010.
- Price, C., Penner, J., and Prather, M.: NO_x from lightning: 1. Global distribution based on

- lightning physics, *J. Geophys. Res.-Atmos.*, 102, 5929-5941, doi:10.1029/96jd03504, 1997.
- Seigneur, C., Karamchandani, P., Lohman, K., Vijayaraghavan, K., and Shia, R. L.: Multiscale modeling of the atmospheric fate and transport of mercury, *J. Geophys. Res.-Atmos.*, 106, 27795-27809, doi:10.1029/2000jd000273, 2001.
- Seigneur, C. and K. Lohman.: Effect of bromine chemistry on the atmospheric mercury cycle. *J. Geophys. Res.*, 113, D23309, doi:10.1029/2008JD010262, 2008.
- Selin, N. E., Jacob, D. J., Park, R. J., Yantosca, R. M., Strode, S., Jaegle, L., and Jaffe, D.: Chemical cycling and deposition of atmospheric mercury: Global constraints from observations, *J. Geophys. Res.-Atmos.*, 112, D02308, doi:10.1029/2006jd007450, 2007.
- Selin, N. E., Jacob, D. J., Yantosca, R. M., Strode, S., Jaegle, L., and Sunderland, E. M.: Global 3-D land-ocean-atmosphere model for mercury: Present-day versus preindustrial cycles and anthropogenic enrichment factors for deposition, *Global Biogeochem. Cy.*, 22, Gb3099, doi:10.1029/2008gb003282, 2008.
- Simone, D. F., C. N. Gencarelli, I. M. Hedgecock and N. Pirrone (2014). Global atmospheric cycle of mercury: a model study on the impact of oxidation mechanisms. *Environmental Science and Pollution Research* 21(6): 4110-4123.
- Soerensen, A. L., Sunderland, E. M., Holmes, C. D., Jacob, D. J., Yantosca, R. M., Skov, H., Christensen, J. H., Strode, S. A., and Mason, R. P.: An improved global model for air-sea exchange of mercury: High concentrations over the North Atlantic, *Environ. Sci. Technol.*, 44, 8574-8580, doi:10.1021/es102032g, 2010.
- Strode, S. A., Jaegle, L., Selin, N. E., Jacob, D. J., Park, R. J., Yantosca, R. M., Mason, R. P., and Slemr, F.: Air-sea exchange in the global mercury cycle, *Global Biogeochem. Cy.*, 21, Gb1017, doi:10.1029/2006gb002766, 2007.
- Temme, C., Blanchard, P., Steffen, A., Banic, C., Beauchamp, S., Poissant, L., Tordon, R., and Wiens, B.: Trend, seasonal and multivariate analysis study of total gaseous mercury data from the Canadian atmospheric mercury measurement network (CAMNet), *Atmos. Environ.*, 41, 5423-5441, doi:10.1016/j.atmosenv.2007.02.021, 2007.
- Wang, L., S. Wang, L. Zhang, Y. Wang, Y. Zhang, C. Nielsen, M. B. McElroy and J. Hao, Source apportionment of atmospheric mercury pollution in China using the GEOS-Chem model. *Environmental Pollution* 190(0): 166-175, 2014.
- Wangberg, I., Munthe, J., Berg, T., Ebinghaus, R., Kock, H. H., Temme, C., Bieber, E., Spain, T. G., and Stolk, A.: Trends in air concentration and deposition of mercury in the coastal environment of the North Sea Area, *Atmos. Environ.*, 41, 2612-2619, doi:10.1016/j.atmosenv.2006.11.024, 2007.
- Zhang, Y., Jaegle, L., van Donkelaar, A., Martin, R. V., Holmes, C. D., Amos, H. M., Wang, Q., Talbot, R., Artz, R., Brooks, S., Luke, W., Holsen, T. M., Felton, D., Miller, E. K., Perry, K. D., Schmeltz, D., Steffen, A., Tordon, R., Weiss-Penzias, P., and Zsolway, R.: Nested-grid simulation of mercury over North America, *Atmos. Chem. Phys.*, 12, 6095-6111, doi:10.5194/acp-12-6095-2012, 2012.

Response to Dr. Robert Marsh:

We thank Dr. Robert Marsh for the reminder.

We have provided information about the means of accessing the model code in our revised manuscript.

We added a section for code availability at the end of the paper. The contents are “Please contact Huansheng Chen (E-mail: chenhuansheng@mail.iap.ac.cn) to obtain the source code of GNAQPMS-Hg”.

The Revised Manuscript

GNAQPMS-Hg v1.0, a global nested atmospheric mercury transport model: Model description, evaluation and application to trans-boundary transport of Chinese anthropogenic emissions

**H. S. Chen¹, Z. F. Wang¹, J. Li¹, X. Tang¹, B. Z. Ge¹, X. L. Wu¹, O. Wild²,
and G. R. Carmichael³**

¹ LAPC, Institute of Atmospheric Physics, Chinese Academy of Sciences, Beijing, China

² Lancaster Environment Centre, Lancaster University, Lancaster, UK

³ Center for Global and Regional Environmental Research (CGRER), University of Iowa, Iowa City, Iowa, USA

Correspondence to: Z. F. Wang (zifawang@mail.iap.ac.cn)

1 **Abstract**

2 Atmospheric mercury (Hg) is a toxic pollutant and can be transported over the whole
3 globe due to its long lifetime in the atmosphere. For the purpose of assessing Hg
4 hemispheric transport and better characterizing regional Hg pollution, a global
5 nested atmospheric Hg transport model (GNAQPMS-Hg) has been developed. In
6 GNAQPMS-Hg, the gas and aqueous phase Hg chemistry representing the
7 transformation among three forms of Hg: elemental mercury (Hg(0)), divalent
8 mercury (Hg(II)), and primary particulate mercury (Hg(P)) are calculated. A detailed
9 description of the model, including mercury emissions, gas and aqueous phase
10 chemistry, and dry and wet deposition is given in this study. Worldwide observations
11 including extensive data in China have been collected for model evaluation.
12 Comparison results show that the model reasonably simulates the global mercury
13 budget and the spatial-temporal variation of surface mercury concentrations and
14 deposition. Overall, model predictions of annual total gaseous mercury (TGM) and
15 wet deposition agree with observations within a factor of two, and within a factor of
16 five for oxidized mercury and dry deposition. The model performs significantly
17 better in North America and Europe than in East Asia. This can probably be
18 attributed to the large uncertainties in emission inventories, coarse model resolution
19 and to the inconsistency between the simulation and observation periods in East Asia.
20 Compared to the global simulation, the nested simulation shows improved skill at
21 capturing the high spatial variability of surface Hg concentrations and deposition
22 over East Asia. In particular, the root mean square error (RMSE) of simulated Hg
23 wet deposition over East Asia is reduced by 24% in the nested simulation. Model
24 sensitivity studies indicate that Chinese primary anthropogenic emissions account
25 for 30% and 62% of surface mercury concentrations and deposition over China,
26 respectively. Along the rim of the western Pacific, the contributions from Chinese
27 sources are 11% and 15.2% over the Korean Peninsula, 10.4% and 8.2% over
28 Southeast Asia, and 5.7% and 5.9% over Japan. But for North America, Europe and
29 West Asia, the contributions from China are all below 5%.

1 Introduction

2 Since the Minamata Event in Japan in the 1960s (Harada, 1995), the toxicity of
3 mercury (Hg) on human health and the environment has caused widespread public
4 concern. Hg is a persistent, bio-accumulated pollutant, and the only heavy metal that
5 can be transported globally in gaseous form (Schroeder and Munthe, 1998). As a
6 result, Hg has been listed as a priority pollutant by many countries and international
7 agencies. After a long struggle, the first global treaty (the Minamata Convention)
8 aimed at reducing Hg emissions and releases, was adopted and signed by 92 countries
9 in 2013 (<http://www.mercuryconvention.org>/~~<http://www.unep.org/>~~). This made an
10 important advance towards joint action to control global Hg pollution and has
11 brought higher requirements for understanding global Hg source-receptor
12 relationships, especially the impacts of high regional emissions (e.g. from China
13 and India) on global Hg levels. However, besides the remaining uncertainties in
14 emission estimates, poor understanding of the chemical transformation of atmospheric
15 mercury has made assessment of long-range transport very challenging (AMAP/UNEP,
16 2013~~Pirrone and Keating, 2010~~).

17 Atmospheric mercury models are powerful tools to assess the fate and transport of
18 mercury in the atmosphere. A number of atmospheric mercury models have been
19 developed to investigate the emissions, transport, chemistry, deposition and
20 source-receptor relationships of Hg at global and regional scales. Global models
21 include the GEOS-Chem model (~~Selin~~Amos et al., 2012; Zhang et al., 2012), the
22 CTM-Hg model (Seigneur et al., 2004), the CAM-Chem-Hg model (Lei et al., 2013),
23 the ECHMERIT model (De Simone~~Jung~~ et al., 2014), the MSCE-Hg-Hem model
24 (Travnikov and Ilyin, 2009), the DEHM model (Christensen et al., 2004), and the
25 GRAHM model (Dastoor and ~~Durnford~~Davignon, 2014). Regional models
26 include the CMAQ-Hg model (~~Bashullock and Brehme~~, 2010), the STEM-Hg
27 model (Pan et al., 2008), ~~and~~ the CAMx-Hg model (ENVIRON, 2011) ~~and the~~
28 WRF-Chem-Hg model (Gencarelli et al., 2014). Application of these models has
29 greatly advanced our understanding of the global Hg cycle. However, several model

1 intercomparison studies (Ryaboshapko et al., 2007; Bullock et al., 2008; Pirrone and
2 Keating, 2010) have found that large uncertainties still exist in Hg models and there is
3 much room for improvement, especially for simulation of reactive gaseous mercury
4 (RGM) and dry deposition.

5 Mercury is released to the atmosphere from both anthropogenic and natural sources.
6 Human activities have increased the amount of mercury cycling through the
7 atmosphere-ocean-terrestrial system by about a factor of three (Selin, 2009), although
8 anthropogenic sources are estimated to account for only 31% of total Hg emissions
9 (Pirrone et al., 2010). China has the world's largest -Hg-production, -consumption
10 and emissions, and suffers the most serious Hg pollution (Jiang et al., 2006), but the
11 impacts of its anthropogenic emissions on global Hg levels are still unclear. Previous
12 modeling studies mainly focused on long-range transport of mercury from Asia.
13 Based on the GEOS-Chem model, about 7-20% of Hg deposition over the United
14 States (US) was found to originate from Asian anthropogenic sources, which was
15 comparable to that from North American sources (Strode et al., 2008; Jaffe and Strode,
16 2008). Another modeling study using the CTM-Hg model with three emission
17 scenarios indicated that Asian anthropogenic emissions accounted for 14–25% of Hg
18 deposition over the US (Seigneur et al., 2004). Travnikov (2005) reported a
19 contribution to Hg deposition from total Asian sources (including both anthropogenic
20 and natural emissions) of 15% over Europe and 33% over the Arctic. Corbitt et al.
21 (2011) further pointed out that Asian emissions are the largest contributors to
22 anthropogenic deposition to all ocean basins and these contributions are expected to
23 further grow in the future. The above studies all treated Asian anthropogenic
24 emissions as a whole, and the effects of anthropogenic emissions from the world's
25 largest single emitter (China) have not been explicitly assessed before. In addition,
26 due to lack of observational data, little model validation has been conducted over East
27 Asia (especially China) in these studies and this leads to -greater uncertainty in
28 the -conclusions. Fu et al. (2012) reviewed previous modeling studies and pointed out
29 that current model simulations tend to underestimate total gaseous mercury (TGM)
30 and total particulate mercury (TPM) concentrations but overestimate reactive gaseous

1 mercury (RGM) concentrations in China. To improve Hg model skill in China, nested
2 simulations with high horizontal resolution might be a good choice. Zhang et al. (2012)
3 demonstrated that a nested-grid model can capture the variation of Hg wet deposition
4 over North America better than a global model. In this study, online nested Hg
5 simulation with flexible horizontal resolution was developed and evaluated.
6 Compared to traditional multi-scale modeling approach (using a global model to
7 provide initial and boundary conditions to a regional model) (Seigneur et al., 2001),
8 online nested method use the same physical and chemical parameterizations in the
9 global and nested domains which could avoid uncertainties induced by different
10 boundary conditions. Compared to offline nested method used in the GEOS-Chem
11 model (Zhang et al., 2012), online nested method can provide boundary conditions
12 with higher time resolution (10 or 5 minutes) from the global domain to the nested
13 domain. Hence, online nested simulation would potentially improve model
14 performance in regional scale.

15 Therefore, a comprehensive evaluation and improvement of Hg model performance
16 in China is needed to effectively reduce the uncertainties in Hg trans-boundary
17 transport and a quantitative assessment of Chinese anthropogenic contribution to
18 global Hg concentration and deposition levels is helpful to determine and fulfill the
19 Hg emission reduction tasks under the Minamata Convention.

20 In this paper, we describe the development of a global nested atmospheric mercury
21 transport model (GNAQPMS-Hg) incorporating the latest available physical and
22 chemical processes essential to the mercury life cycle. The spatial and temporal
23 variability of Hg concentrations and deposition are comprehensively evaluated against
24 available worldwide observations, including extensive data from China. The impact of
25 horizontal resolution ($1^{\circ}\times 1^{\circ}$ in the global domain versus $0.33^{\circ}\times 0.33^{\circ}$ in the nested
26 domain) on model predictions over East Asia is examined. Finally, the trans-boundary
27 transport of Chinese primary anthropogenic Hg emissions is quantified using the
28 model.—

1 **2 Model description and setup**

2 **2.1 General description**

3 The atmospheric physics and chemistry component of GNAQPMS-Hg, with the
4 exception of the mercury module, is based on the Nested Air Quality Prediction
5 Modeling System (NAQPMS) (Wang et al., 2006), developed at the Institute of
6 Atmospheric Physics, Chinese Academy of Sciences. NAQPMS is a 3-D regional
7 Eulerian model which has been rigorously evaluated and widely applied to simulate
8 the chemical evolution and transport of ozone (Li et al., 2007; Tang et al., 2010), the
9 distribution and evolution of aerosol and acid rain over East Asia (Wang et al., 2002;
10 Li et al., 2011; Li et al., 2012) and to provide operational air quality forecasts in mega
11 cities such as Beijing, Shanghai and Guangzhou (Wang et al., 2010; Wu et al., 2012;
12 Wang et al., 2009). GNAQPMS is the global version of NAQPMS and uses the same
13 model framework and physical and chemical parameterization schemes.

14 As a multi-scale model, GNAQPMS can simulate the transportation and formation
15 of primary and secondary pollutants from urban to global scale using an online
16 nesting approach. It includes advection, diffusion and convection processes,
17 gas/aqueous/aerosol chemistry, and modules for dry and wet deposition. The
18 advection process is parameterized based on an accurate mass conservative,
19 peak-preserving algorithm provided by Walcek and Aleksic (1998). The gas phase
20 chemical mechanism is the CBM-Z mechanism (Zaveri and Peters, 1999), including
21 133 reactions for 53 species. The dry deposition module uses the parameterization of
22 Wesely (1989). The wet deposition and aqueous-phase chemistry module is
23 constructed based on a revised version of the RADM mechanism (Chang et al., 1987;
24 Wang et al., 2002; Ge et al., 2014). A mercury module has been developed and
25 coupled into the GNAQPMS model in this study, as described in Sect. 2.2 to 2.4.
26 Hereafter, we call this new model GNAQPMS-Hg. Note that meteorology, emissions,
27 deposition and chemistry are self-consistent between the global and nested domains.

2.2 Mercury chemistry

2.2.1 Basic mechanism

In GNAQPMS-Hg, three forms of mercury are explicitly treated: elemental mercury (Hg(0)), divalent mercury (Hg(II)), and primary particulate mercury (Hg(P)).

Transformations between these three forms include the gas phase oxidation of Hg(0) to Hg(II), the aqueous phase oxidation of Hg(0) to Hg(II), the aqueous phase

reduction of Hg(II) to Hg(0), the aqueous phase equilibria of Hg(II) species and the

aqueous phase adsorption of Hg(II) to PM. ~~Fig. 1~~ depicts the mercury reaction

pathways both in the gas and aqueous phase while the detailed reactions and their rate

constants are summarized in ~~Table 1~~. In line with most global mercury models,

GNAQPMS-Hg does not include ~~bromine (Br) chemistry and~~ dynamic air-surface

exchange during Mercury Depletion Events (MDEs) in Polar regions (Schroeder et al.,

1998) due to lack of fundamental data. ~~Holmes et al. (2010) tested a Br oxidation-~~

~~mechanism in the GEOS-Chem Hg model and found that including atomic Br as the~~

~~sole Hg(0) oxidant produced TGM distributions consistent with most observations.~~

~~However, Lei et al. (2013) demonstrated that adding Br chemistry has little impact on~~

~~overall TGM patterns based on sensitivity experiments using the CAM-Chem Hg-~~

~~model and concluded that at the current level of understanding the O₃-OH oxidation-~~

~~mechanism alone is sufficient for Hg models.~~

In the gas phase, Hg(0) is oxidized to Hg(II) by O₃, OH, hydrogen peroxide (H₂O₂),

hydrogen chloride (HCl) and molecular chlorine (Cl₂). The oxidized products of these

five reactions are assumed to be in the gas phase. According to Lin et al. (2004), OH

and O₃ are the dominant oxidants in the continental troposphere while Cl and Br

dominate Hg(0) oxidation in the marine boundary layer and the upper troposphere. In

the aqueous phase, Hg(0) is oxidized to Hg(II) by dissolved O₃, OH, and Cl₂, and

Hg(II) can be reduced back to Hg(0) via reaction with HO₂ and by the formation of

sulfite complexes. In addition, adsorption of Hg(II) species on atmospheric particulate

matter (PM) is simulated using an adsorption coefficient ($K = 34 \text{ L g}^{-1}$) recommended

by Seigneur et al. (1998).

1 As shown in Table 1~~Table 1~~, the mercury chemistry requires the concentrations of
2 several non-mercury species, among which O₃, OH, HO₂, H₂O₂, SO₂, HCl and PM are
3 simulated online with GNAQPMS-Hg. However, Cl₂ is not explicitly simulated, and a
4 typical vertical profile of Cl₂ concentrations is therefore prescribed. The Cl₂
5 concentrations are specified to be 100 ppt at the surface, 50 ppt aloft at night, 10 ppt
6 during daytime over the oceans, and zero over land (Seigneur et al., 2001).

7 2.2.2 Bromine oxidation

8 In order to test the effect of bromine (Br) oxidation reactions on global Hg
9 concentrations, five Br chemical reactions in the gas phase are added in addition to
10 the O₃-OH oxidation mechanism. The detailed description of the Br chemical
11 reactions and their implementation in the model is shown in Section S1.1 in the
12 supplement. A model sensitivity experiment with additional Br oxidation reactions
13 was conducted and compared to the base case simulation with O₃-OH oxidation
14 mechanism. Fig. S1 in the supplement shows the difference of surface TGM
15 concentrations resulting from introducing Br oxidation reactions. Decrease in TGM
16 concentrations is found in the whole globe. This is because additional Br chemistry
17 transforms more Hg(0) into Hg(II), which subsequently enhances the deposition of
18 Hg(II), leading to the reduction of TGM concentrations. Larger TGM reduction is
19 found in the Northern Hemisphere than in the Southern Hemisphere. In general, the
20 change in TGM concentration is less than 0.2 ng m⁻³ in most areas which indicates
21 that introducing Br chemistry seems to have little impact on overall TGM
22 magnitudes and patterns. These results are similar to Lei et al. (2013) which test the
23 impact of Br chemistry using the CAM-Chem-Hg model. Although adding the Br
24 chemistry does not significantly change the TGM pattern, but it may affect the
25 gaseous Hg partitioning between Hg(0) and Hg(II), and hence may affect the global
26 Hg deposition patterns. More in-depth tests and analysis are needed to address these
27 impacts in the future. In the following sections, we still use the base case simulated
28 results without considering the possible effects of Br chemistry.

2.2.3 Gas-particle partitioning of Hg(II)

Recent studies suggested that gas-particle partitioning of Hg(II) is an important process affected global Hg concentrations and deposition (Amos et al., 2012). To test these effects, an empirical mechanism of gas-particle partitioning of Hg(II) was added to the GNAQPMS-Hg model. The detailed description of this mechanism and its implementation in the model is shown in Section S1.2 in the supplement. A model sensitivity experiment with Hg(II) gas-particle partitioning module was conducted and compared to the base case simulation with all Hg(II) existing in the gas phase. Figs. S2-3 in the supplement show the change fraction of surface TGM concentrations and oxidized Hg concentrations resulting from introducing the Hg(II) gas-particle partitioning mechanism. As expected, TGM concentrations decrease while oxidized Hg concentrations increase in the whole globe. The change fractions of TGM and oxidized Hg concentrations are smaller than 0.1 over the middle latitude of the Northern Hemisphere, and even smaller than 0.05 over China. Considering that the base case simulation has overestimated oxidized Hg concentrations in most areas, introducing the mechanism of gas-particle partitioning of Hg(II) would further increase this model discrepancy. Therefore, we still use the base case simulated results without considering the possible effects of gas-particle partitioning of Hg(II) in the following sections. —

2.3 Mercury deposition

Deposition is the leading removal process of atmospheric mercury, and also a major cause of mercury contamination in soil and water. Studies have shown that both dry and wet removal pathways are equally significant for the total deposition of mercury (Pirrone and Keating, 2010; Lin et al., 2006).

Dry deposition of Hg(0), Hg(II) and Hg(P) is accounted for in the GNAQPMS-Hg model, and simulated with the Wesely (1989) resistance model, which considers the effect of different land cover types and characterizes the diurnal variation of dry deposition velocities. The Henry's Law constant for Hg(0) is set to be 0.11 M atm^{-1}

1 (Lin and Pehkonen, 1999) with a temperature factor of -4970 K (Clever et al., 1985),
2 and the surface reactivity is set to zero. Hg(II) represents HgCl₂ and Hg(OH)₂. Its
3 Henry's Law constant is assumed to be the same as HNO₃ because they have similar
4 solubility (Bullock and Brehme, 2002). Like HNO₃, Hg(II) has a strong tendency to
5 stick to surfaces and its dry deposition occurs readily, so the surface resistance for
6 Hg(II) in the dry deposition scheme is set to zero. The Hg(P) dry deposition velocity
7 is set equal to that for sulfate, similar to that applied in the CMAQ-Hg and
8 STEM-Hg model (Bullock and Brehme, 2002; Pan et al., 2008). [More detailed](#)
9 [description of the dry deposition scheme used in the model is given in Section S2.1](#)
10 [in the supplement.](#) Model intercomparison studies demonstrate that there are still
11 very large uncertainties in Hg dry deposition estimates (Bullock et al., 2008), and
12 this can be ascribed to the wide range of treatments and physical parameters for dry
13 deposition used in different models.

14 The wet deposition of Hg includes in-cloud and below-cloud scavenging. In-cloud
15 scavenging is dependent on cloud and rain water content, species solubility and
16 chemical transformation in the liquid phase, while below-cloud scavenging depends
17 mainly on total rainfall intensity and washout efficiency. Among the three forms of
18 mercury, wet deposition of Hg(0) is minor compared to Hg(II) and Hg(P) due to its
19 low solubility. Therefore, Hg(0) oxidation will enhance total Hg wet deposition. In
20 the GNAQPMS-Hg model, wet deposition of Hg species is calculated through
21 adapting the RADM mechanism. The physical properties (e.g. Henry's Law constant,
22 surface reactivity, molecular diffusivity) used are the same as those in the dry
23 deposition module. [More detailed description of the wet deposition scheme used in](#)
24 [the model is given in Section S2.2 in the supplement.](#) Currently, the uncertainties of
25 Hg wet deposition simulation are mainly from the assumptions made in the cloud
26 scavenging process and the uncertainty associated with the precipitation fields
27 (Seigneur et al., 2001; Lin et al., 2006).

28 **2.4 Mercury emissions**

29 We include anthropogenic emissions, biomass burning emissions, geogenic

1 emissions, land reemission and ocean emissions (including reemission) of Hg in the
2 model. Emissions from artisanal mining and volcanoes are neglected due to lack of
3 fundamental data. The former is estimated to be 400 Mg yr⁻¹, and the latter 90 Mg
4 yr⁻¹, and they account for about 5% and 1% of global total Hg emissions (Pirrone et
5 al., 2010). Note that biomass burning emissions, geogenic emissions, land and ocean
6 emissions are all treated as Hg(0). Global Hg emissions in the model are compared
7 to previous studies in Table 2~~Table-2~~, and their spatial distributions are given in Figs.
8 S41-S63 in the supplement.

9 Anthropogenic emissions in 2000 are derived from the Arctic Monitoring and
10 Assessment Programme (AMAP) inventory (Pacyna et al., 2006; Wilson et al.,
11 2006). This inventory has a horizontal resolution of 0.5°x0.5° and no seasonal
12 variation. Following Selin et al. (2008), we increase the Asian (0~60°N, 65~150°E)
13 Hg(0) emissions in the AMAP inventory by 50% (about 300 Mg yr⁻¹) to account for
14 the regional underestimation identified by Jaffe et al. (2005). The modified inventory
15 has a total emission of 2488 Mg yr⁻¹, with Hg(0), Hg(II) and Hg(P) accounting for
16 63%, 29% and 8% respectively. The major source regions are Asia and Africa,
17 accounting for 59% (1480 Mg yr⁻¹) and 16% (399 Mg yr⁻¹), while Europe and North
18 America contribute only 7% and 6%. China has the largest emissions at country
19 level (about 785 Mg yr⁻¹), contributing 53% and 32% to the Asian and global
20 anthropogenic Hg emissions, respectively. It is noted that the emissions over South
21 Africa in this inventory were reported to be flawed (AMAP/UNEP, 2008) and much
22 higher than reality. The effects of these flawed emissions on the simulated results
23 were assessed in Section S3 in the supplement.

24 Biomass burning emissions are specified by mapping an annual mean value of 675
25 Mg yr⁻¹ (Friedli et al., 2009) to the spatial and temporal distribution of CO biomass
26 burning emissions from the IPCC-AR5 (Intergovernmental Panel on Climate Change
27 Fifth Assessment Report) emissions inventory (Lamarque et al., 2010). The regional
28 and monthly emission amounts are prescribed based on Friedli et al. (2009). A
29 similar method has been used by Jung et al. (2009).

30 The geogenic emissions here represent mobilization of Hg by degassing from

1 geological reservoirs. Following Selin et al. (2007), we consider a geogenic source
2 of 500 Mg yr⁻¹ distributed according to the locations of Hg mines (Frank, 1999) as an
3 indicator of Hg deposits. No temporal variation is applied to the geogenic emissions.

4 Land and ocean emissions are not dynamically calculated in the model due to the
5 large uncertainties associated with current parameterizations. Consistent with several
6 previous studies (Selin et al., 2007; Seigneur et al., 2001), the global annual land
7 reemission of Hg is assumed to be 1500 Mg yr⁻¹. The biogenic CO emissions from
8 the Global Emission Initiative (GEIA) inventory (Guenther et al., 2006) are used as
9 spatial and temporal surrogates to map the land reemission. Regional emission totals
10 from different latitude zones and land uses are prescribed based on Mason (2009).

11 Ocean emissions in our model are specified as 5000 Mg yr⁻¹ (including
12 reemission), close to the estimates of Selin et al. (2008). Similarly, ocean emissions
13 are mapped according to the distribution of ocean biogenic CO emissions from the
14 Precursors of Ozone and their Effects in the Troposphere (POET) inventory (Granier
15 et al., 2005). Additionally, ocean emissions are adjusted to reflect several
16 distribution characteristics: 1) ocean emissions are high in summer but low in winter
17 (Strode et al., 2007), 2) ocean emissions are largest in the Tropics and downwind of
18 industrial regions (Strode et al., 2007; Soerensen et al., 2010b), and 3) ocean
19 emissions are large at mid and high latitudes in the Southern Hemisphere due to high
20 wind speeds (Selin et al., 2008).

21 **2.5 Model setup**

22 Two nested domains covering the whole globe and East Asia are configured in this
23 study. The horizontal resolutions are 1°x1° and 0.33°x0.33°, respectively. Vertically,
24 the model uses 20 terrain-following layers from the surface to 20 km a.s.l., with a
25 decreasing resolution with height. Roughly, the lowest 14-18 layers are in the
26 troposphere and the remaining layers are in the stratosphere. The time step in the
27 model calculation is 600 s. The input/output frequency is 6h in the global domain but
28 3h in the nested domain. The meteorological fields are provided by the global
29 version of the Weather Research and Forecasting (WRF) model. The atmospheric

1 lifetime of Hg(0) is 0.5-2 year (Schroeder and Munthe, 1998), and so to ensure
2 mixing through the global troposphere and approach steady-state, we conduct the
3 simulation for a 4-year period, with the first 3 years used for initialization and the
4 last year (2001) used for analyses.

5 Emissions of reactive gases and aerosols used in this study are from several
6 databases: 1) the IPCC-AR5 anthropogenic and biomass burning emissions for 2000
7 (Lamarque et al., 2010); 2) the GEIA biogenic emissions for 2000 (Guenther et al.,
8 2006) and lightning emissions of nitric oxide (NO_x) for 1983–1990 (Price et al.,
9 1997); 3) the POET ocean emissions of volatile organic compounds (VOCs) for
10 2000 (Granier et al., 2005); 4) the soil NO_x emissions for 2001 from Yan et al. (2005).
11 All emissions are interpolated and remapped to match the model grids of the global
12 and nested domains.

13 The initial and top boundary conditions for O₃, NO_x, and CO are taken from a
14 global chemical transport model (MOZART-V2.4) with 2.8° resolution (Horowitz et
15 al., 2003). ~~Initial surface concentrations for Hg(0) of 1.6 ng m⁻³ in the Northern
16 Hemisphere and 1.2 ng m⁻³ in the Southern Hemisphere are prescribed and these
17 decrease gradually with elevation (Lindberg et al., 2007).~~

18 Two model simulations, with and without Chinese primary anthropogenic Hg
19 emissions, are carried out in this study. The differences between the two simulations
20 are attributed to the influence of Chinese primary anthropogenic Hg emissions.

21 **3 Model evaluation**

22 **3.1 Observational data**

23 Compared to reactive gases and aerosols, atmospheric Hg measurements are still
24 quite sparse. Routine monitoring networks for atmospheric Hg concentrations and
25 deposition have only been established in Europe and North America. Lack of Hg
26 observational data is a great restriction against advancing our understanding of
27 global Hg cycling and improving our skill in modeling. There is an urgent need to
28 establish a coordinated global Hg monitoring network for current Hg study

1 (Sprovieri et al., 2010; Keeler et al., 2009).

2 The observational dataset in this study is based partly on the database shared by the
3 GEOS-Chem Hg modeling group (public access at [https://github.com/noelleselin/](https://github.com/noelleselin/HgBenchmark)
4 HgBenchmark; Selin et al., 2007; Selin et al., 2008; Holmes et al., 2010). This is
5 supplemented with scattered Hg observations across East Asia collected from the
6 literature. The observations used in this study are summarized as follows: 1)
7 long-term TGM/GEM (gaseous elemental mercury) measurements at 51 land sites,
8 with 49 in the Northern Hemisphere and 2 in the Southern Hemisphere; 2) long-term
9 RGM/TPM measurements at 26 land sites, all in the Northern Hemisphere; 3)
10 short-term Hg species measurements from 6 ship cruises; 4) wet deposition
11 measurements from the MDN (the Mercury Deposition Network in North America,
12 <http://nadp.sws.uiuc.edu/nadpdata/mdnalldata.asp>) and EMEP (the European
13 Monitoring and Evaluation Programme, <http://www.nilu.no/projects/ccc/emepdata.html>) monitoring networks, with 51 and 8
14 sites respectively; 5) dry and wet deposition measurements at 19 sites in East Asia.
15
16 Further information about the measurement sites and data sources is given in Tables
17 ~~S21-S54~~ in the supplement. It should be noted that the time periods of the
18 measurements do not all match with those of the simulation, and this difference may
19 partially explain any model–observation discrepancies. The influence of the mismatch
20 of time periods when comparing the simulated results with the observations was
21 qualitatively analyzed and shown in Section S4.1 in the supplement.

22 3.2 Global mercury budget

23 ~~Fig. 2~~ Fig. 2 gives the global mercury budget in GNAQPMS-Hg, including the
24 cycling among atmosphere, ocean and land. The total atmospheric burden of Hg is
25 ~~55468679~~ Mg, with Hg(0), Hg(II), and Hg(P) contributing ~~9092%~~, ~~97%~~ and 1%,
26 respectively. Therefore, mercury in the atmosphere exists mainly as Hg(0). Total
27 emissions and deposition of Hg are 5163 Mg yr⁻¹ and 2866 Mg yr⁻¹ over land (a net
28 source), and are 5000 Mg yr⁻¹ and 7297 Mg yr⁻¹ over ocean (a net sink), indicating
29 that Hg is transported from land to ocean. For total deposition of Hg species, Hg(0)

1 and Hg(II)/Hg(P) account for 38% and 62% over the earth's surface. Over land,
2 deposition of Hg(II)/Hg(P) is more prominent than that of Hg(0), while they are both
3 important over the ocean. Our results for total Hg deposition over ocean and
4 Hg(II)/Hg(P) deposition over land are very close to that of GEOS-Chem (Selin et al.,
5 2008). However, Hg(0) deposition over land derived from GNAQPMS-Hg is much
6 smaller. This may be due to the lower reactivity coefficient used in the dry
7 deposition module in GNAQPMS-Hg (zero in GNAQPMS-Hg but 10^{-5} in
8 GEOS-Chem), which produces a lower dry deposition velocity for Hg(0).

9 ~~Table 2~~ [Table 2](#) compares the GNAQPMS-Hg TGM budget and lifetime to those
10 from previous modeling studies. The TGM sources, sinks, burden and lifetime
11 estimated from GNAQPMS-Hg are all in the range determined by previous studies.
12 Taking the TGM lifetime as an example, the reported range is ~~0.5-1.7~~ [0.5-1.7](#) ~~±0.4~~ years
13 and it is ~~0.854~~ [0.854](#) years for GNAQPMS-Hg. In addition, similar to the results of
14 GEOS-Chem (Selin et al., 2007) ~~and CAM-Chem-Hg (Lei et al., 2013)~~, Hg dry
15 deposition in GNAQPMS-Hg dominates globally over wet deposition. Dry and wet
16 deposition account for 78% and 22%, respectively.

17 3.3 Total gaseous mercury (TGM)

18 As shown in ~~Fig. 3~~ [Fig. 3](#), the main characteristics of the spatial distribution of TGM
19 are captured well by the model. High surface TGM concentrations are found in or
20 downwind of areas with intensive mercury-related mining (e.g. Western USA;
21 ~~Southern Africa~~) and rapid industrialization (e.g. East Asia). In particular, TGM
22 concentrations even exceed 3 ng m^{-3} in eastern China. Both model simulation and
23 observations show a significant surface interhemispheric gradient in TGM (~~Fig. 3~~ [Fig.](#)
24 ~~3~~ and [Fig. 4](#) ~~Fig. 4~~). Based on background observations, Lindberg et al. (2007)
25 reported that mean Hg(0) concentrations were $1.5\text{--}1.7 \text{ ng m}^{-3}$ in the Northern
26 Hemisphere and $1.1\text{--}1.7 \text{ ng m}^{-3}$ in the Southern Hemisphere. Lamborg et al. (2002)
27 also estimated the range of north-south interhemispheric TGM concentration ratios
28 for surface air as 1.2–1.8. Our model results share a general similarity with these
29 studies. In GNAQPMS-Hg, surface mean TGM concentrations in the Northern and

1 Southern Hemisphere are 1.56 and 1.23 ng m⁻³, and the derived interhemispheric
2 ratio is 1.27. However, it should be noted that GNAQPMS-Hg is systematically
3 biased low relative to cruise observations in the Northern Hemisphere, which leads
4 to underestimation of the TGM interhemispheric ratio compared with the range
5 (1.49±0.12) reported by Temme et al. (2003) based on observations from several
6 Atlantic cruises. This disagreement was also found by several previous modeling
7 studies (Seigneur et al., 2004; Selin et al., 2007), and can be attribute to the inability
8 of current models to reproduce the air-sea exchange of Hg reasonably (Soerensen et
9 al., 2010a). More specifically, this discrepancy is due to upwelling mercury from the
10 sub-surface ocean, possibly reflecting the legacy of past anthropogenic emissions
11 (Holmes et al., 2010), and has been partially demonstrated by Soerensen et al. (2012).

12 In general, the simulated TGM concentrations match observations within a factor of
13 two (Fig. 10~~Fig. 10~~). The correlation coefficient (R) and normalized mean bias
14 (NMB) between model results and observations from 51 land sites are 0.7 and -18%,
15 respectively (Table 3~~Table 3~~).

16 Fig. 5~~Fig. 5~~ illustrates the mean seasonal variations of surface TGM
17 concentrations in North America, Europe, East Asia, the Arctic, the Antarctic
18 (Neumayer) and South Africa (Cape Point). In northern mid-latitudes, TGM
19 concentrations are high in winter but low in summer. This seasonality can be
20 reproduced well by GNAQPMS-Hg. The summer low is caused by high OH
21 concentrations and frequent precipitation (Bergan and Rodhe, 2001). Compared with
22 observations, the simulated TGM monthly variations are stronger in North America
23 but weaker in East Asia. The site by site comparisons in East Asia are shown in Fig.
24 S9 in the supplement. We can see that nested simulation can well improve model
25 performance in simulated TGM monthly variation in East Asia. At Arctic and
26 Antarctic sites, TGM shows a spring minimum driven by MDEs and a summer
27 maximum driven by reemission from the snowpack (Steffen et al., 2005). The
28 summer maximum is captured by GNAQPMS-Hg because high reemission in polar
29 summer has been taken into account in our land reemission inventories. However,
30 due to missing halogen chemistry, the model fails to reproduce the spring minimum.

1 At Cape Point, both observed and simulated TGM show little seasonal variation.
2 However, simulated monthly TGM concentrations are systematically biased high
3 (NMB is 87%), which can be attributed to ~~an overestimation~~ the flawed
4 anthropogenic emissions in the AMAP emission inventories ~~over~~ South Africa
5 (AMAP/UNEP, 2008~~Lei et al., 2013~~). By updating the anthropogenic emissions over
6 South Africa, the simulated TGM concentrations at Cape Point decrease from 1.77
7 ng m⁻³ to 1.23 ng m⁻³, more close to the observed values (See Section S3 in the
8 supplement).

9 Additional evaluation and analyses of simulated diurnal and vertical variation of
10 TGM concentrations are given in Section S4.2 in the supplement.

11 3.4 Oxidized mercury

12 ~~Fig. 3~~ Fig. 3 also shows the global distribution of oxidized mercury (defined as the
13 sum of RGM+TPM in the observations and Hg(II)+Hg(P) in the model). Similar to
14 TGM, a pronounced north-south interhemispheric gradient is found for surface
15 concentrations of oxidized mercury, which is consistent with the global distribution
16 of emissions. Both model simulation and observations indicate that oxidized
17 mercury concentrations are much higher in East Asia than North America and
18 Europe. Compared to scarce available observations, oxidized mercury concentrations
19 are overestimated by GNAQPMS-Hg in most parts of the world (except East Asia).
20 This discrepancy may partially be attributed to excessive oxidation of Hg(0) by
21 relatively high concentrations of OH and O₃ (especially over the ocean) and
22 uncertainties concerning Hg chemical speciation in emission inventories. The
23 simulated tropospheric mean OH concentration is 1.41x10⁶ molec cm⁻³. This is at the
24 high end of the concentration range (0.65-1.56x10⁶ molec cm⁻³) summarized by
25 Lawrence et al. (2001) and is about 27% higher than the ensemble mean
26 (11.1±1.8x10⁵ molec cm⁻³) of the Atmospheric Chemistry and Climate Model
27 Intercomparison Project (ACCMIP) models (Voulgarakis et al., 2013). The simulated
28 mean surface O₃ in the North Pacific and North Atlantic is overestimated by 27%
29 and 34% compared to observations from the WDCGG (World Data Centre for

1 Greenhouse Gases) network, although concentrations over land are reproduced
2 relatively well (see Figs. S104-S115 in the supplement). Besides, uncertainties of Hg
3 chemistry (e.g. gas-particle partitioning of RGM, in-plume reduction of RGM) and
4 deposition processes in the present model might also contribute to this discrepancy.
5 Overall, the simulated oxidized mercury concentrations agree with observations
6 within a factor of five (Fig. 10). The statistical indicators, R and NMB,
7 calculated from 26 land sites are 0.53 and 3% (Table 3), respectively.

8 **3.5 Wet deposition**

9 Wet deposition is mainly determined by the distribution of precipitation and Hg
10 concentrations. Fig. 6 and Fig. 7 evaluate the simulated annual Hg wet
11 deposition and accumulated precipitation over North America, Europe and East Asia.
12 In general, GNAQPMS-Hg reproduces the spatial patterns of Hg wet deposition
13 relatively well.

14 Over North America, the maximum wet deposition occurs in the southeast,
15 corresponding to high OH concentrations and frequent precipitation there, while less
16 wet deposition occurs in the west and north, where there is much less precipitation.
17 GNAQPMS-Hg predicts the magnitude of mean wet deposition within 5% and
18 shows a good spatial correlation ($R=0.76$) (Table 3). These results are similar
19 to those of GEOS-Chem (Selin et al., 2007). However, it should be also noted that
20 precipitation in the southeast is slightly overestimated by the model.

21 Over Europe, model performance for wet deposition and precipitation are better
22 than over North America and East Asia. High spatial correlation between the
23 simulated and observed results are found for both wet deposition ($R=0.78$) and
24 precipitation ($R=0.86$), and the NMBs are both less than 5% (Table 3).

25 Over East Asia, Hg wet deposition is not only related to the precipitation pattern
26 but also the local Hg emissions, especially in the southwest and Jilin province of
27 China, and in Central Japan. Model performance for wet deposition over East Asia is
28 poorer than over Europe and North America. Although the spatial distribution and
29 magnitude of precipitation over East Asia are seemingly well reproduced ($R=0.64$

1 and NMB=-6%), a large underestimation (NMB=-61%) of wet deposition is found
2 here. Specifically, this is because the model fails to capture the high wet deposition
3 at certain sites. For example, the observed wet deposition over Shanghai and
4 Changchun are 251 and 108 $\mu\text{g m}^{-2}$ while the corresponding simulated values are
5 only 25 and 13 $\mu\text{g m}^{-2}$. This suggests that it is hard for models with coarse horizontal
6 resolution to characterize the high local mercury pollution in China. The difference
7 between the simulated and observed time periods and uncertainties in the emission
8 inventories may also contribute to these discrepancies.

9 ~~Fig. 8~~ ~~Fig. 8~~ further compares the simulated seasonal cycle of wet deposition with
10 measurements at MDN sites over North America and EMEP sites over Europe. No
11 monthly wet deposition observations are available over East Asia. Wet deposition
12 and precipitation share similar monthly variations, with high values in summer and
13 autumn and low values in winter, as shown by both observations and simulation. In
14 summer and autumn, the variation in wet deposition and precipitation among sites is
15 larger than for other seasons, and this is evident from the greater variability in ~~Fig.~~
16 ~~8~~ ~~Fig. 8~~. GNAQPMS-Hg tends to overestimate wet deposition and precipitation in
17 July and August over North America.

18 3.6 Dry deposition

19 Due to limited observations, only Hg dry deposition over East Asia is evaluated in
20 this study. It should be noted that data (Table S5 in the supplement) used to evaluate
21 model simulation of dry deposition is not directly measured, but is inferred or
22 estimated based on measurements of total Hg in through fall and rainwater, wet
23 deposition and atmospheric concentrations. Associated with local Hg emissions,
24 high dry deposition mainly occurs over central eastern China and central Japan (~~Fig.~~
25 ~~9~~ ~~Fig. 9~~). The modeled dry deposition has a good spatial correlation with
26 observations ($r=0.81$), but there is a substantial negative bias (NMB=-42%, ~~Table~~
27 ~~3~~ ~~Table 3~~). In general, the simulated dry deposition agrees with observations within a
28 factor of five (~~Fig. 10~~ ~~Fig. 10~~). Over Japan, the model results are biased high by a
29 factor of 2-5, which may be caused by overestimation of Hg(II) and Hg(P) emissions

1 [and missing model mechanism to deal with fast in-plume reduction of Hg\(II\)](#)
2 [\(Vijayaraghavan et al., 2008; Amos et al., 2012; Zhang et al., 2012\)](#). Taking Tokyo as
3 an example, observed Hg(P) is only 98 pg m⁻³ while the simulated value is as high as
4 648 pg m⁻³. Modeling studies conducted by Pan et al. (2008) using the STEM-Hg
5 model also found large overestimation in dry deposition over Japan. Conversely, the
6 model results are biased low by a factor of 2-5 over China, which indicates probable
7 underestimation of Chinese Hg emissions.

8 **3.7 Model performance summary and comparison**

9 In this section, we summarize the statistical performance of GNAQPMS-Hg for
10 TGM, oxidized mercury, and wet and dry deposition, compare the model
11 performance over East Asia, North America and Europe, and assess the effects of
12 horizontal resolution on model predictions over East Asia. As shown in [Fig. 10](#)
13 ~~10~~, the simulated TGM and wet deposition are within a factor of two of the
14 corresponding observations and within a factor of five for oxidized mercury and dry
15 deposition. The statistical performance of GNAQPMS-Hg is comparable with that of
16 other state-of-the-art Hg models (Bullock et al., 2008; Ryaboshapko et al., 2007;
17 Pirrone and Keating, 2010).

18 **3.7.1 East Asia versus North America and Europe**

19 As illustrated in [Table 3](#)~~Table-3~~, the model statistical performance for all Hg
20 parameters in North America and Europe is better than in East Asia. For example,
21 the RMSEs between simulated and observed TGM over North America and Europe
22 are 0.58 and 0.17 ng m⁻³ but up to 3.61 ng m⁻³ over East Asia. The poor model
23 performance over East Asia is probably caused by the following reasons. Firstly,
24 there are differences between simulated and observed data periods. Hg
25 measurements over East Asia (especially China) are mainly taken from recent years,
26 and the observed values are higher than in year 2001, which may lead to model
27 underestimation. [Hg anthropogenic emissions in China had increased by 164%](#)
28 [during 1992-2007 \(Liang et al., 2013\) is an evidence.](#) Secondly, there is a much

1 | higher spatial variation ratio (SVR, see [Table 3Table-3](#)) for Hg parameters in East
2 | Asia than North America and Europe. This implies that there are very intense spatial
3 | variations in [surface](#) Hg concentrations and deposition over East Asia which cannot
4 | be resolved at the coarse horizontal resolution used in global models [\(see Section](#)
5 | [3.7.2\)](#). Thirdly, there are large uncertainties in emission inventories over East Asia.
6 | Large underestimations in Hg anthropogenic emissions over East Asia have been
7 | demonstrated in several previous studies (Jaffe et al., 2005; Pan et al., 2007; Friedli
8 | et al., 2004; [Song et al., 2015](#)). This is consistent with the simulated results in this
9 | study. [Except the above factors, missing of some chemical and physical processes](#)
10 | [\(e.g. gas-particle partitioning of Hg\(II\), in-plume reduction of Hg\(II\), dynamic land](#)
11 | [reemission\) in the present model might also contribute to the poor model](#)
12 | [performance over East Asia.](#)

13 | **3.7.2 Global versus nested simulations**

14 | In order to assess the impact of resolution on model predictions, an online nested
15 | simulation with higher resolution ($0.33^{\circ}\times 0.33^{\circ}$) over East Asia was conducted and
16 | compared to the global simulation with lower resolution ($1^{\circ}\times 1^{\circ}$). Emissions,
17 | meteorology, deposition and chemistry are self-consistent between the global and
18 | nested domains. The nested simulation uses higher resolution model inputs (e.g.
19 | topography, meteorology, emissions) and thus has the potential to better resolve high
20 | spatial variability of Hg concentrations and deposition in regional and local scales.

21 | [Fig. 7Fig-7](#) and [Fig. 9Fig-9](#) compare the spatial distributions of simulated annual
22 | mercury wet deposition, accumulated precipitation and dry deposition over East Asia
23 | between the global and nested simulations. Although the global and nested
24 | simulations predict similar large scale patterns for Hg deposition, the nested
25 | simulation resolves many fine features which are lost in the global simulation by
26 | horizontal averaging. Firstly, in the nested domain, high deposition fluxes become
27 | more concentrated in regions with large emissions or precipitation resulting in higher
28 | spatial variability in deposition. Secondly, the nested simulation reveals elevated wet
29 | deposition in southwest China due to frequent orographic and convective

1 precipitation. Finally, the nested simulation shows a more detailed land/ocean
2 contrast in deposition over coastal regions. For example, over the coastal regions of
3 southeast China and Japan, wet deposition increases due to scavenging of local
4 emissions and enhanced precipitation ([Fig. 7](#)) while dry deposition decreases
5 associated with the lower dry deposition velocity of Hg(0) over land than over ocean
6 ([Fig. 9](#)). Our results are similar to those of Zhang et al. (2012) who conducted
7 a nested simulation of Hg over North America using the GEOS-Chem model. [More](#)
8 [comparisons about the differences of dry and wet deposition and Hg budgets over](#)
9 [East Asia between the two simulations are given in Fig. S14 and Table S6 in the](#)
10 [supplement.](#)

11 [Fig. 11](#) and [Table 3](#) further quantitatively compare the model
12 performance over East Asia between the global and nested domains. In the Taylor
13 diagram (Taylor, 2001), the position of each circle (or square) quantifies how closely
14 the simulated results match observations. We can see that the simulated precipitation,
15 oxidized Hg, wet and dry deposition agree better with observations in the nested
16 domain than in the global domain ([Fig. 11](#)). The largest improvement is found
17 in the simulated wet deposition. Specifically, the statistical parameter R for
18 simulated wet deposition increases from 0.36 to 0.78, the NMB decreases from -61%
19 to -28%, and the RMSE decreases by 24% (from 60.1 to 45.5 $\mu\text{g m}^{-2} \text{yr}^{-1}$) ([Table](#)
20 [3](#)). But for TGM, oxidized Hg and dry deposition, the statistical parameters
21 do not change significantly. For example, the RMSEs of simulated oxidized Hg and
22 dry deposition decrease by 7% and 2% respectively, but increase by 7% for
23 simulated TGM.

24 **4 Impacts of Chinese primary anthropogenic sources on global Hg** 25 **levels**

26 [Fig. 12](#) shows the contribution of Chinese primary anthropogenic sources (not
27 including reemission) to annual mercury surface concentrations and total deposition
28 in the Northern Hemisphere, and [Fig. 13](#) gives the corresponding mean

1 | percentage contributions over different world regions (defined in Fig. S156 in the
2 | supplement), as derived from a sensitivity simulation with Chinese anthropogenic
3 | emissions shut off. In general, the largest percentage contribution is found in China
4 | itself, followed by neighbouring regions like the Korean Peninsula, Southeast Asia,
5 | Mongolia and Japan, but they are relatively small in other regions. Specifically,
6 | domestic anthropogenic emissions contribute on average 0.6 ng m^{-3} (ranging from
7 | below 0.1 to above 3.0) to surface Hg concentrations and 18.4 ug m^{-2} (ranging from
8 | below 2.0 to above 50.0) to total deposition in China. They account for about 30%
9 | and 62% on a national basis, respectively. The domestic contribution to deposition
10 | consists mainly of the deposition of directly emitted Hg(II) and Hg(P) near sources
11 | and deposition of Hg(II) formed by oxidation of Chinese Hg(0). For neighboring
12 | regions, the Chinese anthropogenic contributions to surface Hg concentrations and
13 | deposition are also large. For example, the percentage contributions are 11% ($0.2\text{-}0.6$
14 | ng m^{-3}) and 15.2% ($8\text{-}20 \text{ ug m}^{-2}$) over the Korean Peninsula, 10.4% ($0.1\text{-}0.6 \text{ ng m}^{-3}$)
15 | and 8.2% ($1\text{-}12 \text{ ug m}^{-2}$) over Southeast Asia, and 5.7% ($0.1\text{-}0.4 \text{ ng m}^{-3}$) and 5.9%
16 | ($2\text{-}15 \text{ ug m}^{-2}$) over Japan. For regions far away from China, the percentage
17 | contributions are small. They are 4.2% ($0.06\text{-}0.1 \text{ ng m}^{-3}$) and 4.8% ($0.5\text{-}4 \text{ ug m}^{-2}$)
18 | over North America, and 3.5% (below 0.08 ng m^{-3}) and 3.0% (below 2.0 ug m^{-2})
19 | over Europe. The percentage contributions over North America determined from our
20 | simulation are comparable with the modeling study of Lei et al. (2013). They
21 | estimated that around 7% of TGM concentrations and 9% of total Hg deposition in
22 | the United States resulted from transpacific transport of Asian anthropogenic
23 | emissions. Given that about 53% of Asian anthropogenic Hg emissions are from
24 | China, it is reasonable that our estimated contributions are a little smaller than those
25 | reported by Lei et al. (2013).

26 | Finally, there are another two issues which need to be addressed. Firstly, the above
27 | analysis mainly focuses on regional average contributions. However, the percentage
28 | contributions vary geographically inside the region. As shown in Fig. 12~~Fig. 12~~,
29 | contributions of domestic anthropogenic emissions to total deposition in Central
30 | Eastern China can exceed 40 ug m^{-2} , but they are below 5 ug m^{-2} in Western China.

1 Similarly, previous studies have found that Asia emissions make a much larger
2 contribution to Hg deposition in the Western USA than in the Eastern USA (Seigneur
3 et al., 2004; Strode et al., 2008). Secondly, the contributions from reemission of
4 previously deposited anthropogenic Hg (treated as natural land or ocean reemission
5 in GNAQPMS-Hg) are not taken into account in this study. Of the natural emissions,
6 only one-third is considered not to be influenced by anthropogenic activities at all
7 (Jung et al., 2009). In addition, according to the modeling study of Selin et al. (2008),
8 31% (including 22% primary and 9% recycled) of the deposition over USA is from
9 anthropogenic emissions outside of North America. When considering reemission of
10 previously deposited anthropogenic Hg, this suggests that the foreign anthropogenic
11 contribution would increase by about 42% (from 22% to 31%). If we apply the same
12 scaling factor to our attribution results, then the estimated Chinese anthropogenic
13 contributions to Hg deposition over North America would increase from 4.8% to
14 6.8%. Therefore, it is also important to consider the reemission of previously
15 deposited anthropogenic Hg.

16 **5 Conclusions**

17 A global nested atmospheric mercury transport model including Hg emissions,
18 chemical transformation and deposition is introduced in this study. The treatment of
19 Hg chemistry employs the O_3 -OH oxidation and SO_3^{2-} - HO_2 reduction mechanisms.
20 The gas phase reactions of Hg are added to the CBM-Z mechanism, while the
21 aqueous phase reactions and wet deposition of Hg are calculated through adapting
22 the RADM mechanism. The Wesely (1989) resistance model is used to deal with Hg
23 dry deposition. The same meteorological fields, emissions, chemical and physical
24 parameterizations are used in the global and nested domains.

25 The GNAQPMS-Hg model has a global mercury source of 10163 Mg yr^{-1} ,
26 including 2488 Mg yr^{-1} primary anthropogenic emissions, 675 Mg yr^{-1} biomass
27 burning emissions, 2000 Mg yr^{-1} land emissions (of which 75% is reemission), and
28 5000 Mg yr^{-1} from the ocean. Dynamic bidirectional air-surface exchange of Hg is

1 not included in the model. Instead, we simply apply static net emission fluxes to
2 account for natural sources (including reemission) of Hg, with total emission
3 amounts determined based on published estimates.

4 Based on existing routine monitoring networks (e.g. MDN, EMEP) and the
5 published literature, global observations including surface Hg concentrations and
6 deposition are collected for model evaluation. Compared with previous studies,
7 many more observations over East Asia (especially China) are included in our
8 dataset. Model evaluation shows that the spatial distribution and seasonal cycle of
9 Hg concentrations and deposition can be reproduced reasonably well by
10 GNAQPMS-Hg. Overall, the simulated annual TGM and wet deposition match
11 observations within a factor of two, and within a factor of five for oxidized mercury
12 and dry deposition. This performance is comparable with other state-of-the-art Hg
13 models. Some model deficiencies have also been identified. GNAQPMS-Hg is
14 systematically biased low relative to cruise observations in the Northern Hemisphere,
15 due to poor representation of the air-sea exchange mechanism for Hg.
16 GNAQPMS-Hg overestimates oxidized mercury concentrations in most parts of the
17 world which may partially be caused by excessive oxidation of Hg(0) by relatively
18 high concentrations of OH and O₃ and uncertainties associated with Hg chemical
19 speciation in emission inventories. The model performs significantly better in North
20 America and Europe than in East Asia. This can probably be attributed to the large
21 uncertainties in emission inventories, coarse model resolution and inconsistency
22 between the simulation and observation periods in East Asia. An online nested
23 simulation with higher resolution (0.33°x0.33°) over East Asia was conducted to
24 examine the impact of horizontal resolution on model predictions. Relative to the
25 global simulation, the nested simulation can better resolve high spatial variability of
26 Hg concentrations and deposition over East Asia, can better capture features such as
27 higher wet deposition due to orographic and convective precipitation, and land/ocean
28 contrast. Statistically, the RMSE of simulated wet deposition over East Asia is
29 reduced by 24% in the nested simulation.

30 To quantify the impacts of Chinese anthropogenic sources on global Hg levels, a

1 model sensitivity simulation was conducted with Chinese anthropogenic emissions
2 shut off. The results show that these sources contribute 30% and 62% of surface
3 mercury concentrations and deposition over China. Outside of China, the largest
4 percentage contributions of 11% and 15.2% are found in the Korean Peninsula,
5 following by Southeast Asia (10.4% and 8.2%), Mongolia (6.1% and 8.6%), and
6 Japan (5.7% and 5.9%). For regions far away from China, the percentage
7 contributions are relatively small (e.g. 4.2% and 4.8% over North America; 3.5% and
8 3.0% over Europe).

9 To perfect the model, future improvements will be focused on the following
10 aspects: 1) employing dynamic parameterizations for bidirectional air-surface (sea
11 and land) exchange of Hg (Selin et al., 2008; Bash, 2010; Strode et al., 2007) to
12 better reflect natural emissions (including reemission), 2) including [fast in-plume](#)
13 [reduction of Hg\(II\) halogen chemistry](#) to [better](#) characterize [MDEs in the Polar](#)
14 [regions](#) [Hg\(II\) distribution near large point sources](#) ([Amos Holmes](#) et al., 2012⁰), and
15 3) reducing uncertainties in the anthropogenic Hg emission inventory, especially the
16 Hg speciation profile. Finally, establishment of routine Hg monitoring networks
17 would be also very helpful for enhancing and improving modeling studies in East
18 Asia.

19 [Code availability](#)

20 [Please contact Huansheng Chen \(E-mail: chenhuansheng@mail.iap.ac.cn\) to obtain the](#)
21 [source code of GNAQPMS-Hg.](#)

22 **Acknowledgments**

23 This work is funded by the National Natural Science Foundation of China (NO.
24 41405119), the National Basic Research Program of China (2010CB951800) and the
25 CAS Strategic Priority Research Program (XDB05030200 and XDB05030101). We
26 thank the GEOS-Chem Hg modeling group for sharing observational data of Hg.

1 **References**

- 2 [AMAP/UNEP: Technical Background Report to the Global Atmospheric Mercury Assessment,](http://www.unep.org/hazardoussubstances/)
3 [Tech. rep., Arctic Monitoring and Assessment Programme / UNEP Chemicals Branch, http:](http://www.unep.org/hazardoussubstances/)
4 [//www.unep.org/hazardoussubstances/, 2008.](http://www.unep.org/hazardoussubstances/)
- 5 [AMAP/UNEP: Technical Background Report for the Global Mercury Assessment 2013, Tech.](http://www.unep.org/hazardoussubstances/Mercury/Informationmaterials/ReportsandPublications/tabid/3593/Default.aspx)
6 [rep., Arctic Monitoring and Assessment Programme AMAP and United Nations Environment](http://www.unep.org/hazardoussubstances/Mercury/Informationmaterials/ReportsandPublications/tabid/3593/Default.aspx)
7 [Programme \(UNEP\) Chemicals Branch, http://www.unep.org/hazardoussubstances/](http://www.unep.org/hazardoussubstances/Mercury/Informationmaterials/ReportsandPublications/tabid/3593/Default.aspx)
8 [Mercury/Informationmaterials/ReportsandPublications/tabid/3593/Default.aspx, 2013.](http://www.unep.org/hazardoussubstances/Mercury/Informationmaterials/ReportsandPublications/tabid/3593/Default.aspx)
- 9 [Amos, H. M., Jacob, D. J., Holmes, C. D., Fisher, J. A., Wang, Q., Yantosca, R. M., Corbitt, E. S.,](https://doi.org/10.5194/acp-12-591-2012)
10 [Galarneau, E., Rutter, A. P., Gustin, M. S., Steffen, A., Schauer, J. J., Graydon, J. A., Louis, V.](https://doi.org/10.5194/acp-12-591-2012)
11 [L. St., Talbot, R. W., Edgerton, E. S., Zhang, Y., and Sunderland, E. M.: Gas-particle](https://doi.org/10.5194/acp-12-591-2012)
12 [partitioning of atmospheric Hg\(II\) and its effect on global mercury deposition, Atmos. Chem.](https://doi.org/10.5194/acp-12-591-2012)
13 [Phys., 12, 591-603, doi:10.5194/acp-12-591-2012, 2012.](https://doi.org/10.5194/acp-12-591-2012)
- 14 Ariya, P. A., Khalizov, A., and Gidas, A.: Reactions of gaseous mercury with atomic and
15 molecular halogens: Kinetics, product studies, and atmospheric implications, *J. Phys. Chem. A*,
16 106, 7310-7320, doi:10.1021/jp020719o, 2002.
- 17 Bash, J. O.: Description and initial simulation of a dynamic bidirectional air-surface exchange
18 model for mercury in Community Multiscale Air Quality (CMAQ) model, *J. Geophys.*
19 *Res.-Atmos.*, 115, D06305, doi:10.1029/2009jd012834, 2010.
- 20 Bergan, T., and Rodhe, H.: Oxidation of elemental mercury in the atmosphere: constraints
21 imposed by global scale modelling, *J. Atmos. Chem.*, 40, 191-212,
22 doi:10.1023/a:1011929927896, 2001.
- 23 Bullock, O. R., and Brehme, K. A.: Atmospheric mercury simulation using the CMAQ model:
24 formulation description and analysis of wet deposition results, *Atmos. Environ.*, 36,
25 2135-2146, doi:10.1016/s1352-2310(02)00220-0, 2002.
- 26 Bullock, O. R., Jr., Atkinson, D., Braverman, T., Civerolo, K., Dastoor, A., Davignon, D., Ku,
27 J.-Y., Lohman, K., Myers, T. C., Park, R. J., Seigneur, C., Selin, N. E., Sistla, G., and
28 Vijayaraghavan, K.: The North American Mercury Model Intercomparison Study (NAMMIS):
29 Study description and model-to-model comparisons, *J. Geophys. Res.-Atmos.*, 113, D17310,
30 doi:10.1029/2008jd009803, 2008.
- 31 Chang, J. S., Brost, R. A., Isaksen, I. S. A., Madronich, S., Middleton, P., Stockwell, W. R., and
32 Walcek, C. J.: A three-dimensional Eulerian acid deposition model: Physical concepts and
33 formulation, *J. Geophys. Res.-Atmos.*, 92, 14681-14700, doi:10.1029/JD092iD12p14681,
34 1987.
- 35 Christensen, J. H., Brandt, J., Frohn, L. M., and Skov, H.: Modelling of mercury in the Arctic
36 with the Danish Eulerian Hemispheric Model, *Atmos. Chem. Phys.*, 4, 2251-2257, 2004.
- 37 Clever, H. L., Johnson, S. A., and Derrick, M. E.: The solubility of mercury and some sparingly
38 soluble mercury salts in water and aqueous-electrolyte solutions, *J. Phys. Chem. Ref. Data*, 14,
39 631-681, 1985.
- 40 Corbitt, E. S., Jacob, D. J., Holmes, C. D., Streets, D. G., and Sunderland, E. M.: Global
41 source-receptor relationships for mercury deposition under present-day and 2050 emissions
42 scenarios, *Environ. Sci. Technol.*, 45, 10477-10484, doi:10.1021/es202496y, 2011.
- 43 [Dastoor, A. P., and Durnford, D. A.: Arctic Ocean: Is It a Sink or a Source of Atmospheric](https://doi.org/10.5194/acp-12-591-2012)

- 1 [Mercury, Environ. Sci. Technol., 48\(3\), 1707-1717, 2014.](#)~~Dastoor, A., and Davignon, D.: Global~~
2 ~~mercury modelling at Environment Canada, in: Mercury Fate and Transport in the Global~~
3 ~~Atmosphere, edited by: Mason, R., and Pirrone, N., Springer, USA, 519-532, 2009.~~
- 4 [De Simone, F., Gencarelli, C. N., Hedgecok, I. M., Pirrone, N.: Global atmospheric cycle of](#)
5 [mercury: a model study on the impact of oxidation mechanisms, Environ. Sci. Pollut. Res., 21,](#)
6 [4110-4123, 2014.](#)
- 7 ENVIRON: User's guide for Comprehensive Air Quality Model with Extensions Version 5.40,
8 ENVIRON International Corporation, Novato, California, 2011.
- 9 Frank, D. G.: Mineral Resource Data System (MRDS) data in Arc-View shape file format, for
10 spatial data delivery project, U.S. Geol. Surv., Spokane, Wash., 1999.
- 11 Friedli, H. R., Radke, L. F., Prescott, R., Li, P., Woo, J. H., and Carmichael, G. R.: Mercury in
12 the atmosphere around Japan, Korea, and China as observed during the 2001 ACE-Asia field
13 campaign: Measurements, distributions, sources, and implications, J. Geophys. Res.-Atmos.,
14 109, D19s25, doi:10.1029/2003jd004244, 2004.
- 15 Friedli, H. R., Arellano, A. F., Cinnirella, S., and Pirrone, N.: Initial estimates of mercury
16 emissions to the atmosphere from global biomass burning, Environ. Sci. Technol., 43,
17 3507-3513, doi:10.1021/es802703g, 2009.
- 18 Fu, X., Feng, X., Sommar, J., and Wang, S.: A review of studies on atmospheric mercury in
19 China, Sci. Total Environ., 421, 73-81, doi:10.1016/j.scitotenv.2011.09.089, 2012.
- 20 Ge, B., Wang, Z., Xu, X., Wu, J., Yu, X., and Li, J.: Wet deposition of acidifying substances in
21 different regions of China and the rest of East Asia: Modeling with updated NAQPMS,
22 Environ. Pollut., 187, 10-21, doi:http://dx.doi.org/10.1016/j.envpol.2013.12.014, 2014.
- 23 [Gencarelli, C. N., De Simone, F., Hedgecok, I. M., Sprovieri, F., Pirrone, N.: Development and](#)
24 [application of a regional-scale atmospheric mercury model based on WRF/Chem: a](#)
25 [Mediterranean area investigation, Environ. Sci. Pollut. Res., 21, 4095-4109, 2014.](#)
- 26 Granier, C., Lamarque, J. F., Mieville, A., Muller, J. F., and Olivier, J.: POET, a database of
27 surface emissions of ozone precursors , tech. report, available at:
28 http://www.aero.jussieu.fr/projet/ACCENT/POET.php (last access: 10 June 2013), 2005.
- 29 Guenther, A., Karl, T., Harley, P., Wiedinmyer, C., Palmer, P. I., and Geron, C.: Estimates of
30 global terrestrial isoprene emissions using MEGAN (Model of Emissions of Gases and
31 Aerosols from Nature), Atmos. Chem. Phys., 6, 3181-3210, 2006.
- 32 Hall, B., and Bloom, N.: Report to EPRI, Palo Alto, CA., USA, 1993.
- 33 Hall, B.: The gas phase oxidation of elemental mercury by ozone, Water Air Soil Pollut., 80,
34 301-315, doi:10.1007/bf01189680, 1995.
- 35 Harada, M.: Minamata Disease – Methylmercury poisoning in Japan caused by environmental
36 pollution, Crit. Rev. Toxicol., 25, 1-24, doi:10.3109/10408449509089885, 1995.
- 37 Holmes, C. D., Jacob, D. J., Corbitt, E. S., Mao, J., Yang, X., Talbot, R., and Slemr, F.: Global
38 atmospheric model for mercury including oxidation by bromine atoms, Atmos. Chem. Phys.,
39 10, 12037-12057, doi:10.5194/acp-10-12037-2010, 2010.
- 40 Horowitz, L. W., Walters, S., Mauzerall, D. L., Emmons, L. K., Rasch, P. J., Granier, C., Tie, X.
41 X., Lamarque, J. F., Schultz, M. G., Tyndall, G. S., Orlando, J. J., and Brasseur, G. P.: A global
42 simulation of tropospheric ozone and related tracers: Description and evaluation of MOZART,
43 version 2, J. Geophys. Res.-Atmos., 108, 4784, doi:10.1029/2002jd002853, 2003.
- 44 Jaffe, D., Prestbo, E., Swartzendruber, P., Weiss-Penzias, P., Kato, S., Takami, A., Hatakeyama,

1 S., and Kajii, Y.: Export of atmospheric mercury from Asia, *Atmos. Environ.*, 39, 3029-3038,
2 doi:10.1016/j.atmosenv.2005.01.030, 2005.

3 Jaffe, D., and Strode, S.: Sources, fate and transport of atmospheric mercury from Asia, *Environ.*
4 *Chem.*, 5, 121-126, doi:10.1071/en08010, 2008.

5 Jiang, G., Shi, J., and Feng, X.: Mercury pollution in China: An overview of the past and current
6 sources of the toxic metal, *Environ. Sci. Technol.*, 40, 3673-3678, 2006.

7 Jung, G., Hedgecock, I. M., and Pirrone, N.: ECHMERIT V1.0-a new global fully coupled
8 mercury-chemistry and transport model, *Geosci. Model Dev.*, 2, 175-195, 2009.

9 Keeler, G. J., Pirrone, N., Bullock, R., and Sillman, S.: The need for a coordinated global Hg
10 monitoring network for global and regional models validation, in: *Mercury Fate and Transport*
11 *in the Global Atmosphere*, edited by: Mason, R., and Pirrone, N., Springer, USA, 391-424,
12 2009.

13 Lamarque, J. F., Bond, T. C., Eyring, V., Granier, C., Heil, A., Klimont, Z., Lee, D., Lioussé, C.,
14 Mieville, A., Owen, B., Schultz, M. G., Shindell, D., Smith, S. J., Stehfest, E., Van Aardenne,
15 J., Cooper, O. R., Kainuma, M., Mahowald, N., McConnell, J. R., Naik, V., Riahi, K., and van
16 Vuuren, D. P.: Historical (1850-2000) gridded anthropogenic and biomass burning emissions
17 of reactive gases and aerosols: methodology and application, *Atmos. Chem. Phys.*, 10,
18 7017-7039, doi:10.5194/acp-10-7017-2010, 2010.

19 Lamborg, C. H., Fitzgerald, W. F., O'Donnell, J., and Torgersen, T.: A non-steady-state
20 compartmental model of global-scale mercury biogeochemistry with interhemispheric
21 atmospheric gradients, *Geochim. Cosmochim. Ac.*, 66, 1105-1118,
22 doi:10.1016/s0016-7037(01)00841-9, 2002.

23 Lawrence, M. G., Jöckel, P., and von Kuhlmann, R.: What does the global mean OH
24 concentration tell us?, *Atmos. Chem. Phys.*, 1, 37-49, doi:10.5194/acp-1-37-2001, 2001.

25 Lei, H., Liang, X., Wuebbles, D. J., and Tao, Z.: Model analyses of atmospheric mercury: present
26 air quality and effects of transpacific transport on the United States, *Atmos. Chem. Phys.*, 13,
27 10807-10825, doi:10.5194/acp-13-10807-2013, 2013.

28 Li, J., Wang, Z., Akimoto, H., Gao, C., Pochanart, P., and Wang, X.: Modeling study of ozone
29 seasonal cycle in lower troposphere over east Asia, *J. Geophys. Res.-Atmos.*, 112, D22s25,
30 doi:10.1029/2006jd008209, 2007.

31 Li, J., Wang, Z., Wang, X., Yamaji, K., Takigawa, M., Kanaya, Y., Pochanart, P., Liu, Y., Irie, H.,
32 Hu, B., Tanimoto, H., and Akimoto, H.: Impacts of aerosols on summertime tropospheric
33 photolysis frequencies and photochemistry over Central Eastern China, *Atmos. Environ.*, 45,
34 1817-1829, doi:10.1016/j.atmosenv.2011.01.016, 2011.

35 Li, J., Wang, Z., Zhuang, G., Luo, G., Sun, Y., and Wang, Q.: Mixing of Asian mineral dust with
36 anthropogenic pollutants over East Asia: a model case study of a super-duststorm in March
37 2010, *Atmos. Chem. Phys.*, 12, 7591-7607, doi:10.5194/acp-12-7591-2012, 2012.

38 [Liang, S., Xu, M., Liu, Z., Suh, S. and Zhang T.: Socioeconomic Drivers of Mercury Emissions](#)
39 [in China from 1992 to 2007, *Environ. Sci. Technol.*, 47\(7\): 3234-3240, 2013.](#)

40 Lin, C. J., and Pehkonen, S. O.: Aqueous free radical chemistry of mercury in the presence of
41 iron oxides and ambient aerosol, *Atmos. Environ.*, 31, 4125-4137,
42 doi:http://dx.doi.org/10.1016/S1352-2310(97)00269-0, 1997.

43 Lin, C. J., and Pehkonen, S. O.: Oxidation of elemental mercury by aqueous chlorine
44 (HOCl/OCl⁻): Implications for tropospheric mercury chemistry, *J. Geophys. Res.-Atmos.*, 103,

1 28093-28102, doi:10.1029/98jd02304, 1998.

2 Lin, C. J., Pongprueksa, P., Lindberg, S. E., Pehkonen, S. O., Byun, D., and Jang, C.: Scientific
3 uncertainties in atmospheric mercury models I: Model science evaluation, *Atmos. Environ.*, 40,
4 doi:2911-2928, 10.1016/j.atmosenv.2006.01.009, 2006.

5 Lin, C. J., and Pehkonen, S. O.: The chemistry of atmospheric mercury: a review, *Atmos.*
6 *Environ.*, 33, 2067-2079, doi:10.1016/s1352-2310(98)00387-2, 1999.

7 Lin, C. J., Pongprueks, P., Ho, T. C., and Jang, C.: Development of mercury modeling schemes
8 within CMAQ framework: Science and model implementation issues, In: *Proceedings of the*
9 *2004 CMAS Models-3 Conference*, Research Triangle Park, NC, October 18-20 (CD-ROM).
10 2004.

11 Lindberg, S., Bullock, R., Ebinghaus, R., Engstrom, D., Feng, X., Fitzgerald, W., Pirrone, N.,
12 Prestbo, E., and Seigneur, C.: A synthesis of progress and uncertainties in attributing the
13 sources of mercury in deposition, *Ambio*, 36, 19-32, 2007.

14 Lindqvist, O., and Rodhe, H.: Atmospheric mercury – A review, *Tellus B*, 37, 136-159, 1985.

15 Mason, R.: Mercury emissions from natural processes and their importance in the global mercury
16 cycle, in: *Mercury Fate and Transport in the Global Atmosphere*, edited by: Mason, R., and
17 Pirrone, N., Springer, USA, 173-191, 2009.

18 Munthe, J.: The aqueous oxidation of elemental mercury by ozone, *Atmos. Environ.*, 26,
19 1461-1468, doi:10.1016/0960-1686(92)90131-4, 1992.

20 Pacyna, E. G., Pacyna, J. M., Steenhuisen, F., and Wilson, S.: Global anthropogenic mercury
21 emission inventory for 2000, *Atmos. Environ.*, 40, 4048-4063,
22 doi:http://dx.doi.org/10.1016/j.atmosenv.2006.03.041, 2006.

23 Pan, L., Chai, T., Carmichael, G. R., Tang, Y., Streets, D., Woo, J.-H., Friedli, H. R., and Radke,
24 L. F.: Top-down estimate of mercury emissions in China using four-dimensional variational
25 data assimilation, *Atmos. Environ.*, 41, 2804-2819,
26 doi:http://dx.doi.org/10.1016/j.atmosenv.2006.11.048, 2007.

27 Pan, L., Carmichael, G. R., Adhikary, B., Tang, Y., Streets, D., Woo, J.-H., Friedli, H. R., and
28 Radke, L. F.: A regional analysis of the fate and transport of mercury in East Asia and an
29 assessment of major uncertainties, *Atmos. Environ.*, 42, 1144-1159,
30 doi:10.1016/j.atmosenv.2007.10.045, 2008.

31 Pehkonen, S. O., and Lin, C. J.: Aqueous photochemistry of mercury with organic acids, *J. Air*
32 *Waste Manage. Assoc.*, 48, 144-150, doi:10.1080/10473289.1998.10463661, 1998.

33 Pirrone, N., Cinnirella, S., Feng, X., Finkelman, R. B., Friedli, H. R., Leaner, J., Mason, R.,
34 Mukherjee, A. B., Stracher, G. B., Streets, D. G., and Telmer, K.: Global mercury emissions to
35 the atmosphere from anthropogenic and natural sources, *Atmos. Chem. Phys.*, 10, 5951-5964,
36 doi:10.5194/acp-10-5951-2010, 2010.

37 Pirrone, N., and Keating, T.: *Hemispheric Transport of Air Pollution 2010 Part B: Mercury*,
38 United Nations, New York and Geneva, 210 pp., 2010.

39 Price, C., Penner, J., and Prather, M.: NO_x from lightning: 1. Global distribution based on
40 lightning physics, *J. Geophys. Res.-Atmos.*, 102, 5929-5941, doi:10.1029/96jd03504, 1997.

41 Ryaboshapko, A., Bullock, O. R., Jr., Christensen, J., Cohen, M., Dastoor, A., Ilyin, I., Petersen,
42 G., Syrakov, D., Travnikov, O., Artz, R. S., Davignon, D., Draxler, R. R., Munthe, J., and
43 Pacyna, J.: Intercomparison study of atmospheric mercury models: 2. Modelling results vs.
44 long-term observations and comparison of country deposition budgets, *Sci. Total Environ.*,

1 377, 319-333, doi:10.1016/j.scitotenv.2007.01.071, 2007.

2 Sanemasa, I.: The solubility of elemental mercury vapor in water, *Bull. Chem. Soc. Jpn.*, 48,
3 1795-1798, 1975.

4 Schroeder, W. H., Anlauf, K. G., Barrie, L. A., Lu, J. Y., Steffen, A., Schneeberger, D. R., and
5 Berg, T.: Arctic springtime depletion of mercury, *Nature*, 394, 331-332, doi:10.1038/28530,
6 1998.

7 Schroeder, W. H., and Munthe, J.: Atmospheric mercury - An overview, *Atmos. Environ.*, 32,
8 809-822, doi:10.1016/s1352-2310(97)00293-8, 1998.

9 Seigneur, C., Abeck, H., Chia, G., Reinhard, M., Bloom, N. S., Prestbo, E., and Saxena, P.:
10 Mercury adsorption to elemental carbon (soot) particles and atmospheric particulate matter,
11 *Atmos. Environ.*, 32, 2649-2657, doi:http://dx.doi.org/10.1016/S1352-2310(97)00415-9, 1998.

12 Seigneur, C., Karamchandani, P., Lohman, K., Vijayaraghavan, K., and Shia, R. L.: Multiscale
13 modeling of the atmospheric fate and transport of mercury, *J. Geophys. Res.-Atmos.*, 106,
14 27795-27809, doi:10.1029/2000jd000273, 2001.

15 Seigneur, C., Vijayaraghavan, K., Lohman, K., Karamchandani, P., and Scott, C.: Global source
16 attribution for mercury deposition in the United States, *Environ. Sci. Technol.*, 38, 555-569,
17 doi:10.1021/es034109t, 2004.

18 Selin, N. E., Jacob, D. J., Park, R. J., Yantosca, R. M., Strode, S., Jaegle, L., and Jaffe, D.:
19 Chemical cycling and deposition of atmospheric mercury: Global constraints from
20 observations, *J. Geophys. Res.-Atmos.*, 112, D02308, doi:10.1029/2006jd007450, 2007.

21 Selin, N. E., Jacob, D. J., Yantosca, R. M., Strode, S., Jaegle, L., and Sunderland, E. M.: Global
22 3-D land-ocean-atmosphere model for mercury: Present-day versus preindustrial cycles and
23 anthropogenic enrichment factors for deposition, *Global Biogeochem. Cy.*, 22, Gb3099,
24 doi:10.1029/2008gb003282, 2008.

25 Selin, N. E.: Global biogeochemical cycling of mercury: A review, *Annu. Rev. Environ. Resour.*,
26 34, 43, 2009.

27 Sillen, L. G., Martell, A. E., and Bjerrum, J.: Stability constants of metal-ion complexes, *Chem.*
28 *Soc.*, 17, 754, 1964.

29 Soerensen, A. L., Skov, H., Jacob, D. J., Soerensen, B. T., and Johnson, M. S.: Global
30 concentrations of gaseous elemental mercury and reactive gaseous mercury in the marine
31 boundary layer, *Environ. Sci. Technol.*, 44, 7425-7430, doi:10.1021/es903839n, 2010a.

32 Soerensen, A. L., Sunderland, E. M., Holmes, C. D., Jacob, D. J., Yantosca, R. M., Skov, H.,
33 Christensen, J. H., Strode, S. A., and Mason, R. P.: An improved global model for air-sea
34 exchange of mercury: High concentrations over the North Atlantic, *Environ. Sci. Technol.*, 44,
35 8574-8580, doi:10.1021/es102032g, 2010b.

36 [Soerensen, A. L., Jacob, D. J., Streets, D., Witt, M., Ebinghaus, R., Mason, R. P., Andersson, M.](#)
37 [and Sunderland E. M.: Multi-decadal decline of mercury in the North Atlantic atmosphere](#)
38 [explained by changing subsurface seawater concentrations, *Geophys. Res. Lett.* 39: Art](#)
39 [#L21810, 2012.](#)

40 Sommar, J., Gardfeldt, K., Stromberg, D., and Feng, X. B.: A kinetic study of the gas-phase
41 reaction between the hydroxyl radical and atomic mercury, *Atmos. Environ.*, 35, 3049-3054,
42 doi:10.1016/s1352-2310(01)00108-x, 2001.

43 [Song, S., Selin, N. E., Soerensen, A. L., Angot, H., Artz, R., Brooks, S., Brunke, E.-G., Conley,](#)
44 [G., Dommergue, A., Ebinghaus, R., Holsen, T. M., Jaffe, D. A., Kang, S., Kelley, P., Luke, W.](#)

- 1 [T., Magand, O., Marumoto, K., Pfaffhuber, K. A., Ren, X., Sheu, G.-R., Slemr, F., Warneke, T.,](#)
2 [Weigelt, A., Weiss-Penzias, P., Wip, D. C., and Zhang, Q.: Top-down constraints on](#)
3 [atmospheric mercury emissions and implications for global biogeochemical cycling, *Atmos.*](#)
4 [Chem. Phys., 15, 7103-7125, doi:10.5194/acp-15-7103-2015, 2015.](#)
- 5 Sprovieri, F., Pirrone, N., Ebinghaus, R., Kock, H., and Dommergue, A.: A review of worldwide
6 atmospheric mercury measurements, *Atmos. Chem. Phys.*, 10, 8245-8265,
7 doi:10.5194/acp-10-8245-2010, 2010.
- 8 Steffen, A., Schroeder, W., Macdonald, R., Poissant, L., and Konoplev, A.: Mercury in the Arctic
9 atmosphere: An analysis of eight years of measurements of GEM at Alert (Canada) and a
10 comparison with observations at Amderma (Russia) and Kuujjuarapik (Canada), *Sci. Total*
11 *Environ.*, 342, 185-198, doi:10.1016/j.scitotenv.2004.12.048, 2005.
- 12 Strode, S. A., Jaegle, L., Selin, N. E., Jacob, D. J., Park, R. J., Yantosca, R. M., Mason, R. P., and
13 Slemr, F.: Air-sea exchange in the global mercury cycle, *Global Biogeochem. Cy.*, 21, Gb1017,
14 doi:10.1029/2006gb002766, 2007.
- 15 Strode, S. A., Jaegle, L., Jaffe, D. A., Swartzendruber, P. C., Selin, N. E., Holmes, C., and
16 Yantosca, R. M.: Trans-Pacific transport of mercury, *J. Geophys. Res.-Atmos.*, 113, D15305,
17 doi:10.1029/2007jd009428, 2008.
- 18 Tang, X., Wang, Z., Zhu, J., Gbaguidi, A. E., Wu, Q., Li, J., and Zhu, T.: Sensitivity of ozone to
19 precursor emissions in urban Beijing with a Monte Carlo scheme, *Atmos. Environ.*, 44,
20 3833-3842, doi:http://dx.doi.org/10.1016/j.atmosenv.2010.06.026, 2010.
- 21 Taylor, K. E.: Summarizing multiple aspects of model performance in a single diagram, *J.*
22 *Geophys. Res.-Atmos.*, 106, 7183-7192, doi:10.1029/2000jd900719, 2001.
- 23 Temme, C., Slemr, F., Ebinghaus, R., and Einax, J. W.: Distribution of mercury over the Atlantic
24 Ocean in 1996 and 1999-2001, *Atmos. Environ.*, 37, 1889-1897,
25 doi:10.1016/s1352-2310(03)00069-4, 2003.
- 26 Tokos, J. J. S., Hall, B., Calhoun, J. A., and Prestbo, E. M.: Homogeneous gas-phase reaction of
27 Hg⁰ with H₂O₂, O₃, CH₃I, and (CH₃)₂S: Implications for atmospheric Hg cycling, *Atmos.*
28 *Environ.*, 32, 823-827, doi:10.1016/s1352-2310(97)00171-4, 1998.
- 29 Travnikov, O.: Contribution of the intercontinental atmospheric transport to mercury pollution in
30 the Northern Hemisphere, *Atmos. Environ.*, 39, 7541-7548,
31 doi:10.1016/j.atmosenv.2005.07.066, 2005.
- 32 Travnikov, O., and Ilyin, I.: The EMEP/MSCE mercury modeling system, in: *Mercury Fate and*
33 *Transport in the Global Atmosphere*, edited by: Mason, R., and Pirrone, N., Springer, USA,
34 571-587, 2009.
- 35 Van Loon, L., Mader, E., and Scott, S. L.: Reduction of the aqueous mercuric ion by sulfite: UV
36 spectrum of HgSO₃ and its intramolecular redox reaction, *J. Phys. Chem. A*, 104, 1621-1626,
37 doi:10.1021/jp994268s, 2000.
- 38 Van Loon, L. L., Mader, E. A., and Scott, S. L.: Sulfite stabilization and reduction of the aqueous
39 mercuric ion: Kinetic determination of sequential formation constants, *J. Phys. Chem. A*, 105,
40 3190-3195, doi:10.1021/jp003803h, 2001.
- 41 [Vijayaraghavan, K., P. Karamchandani, C. Seigneur, R. Balmori, and S.-Y. Chen: Plume-in-grid](#)
42 [modeling of atmospheric mercury, *J. Geophys. Res.*, 113, D24305,](#)
43 [doi:10.1029/2008JD010580, 2008.](#)
- 44 Voulgarakis, A., Naik, V., Lamarque, J. F., Shindell, D. T., Young, P. J., Prather, M. J., Wild, O.,

- 1 Field, R. D., Bergmann, D., Cameron-Smith, P., Cionni, I., Collins, W. J., Dalsøren, S. B.,
2 Doherty, R. M., Eyring, V., Faluvegi, G., Folberth, G. A., Horowitz, L. W., Josse, B.,
3 MacKenzie, I. A., Nagashima, T., Plummer, D. A., Righi, M., Rumbold, S. T., Stevenson, D. S.,
4 Strode, S. A., Sudo, K., Szopa, S., and Zeng, G.: Analysis of present day and future OH and
5 methane lifetime in the ACCMIP simulations, *Atmos. Chem. Phys.*, 13, 2563-2587,
6 doi:10.5194/acp-13-2563-2013, 2013.
- 7 Walcek, C. J., and Aleksic, N. M.: A simple but accurate mass conservative, peak-preserving,
8 mixing ratio bounded advection algorithm with Fortran code, *Atmos. Environ.*, 32, 3863-3880,
9 doi:10.1016/s1352-2310(98)00099-5, 1998.
- 10 Wang, Q., Fu, Q., Wang, Z., Wang, T., Liu, P., Lu, T., Duan, Y., and Huang, Y.: Application of
11 ensemble numerical model system on the air quality forecast in Shanghai (in Chinese),
12 *Environmental Monitoring and Forewarning*, 2(4), 1-6+11, 2010.
- 13 Wang, Z., Akimoto, H., and Uno, I.: Neutralization of soil aerosol and its impact on the
14 distribution of acid rain over east Asia: Observations and model results, *J. Geophys.*
15 *Res.-Atmos.*, 107, 4389, doi:10.1029/2001jd001040, 2002.
- 16 Wang, Z., Xie, F., Wang, X., An, J., and Zhu, J.: Development and application of Nested Air
17 Quality Prediction Modeling System (in Chinese), *Chinese Journal of Atmospheric Sciences*,
18 30(5), 778-790, 2006.
- 19 Wang, Z., Wu, Q., Gbaguidi, A., Yan, P., Zhang, W., Wang, W., and Tang, X.: Ensemble air
20 quality multi-model forecast system for Beijing (EMS-Beijing): Model description and
21 preliminary application (in Chinese), *Journal of Nanjing University of Information Science &*
22 *Technology (Natural Science Edition)*, 1(1), 19-26, 2009.
- 23 Wesely, M. L.: Parameterization of surface resistances to gaseous dry deposition in
24 regional-scale numerical models, *Atmos. Environ.*, 23, 1293-1304,
25 doi:http://dx.doi.org/10.1016/0004-6981(89)90153-4, 1989.
- 26 Wilson, S. J., Steenhuisen, F., Pacyna, J. M., and Pacyna, E. G.: Mapping the spatial distribution
27 of global anthropogenic mercury atmospheric emission inventories, *Atmos. Environ.*, 40,
28 4621-4632, doi:http://dx.doi.org/10.1016/j.atmosenv.2006.03.042, 2006.
- 29 Wu, Q., Wang, Z., Chen, H., Zhou, W., and Wenig, M.: An evaluation of air quality modeling
30 over the Pearl River Delta during November 2006, *Meteorol. Atmos. Phys.*, 116, 113-132,
31 doi:10.1007/s00703-011-0179-z, 2012.
- 32 Yan, X., Ohara, T., and Akimoto, H.: Statistical modeling of global soil NO_x emissions, *Global*
33 *Biogeochem. Cy.*, 19, 2005.
- 34 Zhang, Y., Jaegle, L., van Donkelaar, A., Martin, R. V., Holmes, C. D., Amos, H. M., Wang, Q.,
35 Talbot, R., Artz, R., Brooks, S., Luke, W., Holsen, T. M., Felton, D., Miller, E. K., Perry, K. D.,
36 Schmeltz, D., Steffen, A., Tordon, R., Weiss-Penzias, P., and Zsolway, R.: Nested-grid
37 simulation of mercury over North America, *Atmos. Chem. Phys.*, 12, 6095-6111,
38 doi:10.5194/acp-12-6095-2012, 2012.
- 39 Zaveri, R., and Peters, L.: A new lumped structure photochemical mechanism for large-scale
40 applications, *J. Geophys. Res.-Atmos.*, 104, 30387-30415, 1999.
- 41

Table 1. Reactions and rate constants used in the GNAQPMS-Hg model.

NO.	Reaction	Rates (k or K) ^a	References
Gas-phase reactions			
RG1	Hg(0)(g)+O ₃ (g)→Hg(II)(g)	3x10 ⁻²⁰ cm ³ molec ⁻¹ s ⁻¹	Hall (1995)
RG2	Hg(0)(g)+HCl(g)→HgCl ₂ (g)	1x10 ⁻¹⁹ cm ³ molec ⁻¹ s ⁻¹	Hall and Bloom (1993)
RG3	Hg(0)(g)+H ₂ O ₂ (g)→Hg(OH) ₂ (g)	8.5x10 ⁻¹⁹ cm ³ molec ⁻¹ s ⁻¹	Tokos et al. (1998)
RG4	Hg(0)(g)+Cl ₂ (g)→HgCl ₂ (g)	2.6x10 ⁻¹⁸ cm ³ molec ⁻¹ s ⁻¹	Ariya et al. (2002)
RG5	Hg(0)(g)+OH(g)→Hg(OH) ₂ (g)	8x10 ⁻¹⁴ cm ³ molec ⁻¹ s ⁻¹	Sommar et al. (2001)
Gas-liquid equilibria			
GL1	Hg(0)(g)↔Hg(0)(aq)	0.11 M atm ⁻¹	Sanemasa (1975)
GL2	HgCl ₂ (g)↔HgCl ₂ (aq)	1.4x10 ⁶ M atm ⁻¹	Lindqvist and Rodhe (1985)
GL3	Hg(OH) ₂ (g)↔Hg(OH) ₂ (aq)	1.2x10 ⁴ M atm ⁻¹	Lindqvist and Rodhe (1985)
Aqueous-phase equilibria			
AE1	HgCl ₂ (aq)↔Hg ²⁺ +2Cl ⁻	1x10 ⁻¹⁴ M ²	Sillen et al. (1964)
AE2	Hg(OH) ₂ (aq)↔Hg ²⁺ +2OH ⁻	1x10 ⁻²² M ²	Sillen et al. (1964)
AE3	Hg ²⁺ +SO ₃ ²⁻ ↔HgSO ₃	2.1x10 ¹³ M ⁻¹	Van Loon et al. (2001)
AE4	HgSO ₃ +SO ₃ ²⁻ ↔Hg(SO ₃) ₂ ²⁻	1x10 ¹⁰ M ⁻¹	Van Loon et al. (2001)
Aqueous-phase reaction			
RA1	Hg(0)(aq)+O ₃ (aq)→Hg ²⁺	4.7x10 ⁷ M ⁻¹ s ⁻¹	Munthe (1992)
RA2	Hg(0)(aq)+OH(aq)→Hg ²⁺	2x10 ⁹ M ⁻¹ s ⁻¹	Lin and Pehkonen (1997)
RA3	HgSO ₃ (aq)→Hg(0)(aq)	0.0106 s ⁻¹	Van Loon et al. (2000)
RA4	Hg(II)(aq)+HO ₂ (aq)→Hg(0)(aq)	1.7x10 ⁴ M ⁻¹ s ⁻¹	Pehkonen and Lin (1998)
RA5	Hg(0)(aq)+HOCl(aq)→Hg ²⁺	2.09x10 ⁶ M ⁻¹ s ⁻¹	Lin and Pehkonen (1998)
RA6	Hg(0)(aq)+OCl ⁻ →Hg ²⁺	1.99x10 ⁶ M ⁻¹ s ⁻¹	Lin and Pehkonen (1998)
Adsorption of Hg(II) on PM in the aqueous-phase			
AD1	Hg(II)(aq)↔Hg(II)(p)	34 L g ⁻¹	Seigneur et al. (1998)

^a The reaction rate constants are for temperatures in the range of 20 to 25⁰C. No temperature dependence information is available.

Table 2. Global budgets of TGM in the literature (Unit: Mg yr⁻¹).

	Bergan et al. (1999)	Shia et al. (1999)	Lamborg et al. (2002)	Mason et al. (2002)	Seigneur et al. (2004)	Selin et al. (2007)	Selin et al. (2008)	This work
Total Sources	6050	6100	4400	6600	6411	7000	11200	10163
anthropogenic	2150	2100	2600	2400	2143	2200	3400	2488
land	2500	2000	1000	1600	2290	2000	2800	2675
ocean	1400	2000	800	2600	1978	2800	5000	5000
Total Sinks	6050	6100	4200	6600	6411	7000	11200	10163
Wet deposition		2800		3920		2100		2283
Dry deposition		3300		2680		4700		7880
TGM Burden	6050	10400	5220	5000	7690	5360	5600	5507 19
TGM lifetime(y)	1	1.7	1.3	0.76	1.2	0.79	0.5	0.86 0.854

Table 3. Statistical summary of comparisons of the model results with observations^a.

Parameter	Region	R	NMB	RMSE	SVR ^b
TGM	East Asia Nested	0.51	-39%	3.87	2.56
	East Asia	0.54	-32%	3.61	2.56
	North America	0.69	18%	0.58	0.48
	Europe	0.57	-8%	0.17	0.35
	Global	0.70	-18%	2.22	-
Oxidized mercury	East Asia Nested	0.45	-12%	242	3.66
	East Asia	0.31	-10%	259	3.66
	North America	0.53	148%	28	1.61
	Europe	0.91	155%	48	1.00
	Global	0.53	3%	185	-
Wet deposition	East Asia Nested	0.78	-28%	45.5	6.69
	East Asia	0.36	-61%	60.1	6.69
	North America	0.76	-4%	4.3	1.89
	Europe	0.78	4%	1.5	1.40
	Global	0.38	-36%	29.3	-
Dry deposition	East Asia Nested	0.88	-42%	87.0	-
	East Asia	0.81	-42%	88.5	-

^a R, NMB, RMSE, SVR represent correlation coefficient, normalized mean bias, root mean square error, spatial variation ratio. Units of TGM, oxidized mercury, wet and dry deposition are ng m⁻³, pg m⁻³, ug m⁻² yr⁻¹, ug m⁻² yr⁻¹ respectively.

^b SVR defines as (max-min)/mean observations over all sites.

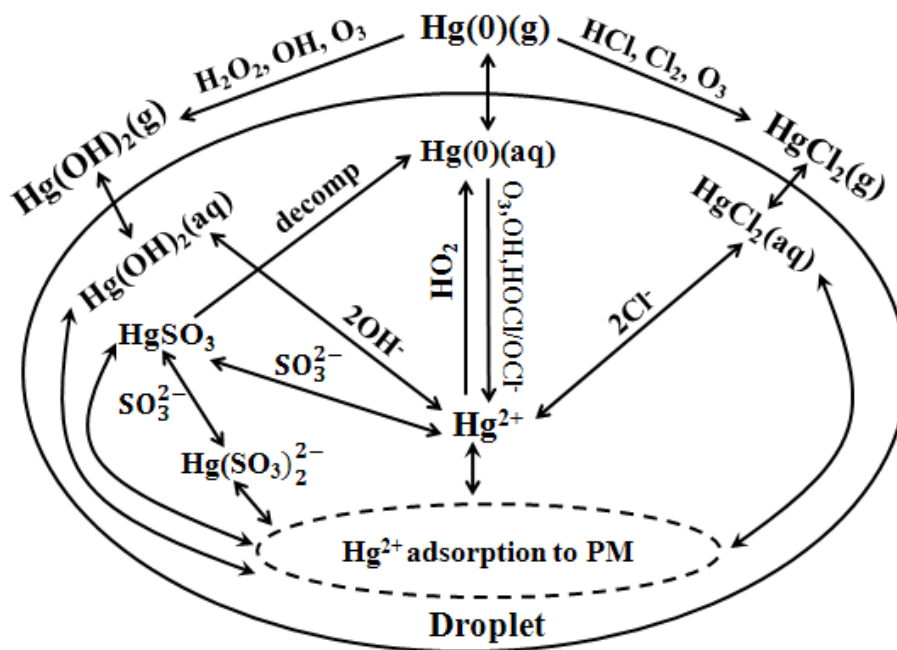
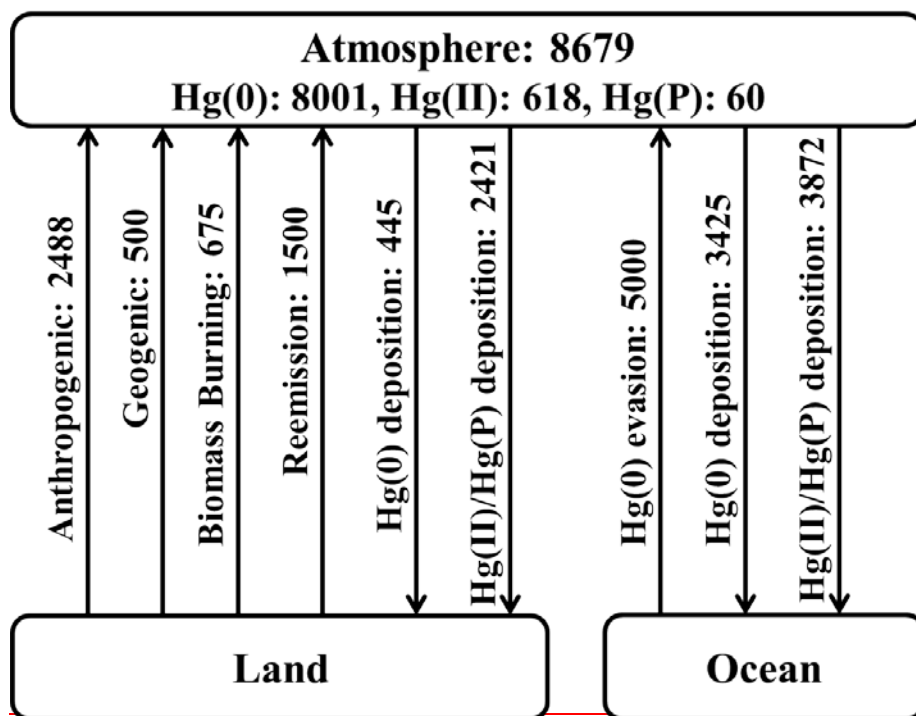


Fig. 1. Schematic of different mercury reactions utilized in the GNAQPMS-Hg model.



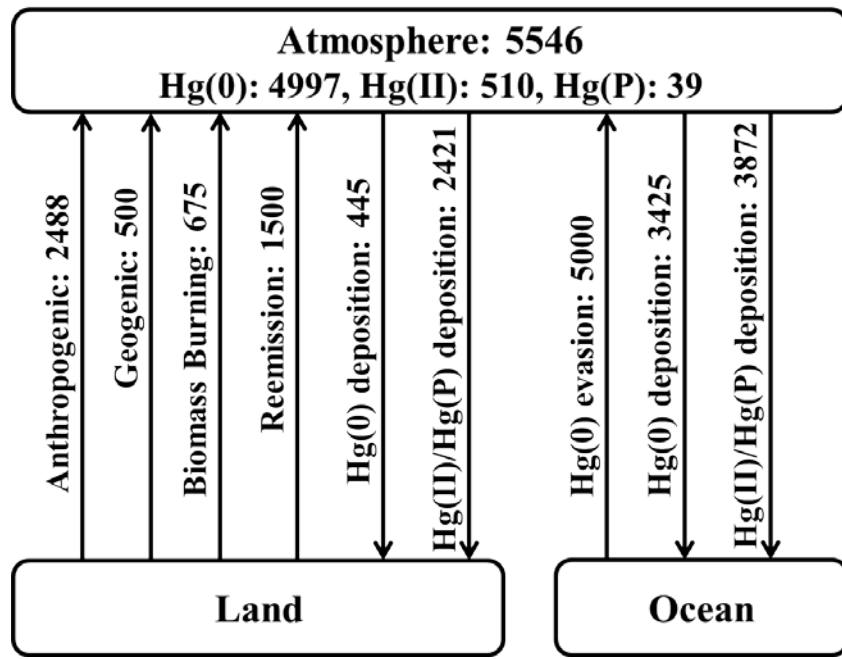


Fig. 2. Global atmospheric mercury budget in GNAQPMS-Hg. Units are Mg yr⁻¹.

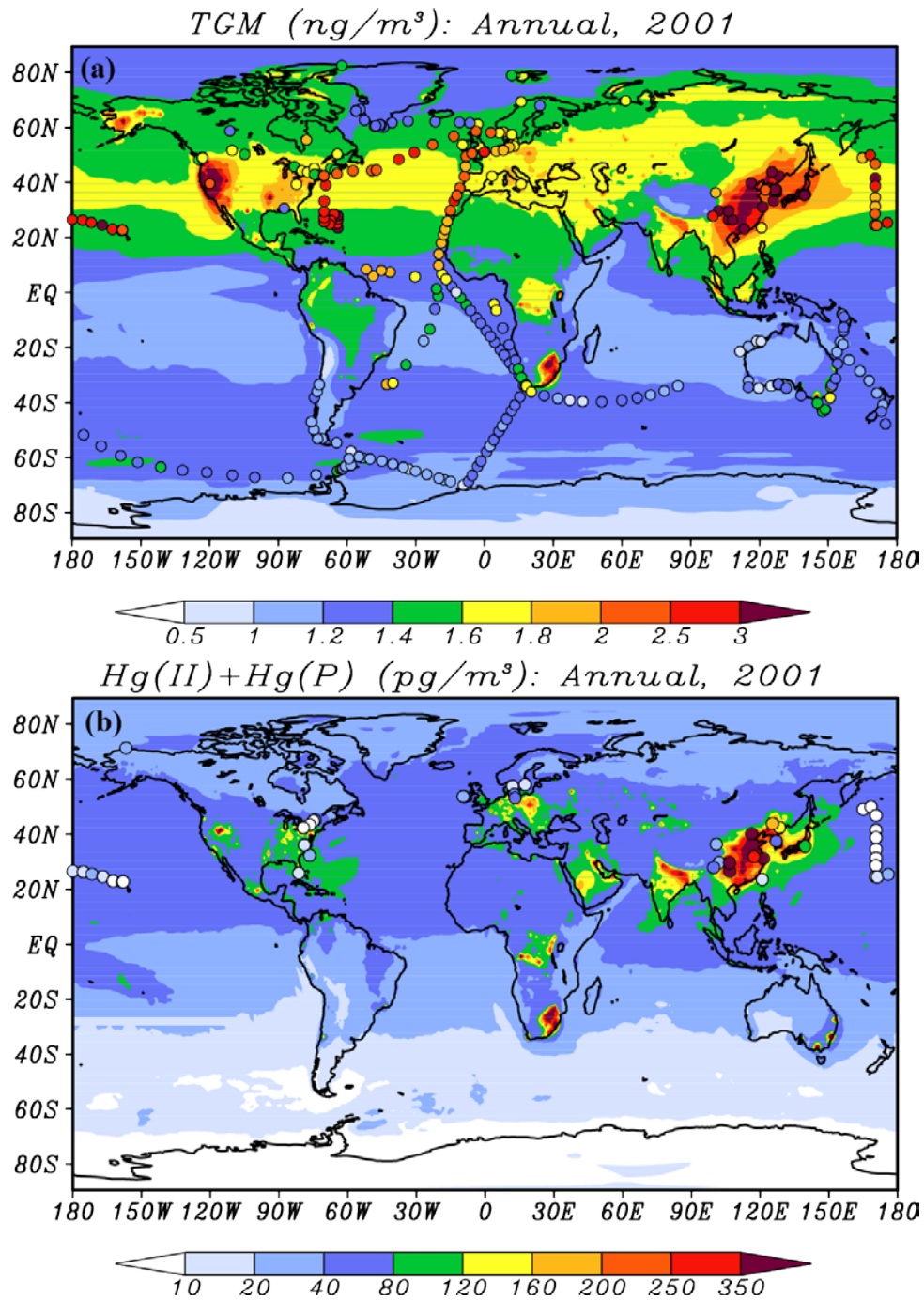


Fig. 3. Annual average TGM (a) and oxidized mercury (Hg(II)+Hg(P),b) concentrations in surface air. Model results (background, for year 2001) are compared to observations (circles) from long-term surface sites and short-term ship cruises.

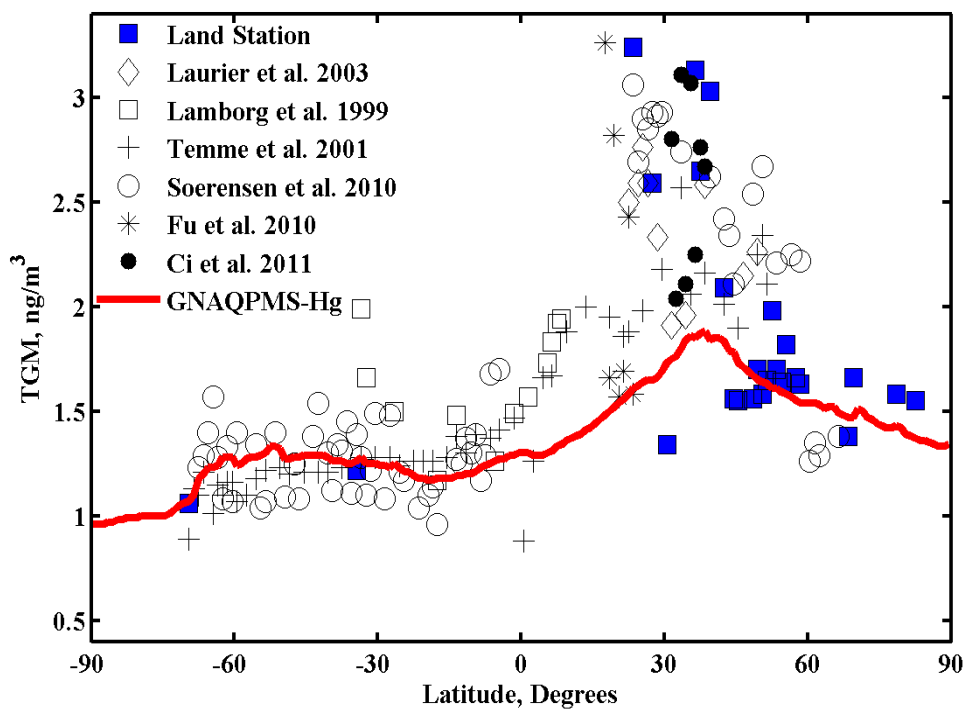


Fig. 4. Variation of TGM surface concentrations with latitude. Zonally averaged, annual mean model results (line) are compared to observations (symbols).

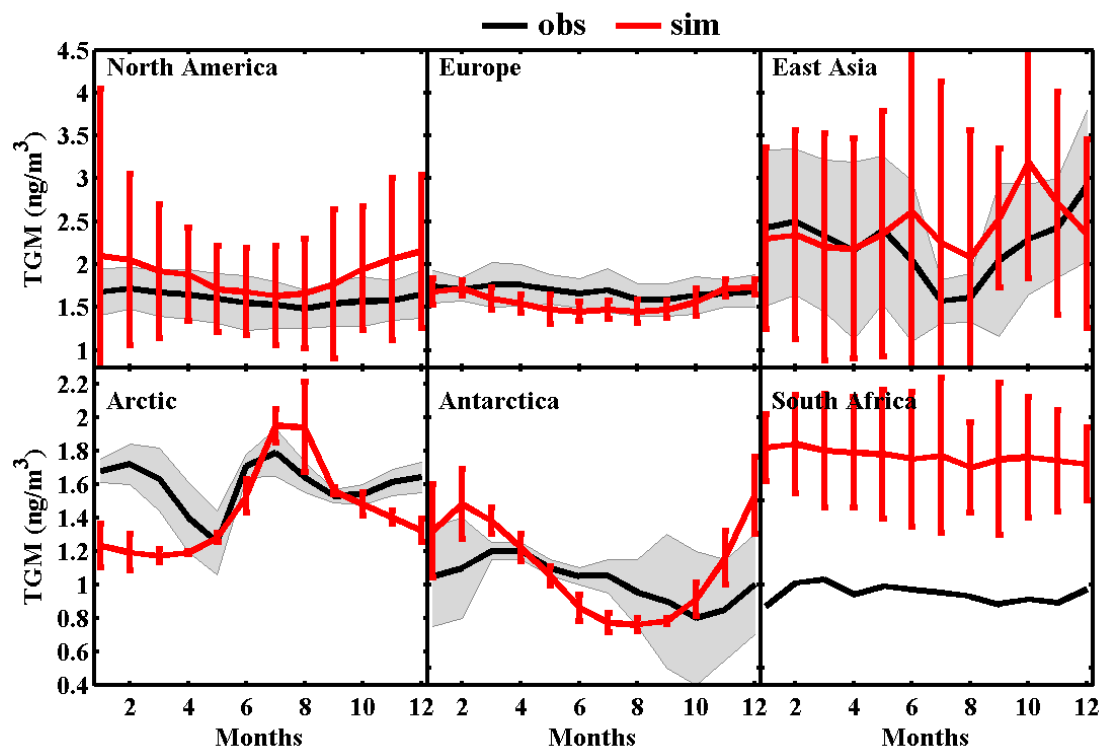


Fig. 5. Mean seasonal variation of TGM at North America, Europe, East Asia, Arctic, Antarctica and South Africa sites. Gray shaded areas and red vertical bars show one standard deviation over the sites for observations and for model results.

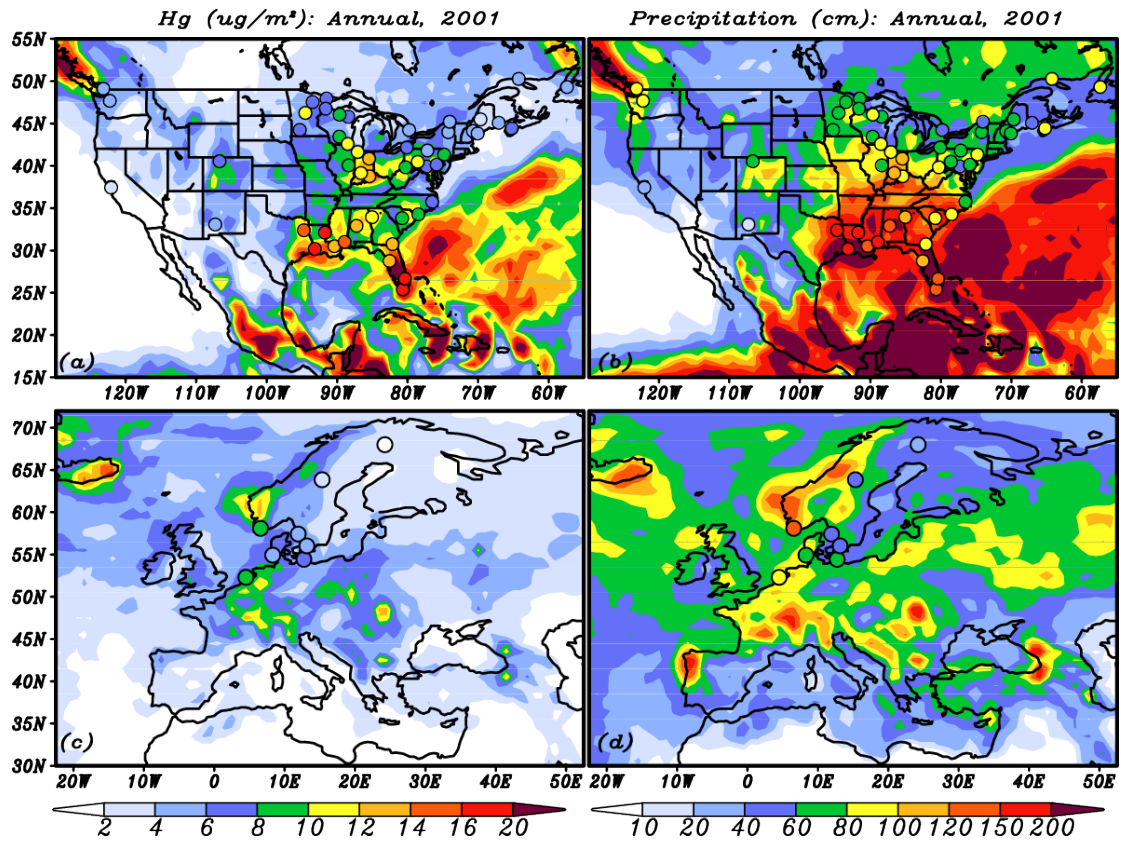


Fig. 6. Simulated annual mercury wet deposition and accumulated precipitation over North America (a, b) and Europe (c, d) in 2001. Overlaid points show observations for the same year from the Mercury Deposition Network (MDN) over North America, and the European Monitoring and Evaluation Programme (EMEP) over Europe.

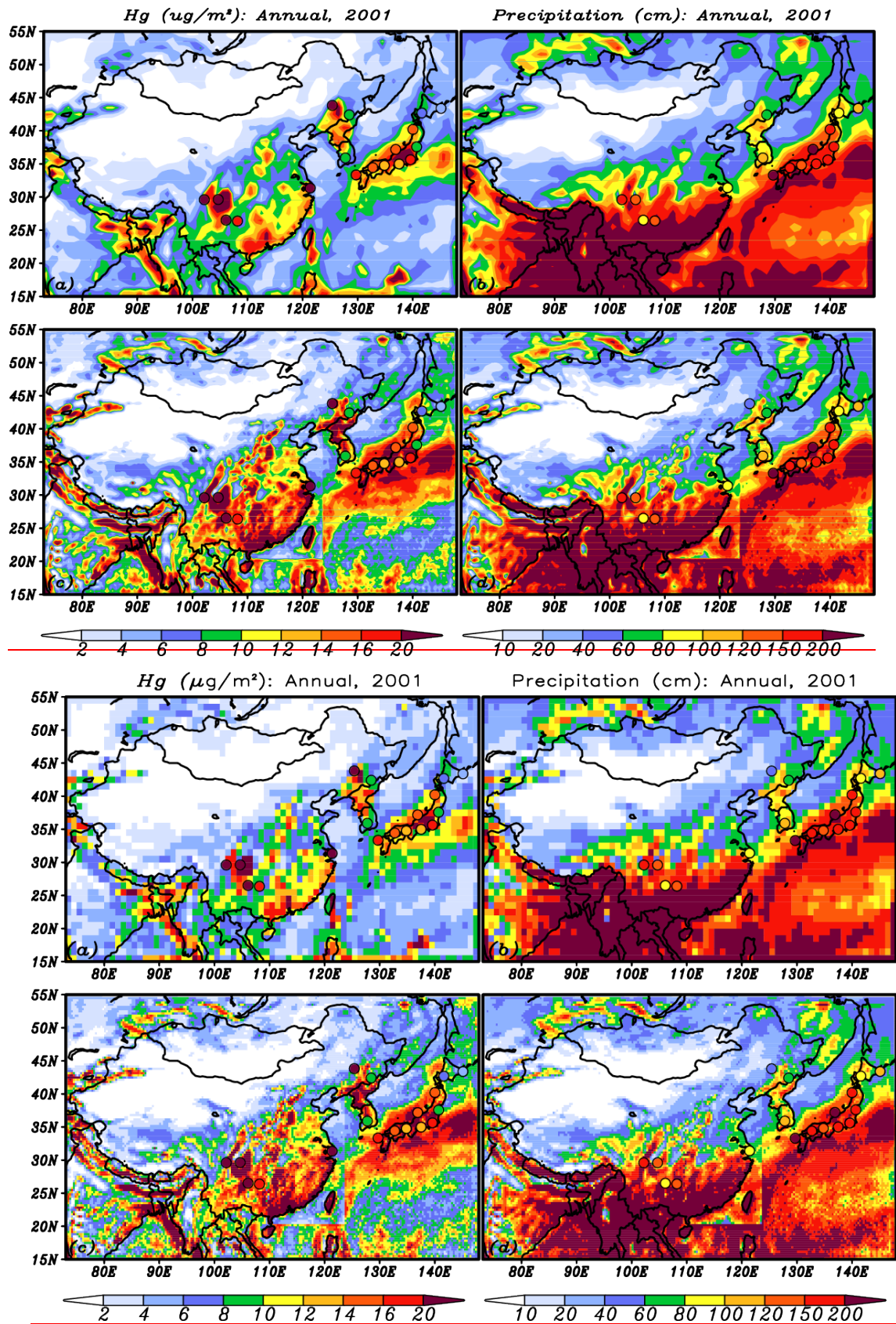


Fig. 7. Simulated annual mercury wet deposition and accumulated precipitation over East Asia in the global (a, b) and nested (c, d) domains in 2001. Overlaid points show observations collected

from the literature. Note that observations and simulated results are not in the same year.

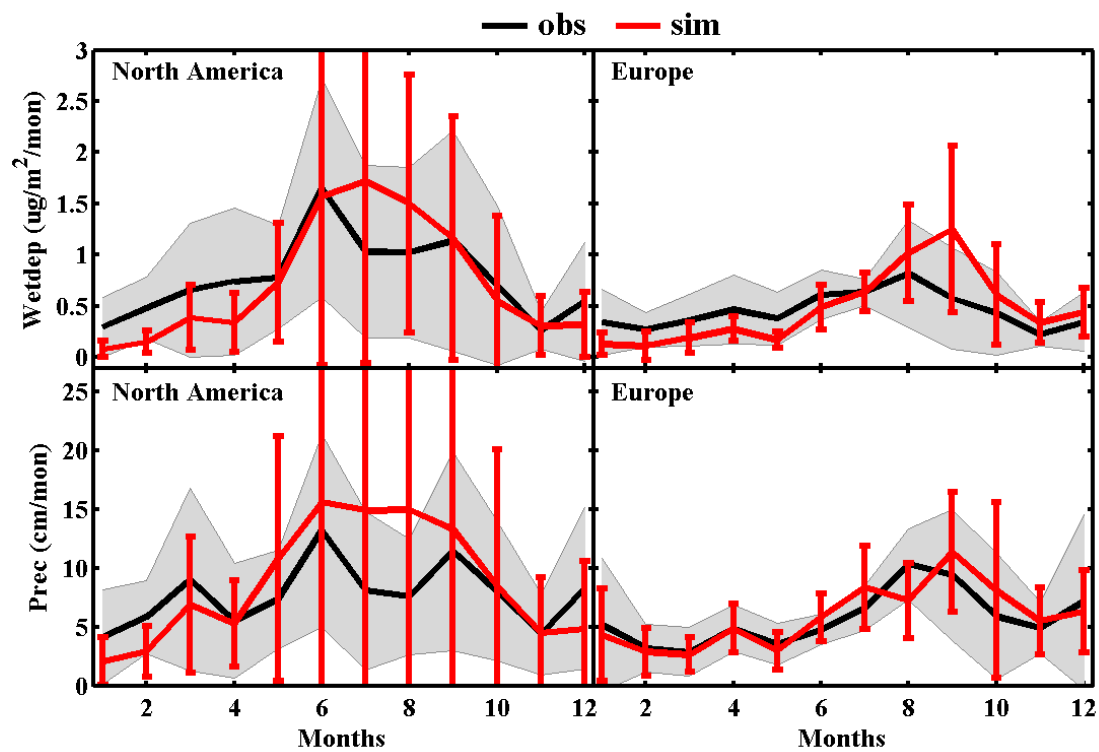


Fig. 8. Mean seasonal variation of mercury wet deposition and accumulated precipitation at North America (51 sites averaged) and Europe (8 sites averaged) sites in 2001. Gray shaded areas and red vertical bars show one standard deviation over the sites for observations and for model results.

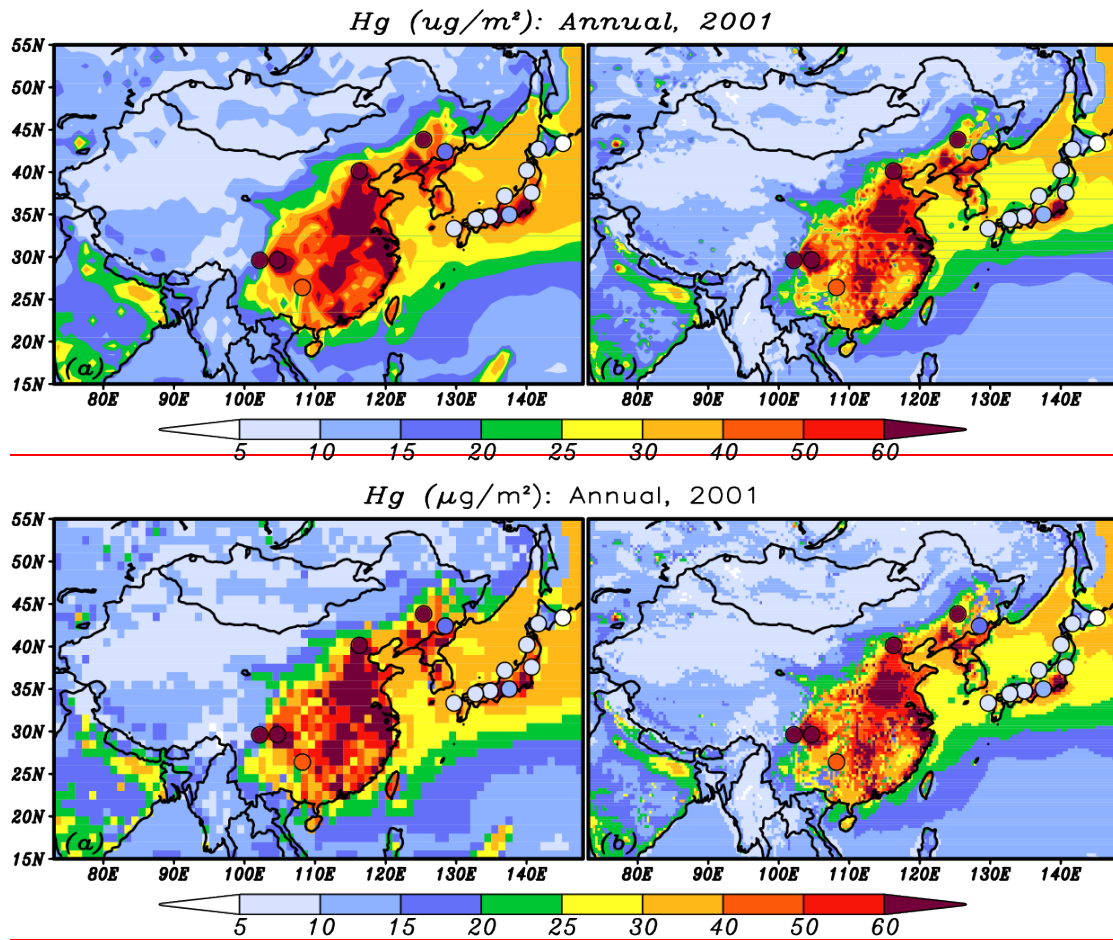


Fig. 9. Simulated annual mercury dry deposition over East Asia in the global (a) and nested (b) domains in 2001. Overlaid points show observations collected from the literature. Note that observations and simulated results are not in the same year.

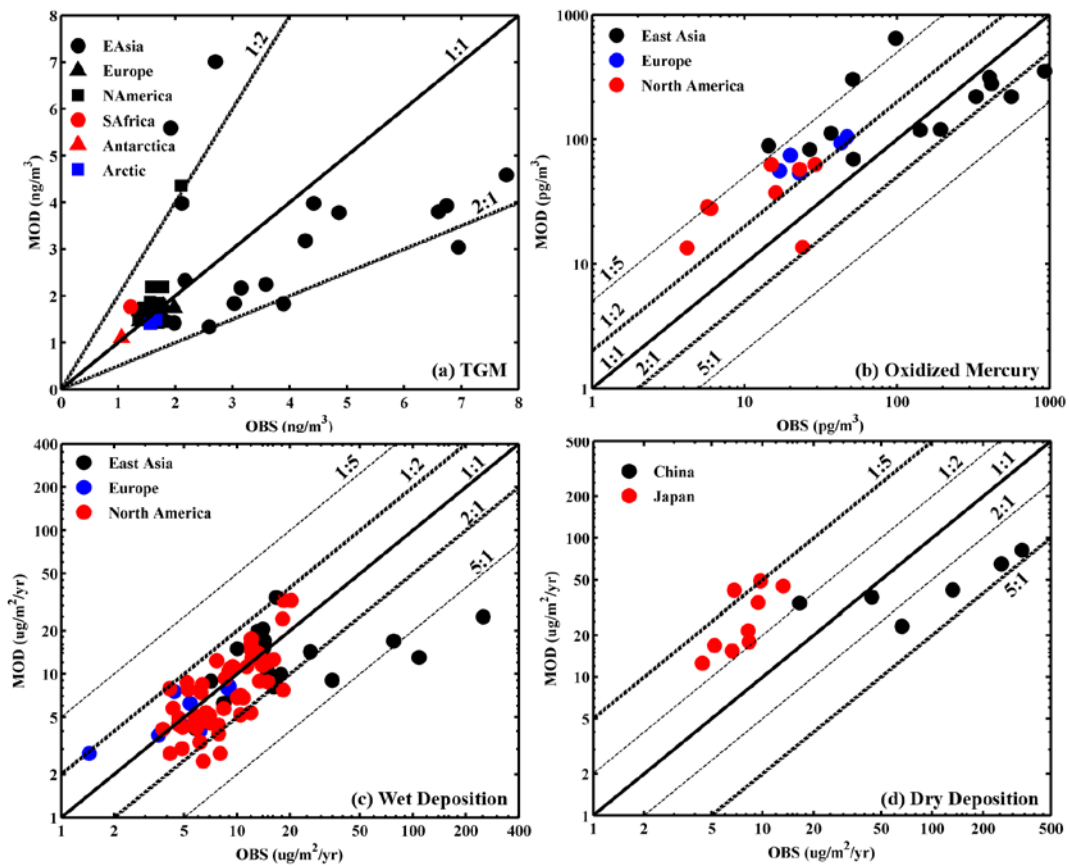


Fig. 10. Simulated vs. observed TGM (a), oxidized mercury (b), wet deposition (c), dry deposition (d) in different regions. Note that coordinates are different in different panels.

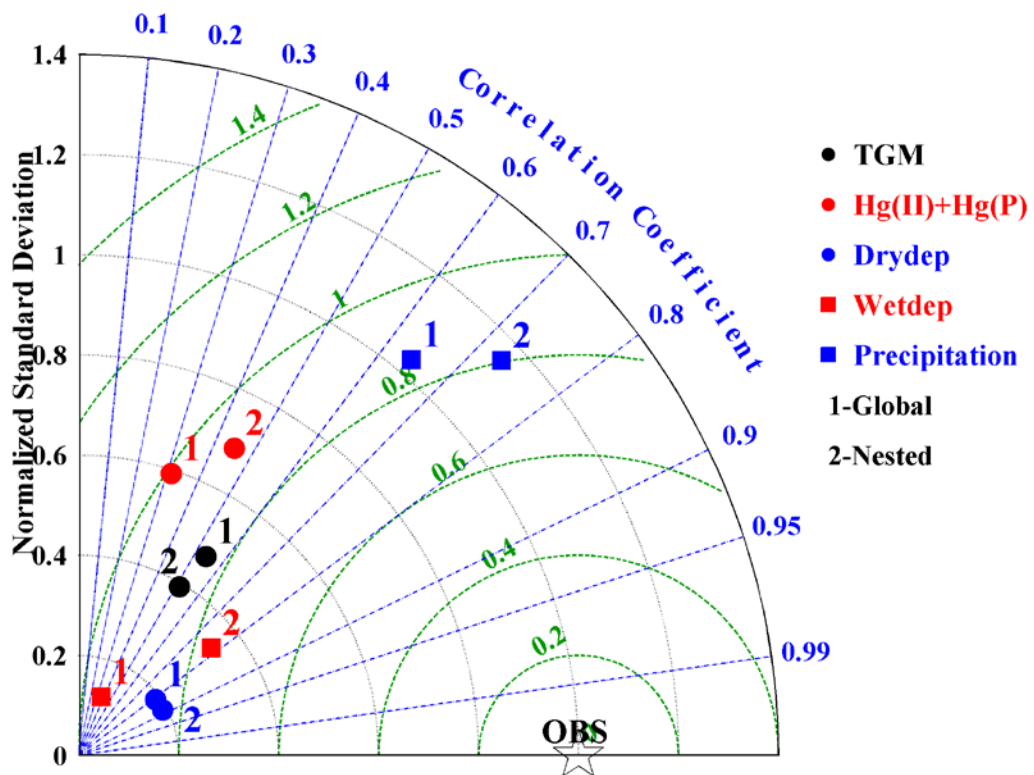


Fig. 11. Taylor Diagram of simulated annual TGM, Hg(II)+Hg(P), dry deposition, wet deposition and precipitation over East Asia in the global and nested domains (denoted by 1 and 2).

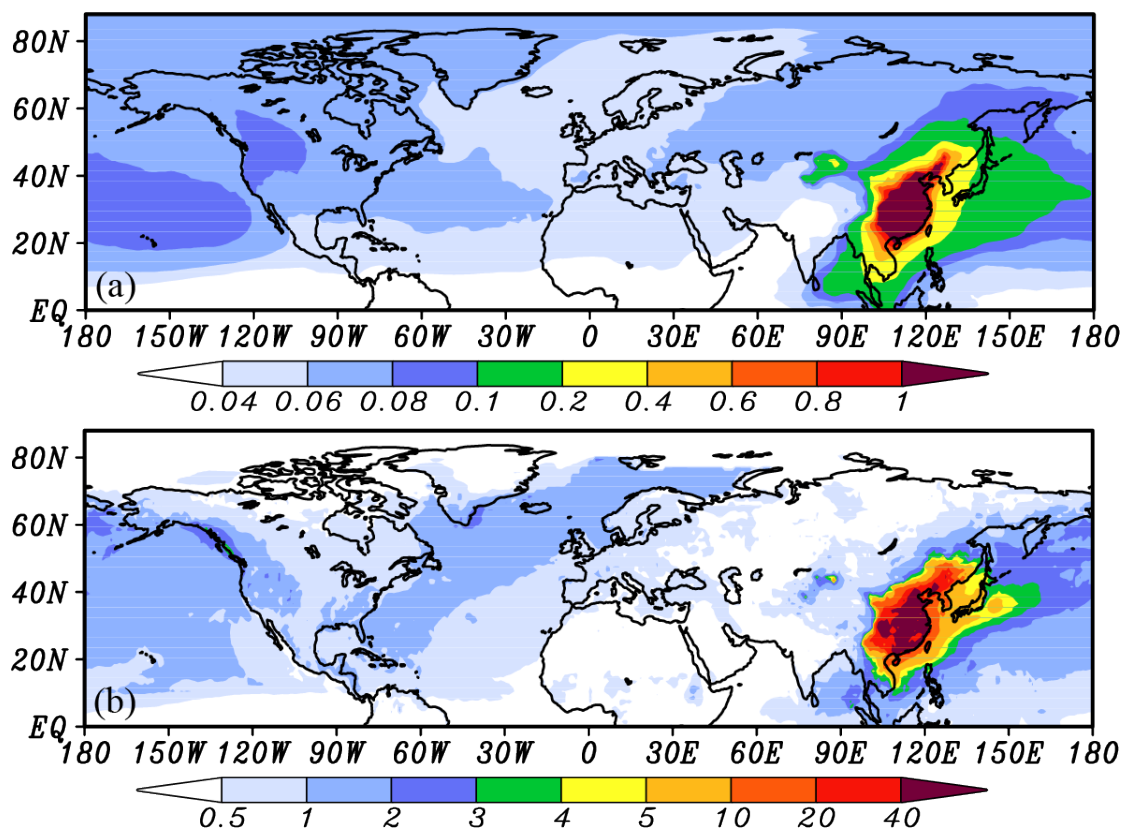


Fig. 12. Contributions of Chinese primary anthropogenic sources to (a) annual mercury surface concentrations and (b) total (wet plus dry) deposition in the Northern Hemisphere. The units for mercury concentrations and deposition are ng m^{-3} and ug m^{-2} , respectively.

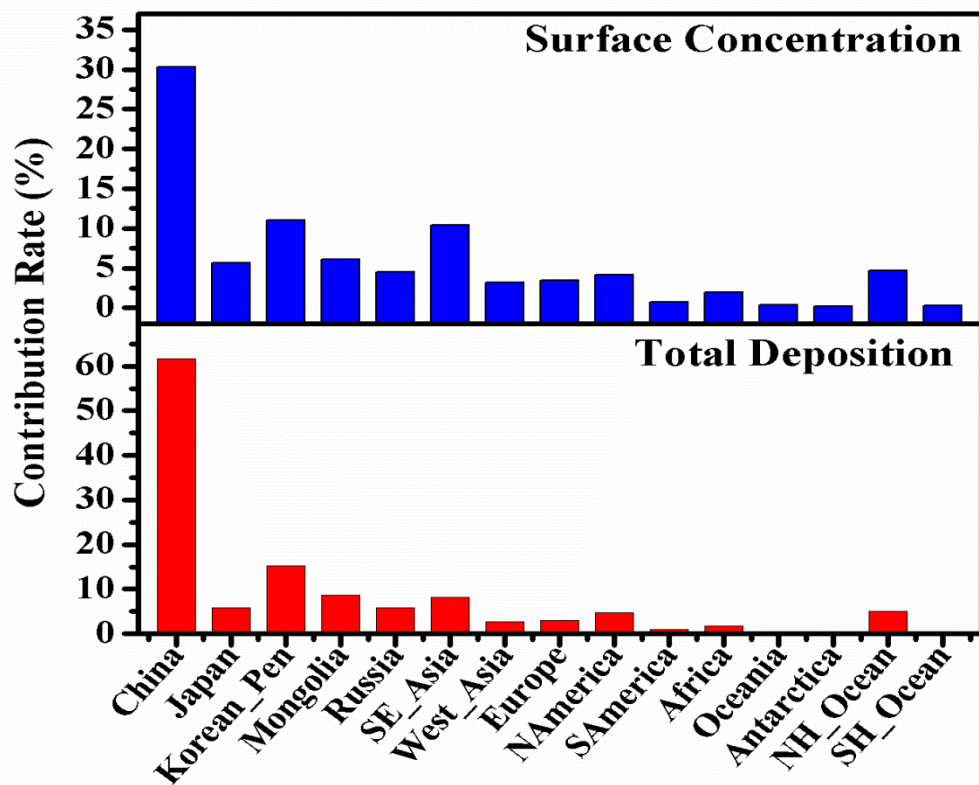


Fig. 13. Mean percentage contributions from Chinese primary anthropogenic sources to annual mercury surface concentrations and total (wet plus dry) deposition over different world regions.

The Supplement

Supplementary Material: GNAQPMS-Hg v1.0, a global nested atmospheric mercury transport model: Model description, evaluation and application to trans-boundary transport of Chinese anthropogenic emissions

H. S. Chen¹, Z. F. Wang¹, J. Li¹, X. Tang¹, B. Z. Ge¹, X. L. Wu¹, O. Wild², and G. R. Carmichael³

¹ LAPC, Institute of Atmospheric Physics, Chinese Academy of Sciences, Beijing, China

² Lancaster Environment Centre, Lancaster University, Lancaster, UK

³ Center for Global and Regional Environmental Research (CGRER), University of Iowa, Iowa City, Iowa, USA

Correspondence to: Z. F. Wang (zifawang@mail.iap.ac.cn)

S1 Mercury chemistry

S1.1 Bromine oxidation

As shown in Table S1, we add five Br chemical reactions in the gas phase (Seigneur and Lohman, 2008) in addition to the O₃-OH oxidation mechanism to test how the Br oxidation reactions affect the Hg distributions. Similar to the treatment of Holmes et al. (2006, 2010), the five reactions are treated as a single reaction, with an effective Hg(0) first-order rate constant that is a function of the individual reaction rates and the concentrations of Br, BrO and OH based on the assumption that Br, BrO and OH concentrations don't change by their reactions with Hg. This is also the same with the implementation described in CAMx (2014). The effective first-order rate constant is calculated as follows:

$$k_{eff} = \frac{k_1[Br](k_3[Br]+k_4[OH])}{k_2+k_3[Br]+k_4[OH]} + k_5[BrO] \text{ s}^{-1}$$

In the GNAQPMS-Hg model, Br and BrO are not explicitly simulated. Therefore, we specify typical vertical profiles of Br and BrO concentrations over land and ocean, with higher values over ocean (2.9x10⁻⁸ and 2.9x10⁻⁷ ppm for Br and BrO) than over land (5.0x10⁻⁹ and 5.0x10⁻⁸ ppm for Br and BrO). During the night, the concentrations of Br and BrO are assumed to be zero, considering that the photolysis of Br₂ is the primary source for these radicals.

S1.2 Gas-particle partitioning of Hg(II)

The mechanism of gas-particle partitioning of Hg(II) implemented in GNAQPMS-Hg is based on the studies of Rutter and Schauer (2007a, b). Similar mechanisms are also used by the CAMx model and Vijayaraghvan et al. (2008). Rutter and Schauer (2007a) suggest that surface area rather than particulate matter (PM) mass controls the Hg(II) partitioning process. The surface-area adsorption coefficient (K_{sa}) is calculated as follows:

$$K_{sa} = Hg_{p,ads} / (RGM \times A_{sp} \times PM)$$

where K_{sa} is in m³m⁻², $Hg_{p,ads}$ and RGM are in pg m⁻³, A_{sp} is the specific surface

area of PM in $\text{m}^2 \mu\text{r}^{-1}$ and PM is the ambient urban PM concentration in $\mu\text{g m}^{-3}$. Further, they also found that the K_{sa} obtained for urban PM falls between that of ammonium sulfate and adipic acid and it can be expressed as a function of temperature (K):

$$K_{sa} = 10^{\left(\frac{4250}{T} - 10\right)}$$

Besides, studies also found a ten-fold increase in adsorption of RGM to sodium chloride compared to ammonium sulfate and organic particulate compounds. Therefore, K_{sa} for sea-salt is about 10 times that for urban PM:

$$K_{sa} = 10^{\left(\frac{4250}{T} - 9\right)}$$

For simplicity, we treat all non-sea-salt PM as urban PM and use the above two equations to simulate RGM adsorption to urban PM and sea-salt PM, respectively. Therefore, the effective adsorption coefficient for each aerosol size section is calculated as follows:

$$K_{sa,eff} = 10^{\left(\frac{4250}{T} - 9\right)} \times F_{ss} + 10^{\left(\frac{4250}{T} - 10\right)} \times (1 - F_{ss})$$

where is F_{ss} the fraction of sea-salt in that size section.

S2 Mercury deposition

S2.1 Dry deposition

In the model, dry deposition is treated as a first-order removal mechanism. The deposition flux of a pollutant to the surface is the product of a characteristic deposition velocity and its concentration in the surface layer. Deposition velocities are derived from models that account for the reactivity, solubility, and diffusivity of gases, the sizes of particles, local meteorological conditions, and season-dependent surface characteristics. Dry deposition parameterizations of gases and aerosols are based on the work of Wesely (1989) and Slinn and Slinn (1980), respectively.

For gases, deposition velocity V_d is calculated from three primary resistances r (s m^{-1}) in series as described below.

$$V_d = \frac{1}{r_a + r_b + r_s}$$

The aerodynamic resistance r_a represents bulk transport through the lowest model layer by turbulent diffusion. The quasi-laminar sub-layer resistance r_b represents molecular diffusion through the thin layer of air directly in contact with the particular surface to which material is being deposited. The surface resistance r_c depends upon the physical and chemical properties of the surface.

For particles, surface deposition occurs via diffusion, impaction, and gravitational settling. Particle size is the dominant variable controlling these processes. Particle deposition velocity for a given aerosol size is calculated using the following resistance equation.

$$V_d = V_{sed} + \frac{1}{r_a + r_b + r_a r_b v_{sed}}$$

V_{sed} is the gravitational settling (or sedimentation) velocity which is dependent on aerosol size and density.

The detail formulations of how to calculate r_a , r_b , r_s and V_{sed} for gases and aerosols can be found in Wesely (1989) and Slinn and Slinn (1980) or the user's guide of the CAMx model (CAMx, 2014).

In the GNAQPMS-Hg model, dry deposition of Hg(0), Hg(II) and Hg(P) are all accounted for by adaption the parameterizations described above. Several physical properties (e.g. Henry's law constant, molecular weight, surface reactivity) of the Hg species are specified in order to calculate their deposition velocities. The Henry's Law constant for Hg(0) is set to be 0.11 M atm⁻¹ (Lin and Pehkonen, 1999) with a temperature factor of -4970 K (Clever et al., 1985), and the surface reactivity is set to zero. Hg(II) represents HgCl₂ and Hg(OH)₂. Its Henry's Law constant is assumed to be the same as HNO₃ because they have similar solubility (Bullock and Brehme, 2002). Like HNO₃, Hg(II) has a strong tendency to stick to surfaces and its dry deposition occurs readily, so the surface resistance for Hg(II) in the dry deposition scheme is set to zero. The Hg(P) dry deposition velocity is set equal to that for sulfate, similar to that applied in the CMAQ-Hg and STEM-Hg model (Bullock and Brehme, 2002; Pan et al., 2008).

S2.2 Wet deposition

In the model, wet deposition of the chemical species are calculated using an approach with medium complexity. In-cloud and below-cloud scavenging are included. The basic formulation implemented in the model is a scavenging approach in which the local rate of concentration change $\frac{\partial c}{\partial t}$ within or below a precipitating cloud depends on a scavenging coefficient Λ :

$$\frac{\partial c}{\partial t} = -\Lambda c$$

The scavenging coefficient is estimated differently for gases and particles, based on relationships described by Seinfeld and Pandis (1998). For gases, two components are calculated: 1) direct diffusive uptake of ambient gases into falling precipitation; and 2) accretion of cloud droplets that contain dissolved gases. For particles, there are also two components: 1) impaction of ambient particles into falling precipitation with an efficiency that is dependent upon particle size; and (2) accretion of cloud droplets that contain particle mass. Overall, the scavenging coefficient depends on an assumed scavenging efficiency, the total rainfall intensity (large-scale and convective precipitation), cloud water content and species solubility according to Henry's law, a mean cloud or rain droplet radius and rain droplet falling velocity. The large-scale and convective precipitation are not distinguished in this method. For species with low solubility (with a Henry's law constant of less than 100 M atm⁻¹), no wet deposition is calculated. More detail description of how to calculate the scavenging coefficients for gases and particles can be found in Seinfeld and Pandis (1998) or the user's guide of the CAMx model (CAMx, 2014). The physical properties (e.g. Henry's Law constant, surface reactivity, molecular diffusivity) of Hg species used in the wet deposition module are the same as those in the dry deposition module.

S3 Mercury emissions

The AMAP 2000 anthropogenic emission inventory was used in the model simulation. However, the emissions over South Africa in this inventory were reported to be flawed (AMAP/UNEP, 2008). Here, we assessed the effects of these flawed

emissions on the simulated results. As shown by Figure S7, we replaced the anthropogenic Hg emissions in South Africa by using the AMAP 2010 inventory and assessed this emission update on the simulated results. The emission amounts in South Africa decrease by about a factor of 4 (from 259 Mg to 64 Mg). After updating the emissions, the surface Hg concentrations in South Africa decrease by up to 1 ng m⁻³, but have little changes elsewhere (the differences of concentrations are smaller than 0.01 ng m⁻³ in most areas) as shown by Figure S8. The simulated TGM concentrations at Cape Point decrease from 1.77 ng m⁻³ to 1.23 ng m⁻³, more close to the observed values.

S4 Model evaluation

S4.1 Observational data

Due to limited public Hg observations, some model results were compared to observations with mismatched time periods. Actually, observations of wet deposition and precipitation in Europe and North America are from EMEP and MDN respectively, and the time periods are exactly the same with the simulation results. In contrast, no public Hg observation datasets are available in East Asia. So we used observations (collected from literatures) with mismatched time periods in East Asia.

All observations of Hg concentrations at land sites used in this study are averaged over time periods larger than 1 year. Analyses of long-term measurements show that trends in mean TGM during the last decade are small (of order 1%a⁻¹) or negligible at most background sites in the Northern Hemisphere (Temme et al., 2007; Wangberg et al., 2007). Therefore, the influences of the mismatch of time periods between model results and Hg concentration observations would not be large. Similar observational datasets (as shown in Table S2-S4) are also used by previous modeling studies (Selin et al., 2007, 2008; Holmes et al., 2010).

Observations from ship cruises are just used for initial comparison of simulated results over ocean following previous studies (Selin et al., 2007, 2008; Holmes et al., 2010). These observations are not used for quantitative model evaluation and not

including in the calculation of statistical parameters of model performance.

Annual dry and wet deposition measurements in East Asia (Table S5) are all obtained from literatures. Considering that dry and wet deposition fluxes are affected by environmental factors (e.g. precipitation) and they might differ from one year to another, so the influence of the mismatched time periods would be relatively larger. Again, no observations of Hg deposition are available at present. So there are no better choice.

Overall, the influence of the mismatch of the time periods between model results and observations is relatively large for dry and wet deposition comparisons in East Asia but relatively small for other comparisons. Quantitative assessments of the influence are difficult and outside the scope of this study.

S4.2 Diurnal and vertical variation

Fig. S12 shows the simulated averaged diurnal variation of surface TGM concentrations in Mt. Lulin (2862 m a.s.l.), Mt. Leigong (2178 m a.s.l.) and Mt. Changbai (741 m a.s.l.) in China. In Mt. Lulin, the simulated TGM concentrations exhibit a clear diurnal pattern, with higher concentrations in daytime but lower concentrations in nighttime. The daily maxima occurs in the afternoon. This simulated pattern is consistent with the observed results reported by Sheu et al. (2010). And they pointed out that this diurnal variation resulted from upslope movement of boundary layer air in daytime and subsidence of free troposphere air at night. The variation of TGM concentrations in Mt. Leigong is similar to that in Mt. Lulin and also agree with filed observations (Fu et al., 2010c). In Mt. Changbai, the diurnal variation of TGM shows different pattern. TGM peaks after sunrise and then decrease to the valley in the afternoon. Fu et al. (2012b) concluded that this variation was caused by regional transport.

Fig. S13 illustrates the simulated averaged vertical variation of TGM concentrations over the North Pacific Ocean (NPO) during April-May 2001. TGM concentrations over the south and north parts of NPO show similar vertical patterns. The highest concentrations are found at surface and then slowly decrease with altitude.

At all levels, higher TGM concentrations occur over the north part of NPO which is related to long-range transport of Hg(0) from mainland in middle latitude. These simulated results agree with aircraft observations conducted in the INTEX-B filed experiment (Singh et al., 2009) and are also comparable to the simulated results from GEOS-Chem (Holmes et al., 2010).

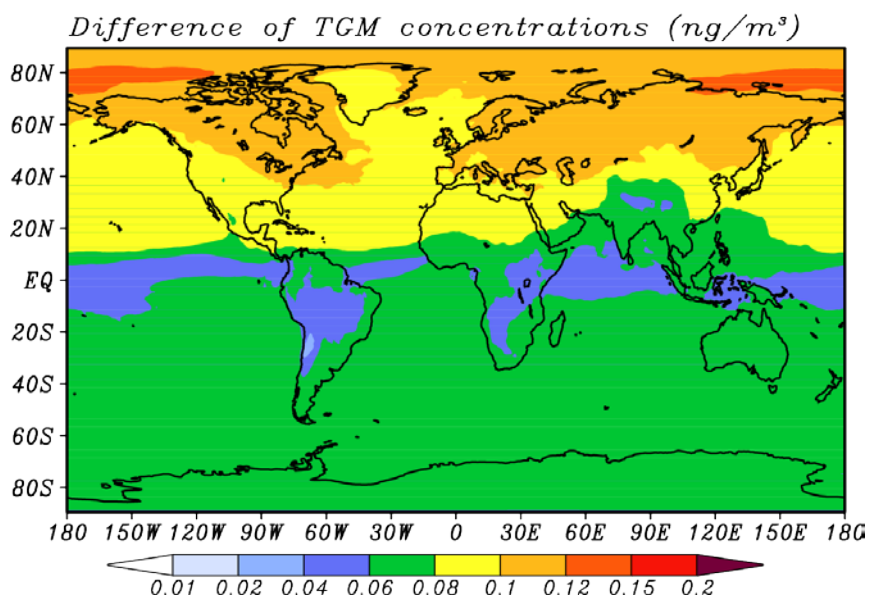


Fig. S1. Change in surface TGM concentrations (ng m⁻³) by introducing bromine chemistry (positive value means the TGM concentrations decrease after added bromine chemistry).

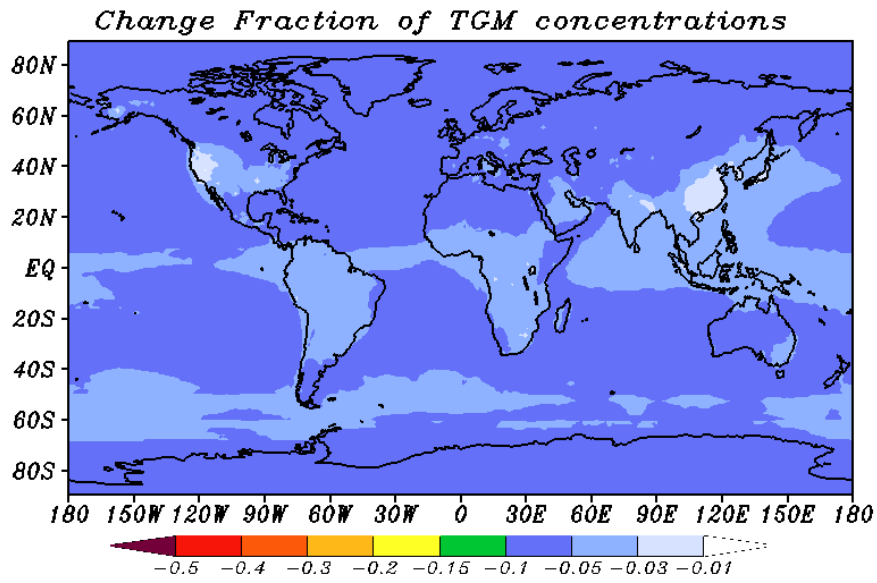


Fig. S2. Change fraction of surface TGM concentrations by introducing the mechanism of gas-particle partitioning of Hg(II) (negative value means the TGM concentrations decrease after introducing the mechanism).

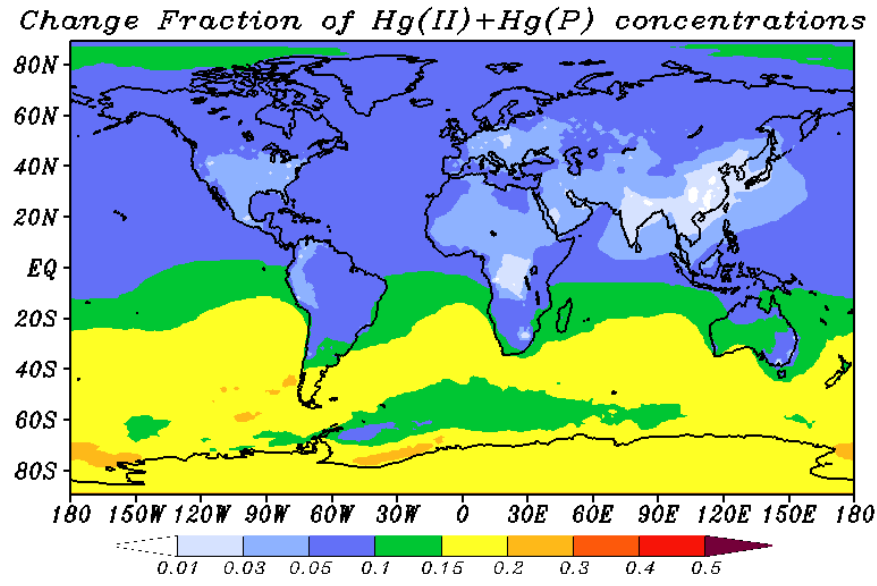


Fig. S3. Change fraction of surface Hg(II)+Hg(P) concentrations by introducing the mechanism of gas-particle partitioning of Hg(II) (positive value means the Hg(II)+Hg(P) concentrations increase after introducing the mechanism).

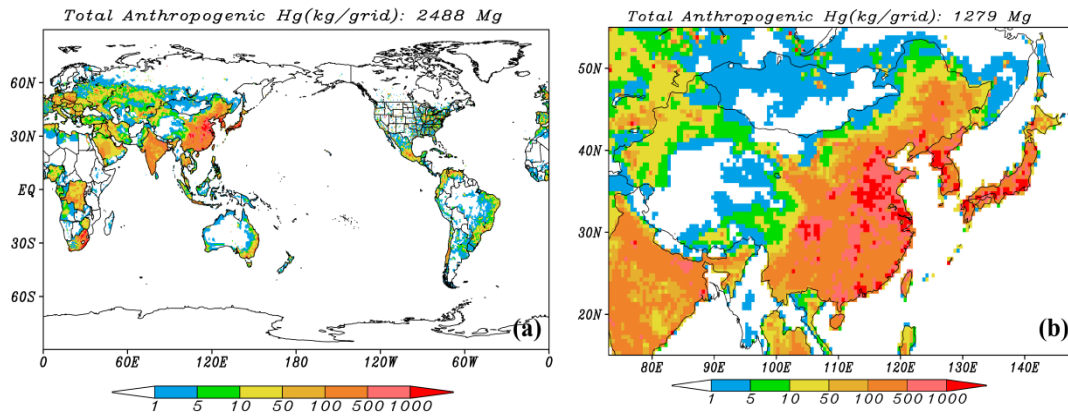


Fig. S41. Global (a) and East Asia (b) annual anthropogenic Hg emissions (kg/grid).

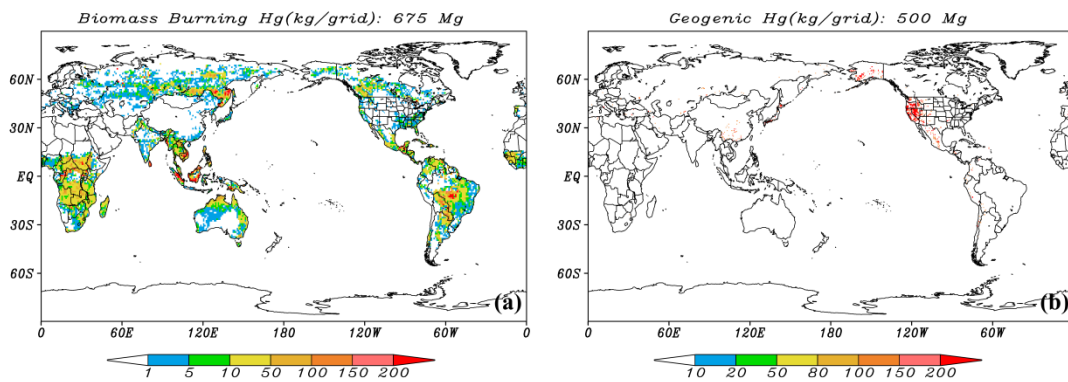


Fig. S52. Global annual biomass burning (a) and geogenic (b) Hg emissions (kg/grid).

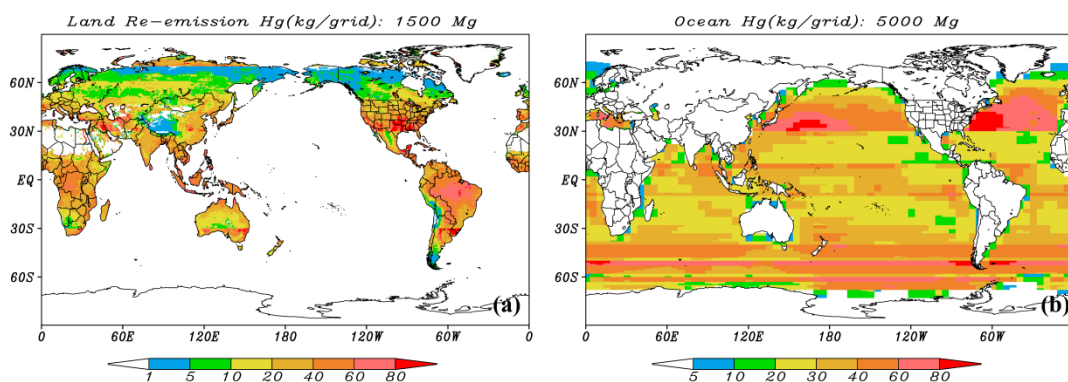


Fig. S63. Global annual land re-emission (a) and total ocean emissions (b) of Hg (kg/grid).

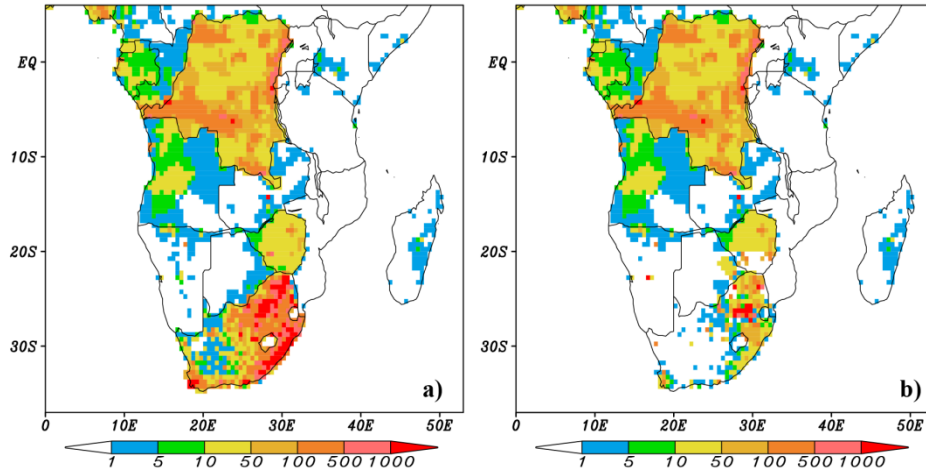


Figure S7. Annual anthropogenic Hg emissions (kg/grid) in South Africa, a) the AMAP 2000 inventory and b) the AMAP 2010 inventory in South Africa (16-34°E, 36-20°S) + the AMAP 2000 inventory elsewhere.

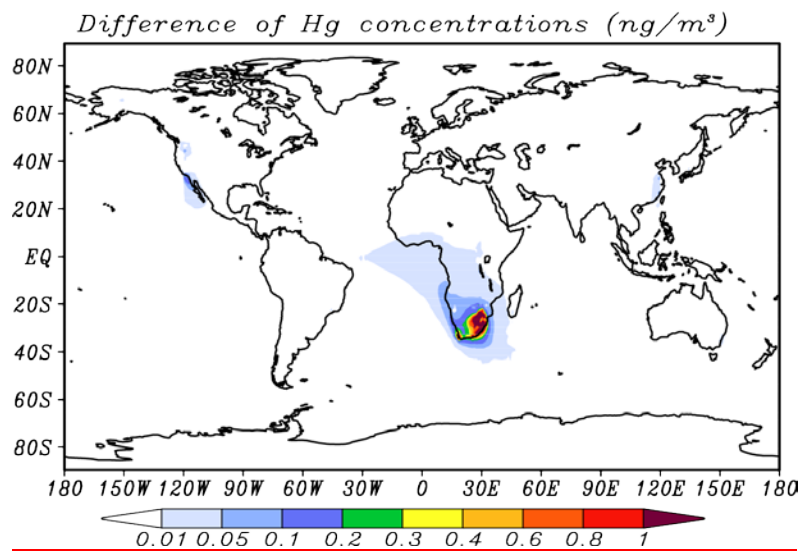


Figure S8. Difference of global surface Hg concentrations after updating the anthropogenic emissions in South Africa by using the AMAP 2010 inventory.

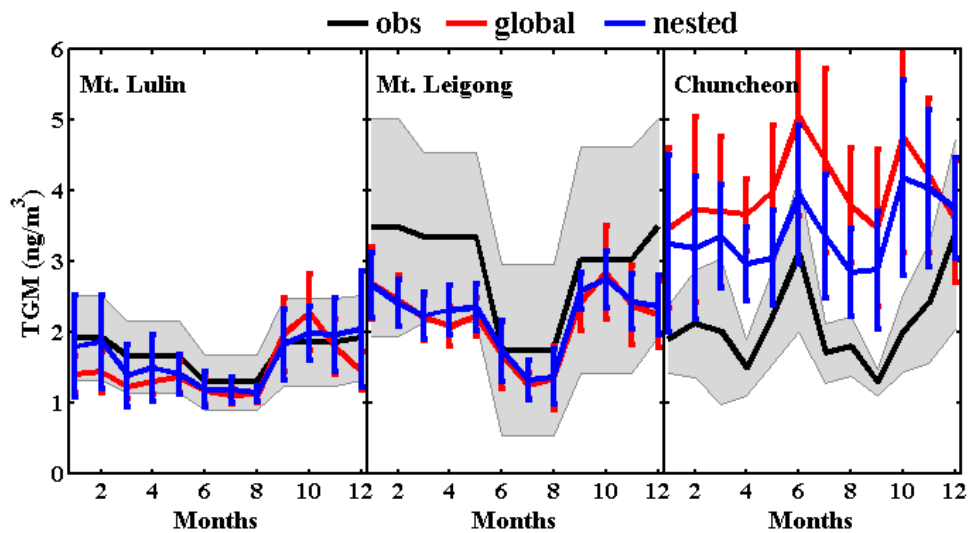


Fig. S9. Mean seasonal variation of TGM in Mt. Lulin and Mt. Leigong in China, and Chuncheon in Korea. Shaded areas and vertical bars show one standard deviation for observations and for model results.

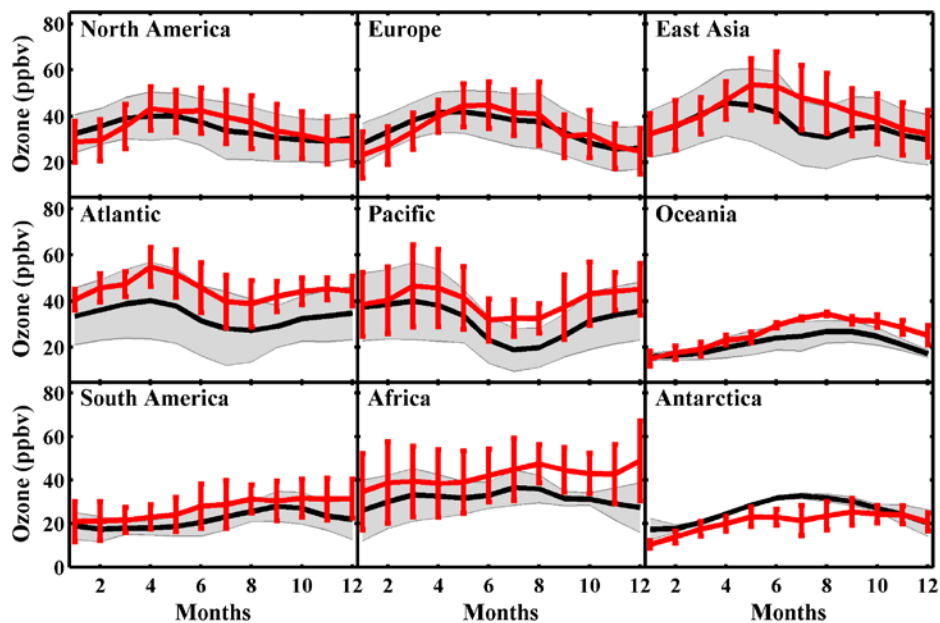


Fig. S104. Mean seasonal variation of surface ozone at 9 subregions in 2001. Gray shaded areas and red vertical bars show one standard deviation over the sites for observations and for model results. Observations are from the WDCGG (World Data Centre for Greenhouse Gases) and EANET (Acid Deposition Monitoring Network in East Asia) network.

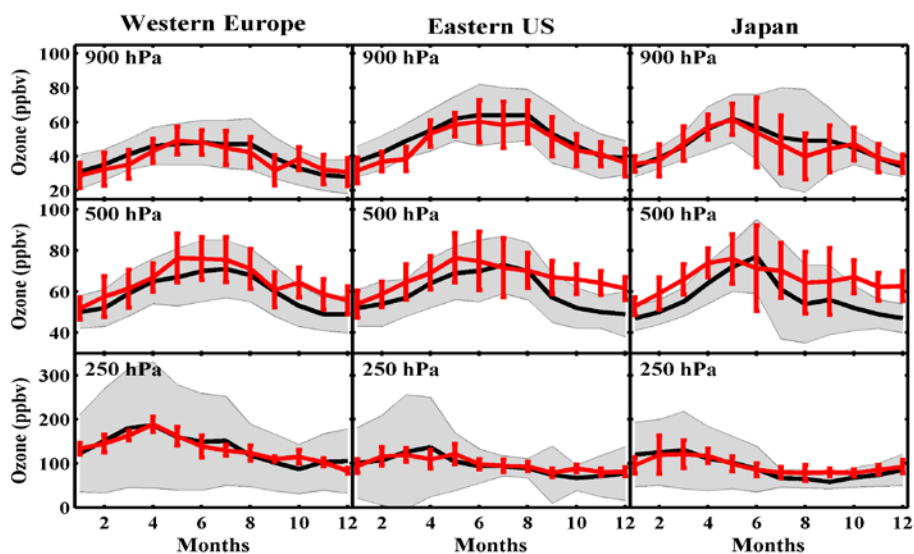


Fig. S115. Comparison of the ozone seasonal cycle between ozonesonde observations (black lines) and model results (red lines) in 900, 500 and 250 hPa in Western Europe, Eastern US and Japan. Gray shaded areas and red vertical bars show one standard deviation over the ozonesonde locations for observations and for model results. Observations are from Tilmes et al. (2012).

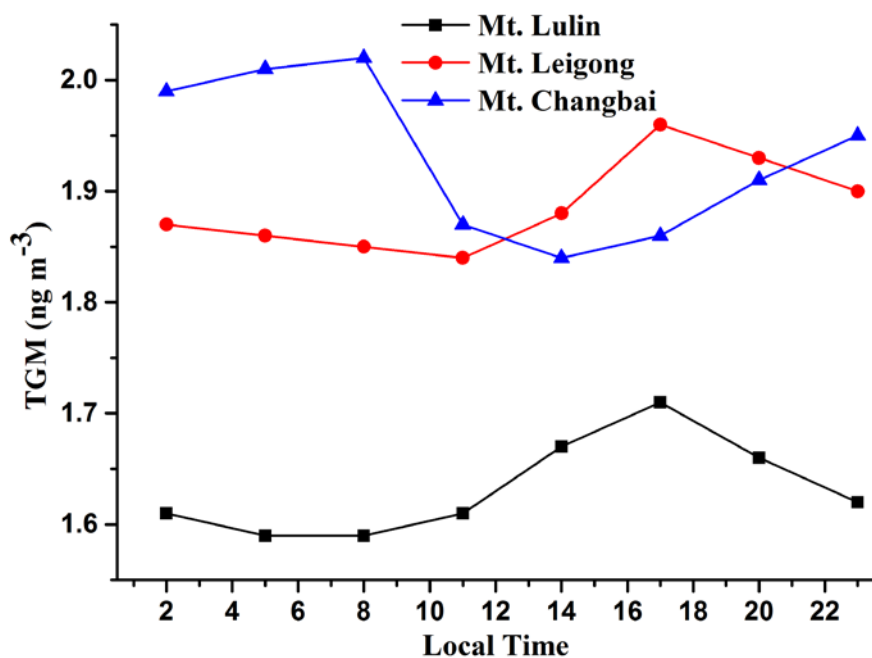


Fig. S12. Simulated averaged diurnal variation of surface TGM concentrations in Mt. Lulin, Mt. Leigong and Mt. Changbai in 2001.

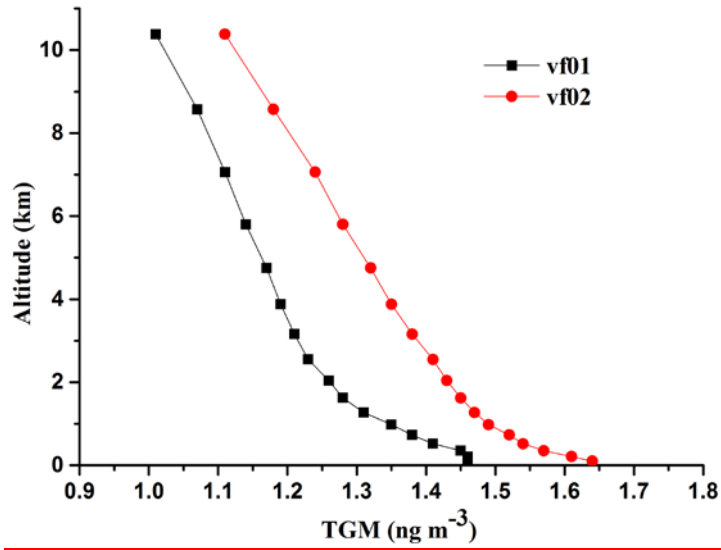


Fig. S13. Simulated averaged vertical variation of TGM concentrations over the North Pacific Ocean during April-May 2001. vf01 and vf02 stand for the vertical profile of TGM averaged over (19-25 N, 120° E-120° W) and (30-55°N, 150°E-150°W) respectively.

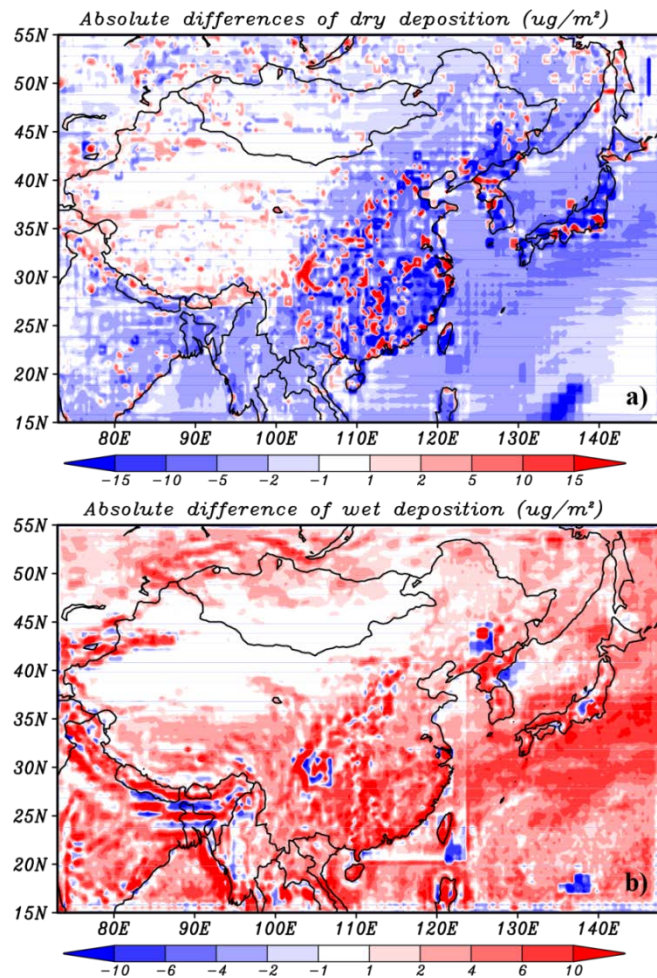


Figure S14. Absolute differences of annual dry and wet deposition over East Asia between the global and nested simulations (Nested-Global).

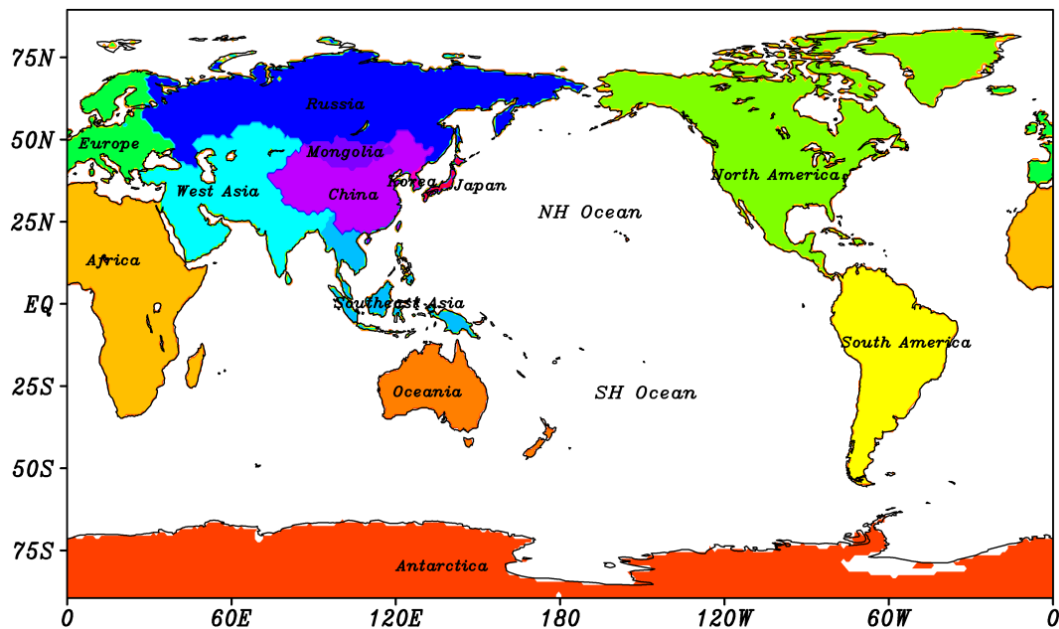


Fig. S156. 15 geographical areas used in this study, colors represent subregions over land while ocean is divided into two parts used the equator as boundary.

Table S1. Bromine reactions added in the model (T is the temperature in degrees Kelvin, and P is the pressure in atmospheres).

<u>NO.</u>	<u>Reaction</u>	<u>Rates</u>
<u>BR1</u>	<u>Hg(0)(g)+Br(g)→HgBr(g)</u>	$k1 = 3.6 \times 10^{-13} P \left(\frac{T}{298}\right)^{-1.86} \text{ cm}^3 \text{ molec}^{-1} \text{ s}^{-1}$
<u>BR2</u>	<u>HgBr(g)→Hg(0)(g)</u>	$k2 = 3.9 \times 10^9 \exp\left(\frac{-8537}{T}\right) \text{ s}^{-1}$
<u>BR3</u>	<u>HgBr(g)+Br(g)→HgBr₂(g)</u>	$k3 = 2.5 \times 10^{-10} \left(\frac{T}{298}\right)^{-0.57} \text{ cm}^3 \text{ molec}^{-1} \text{ s}^{-1}$
<u>BR4</u>	<u>HgBr(g)+OH(g)→HgBrOH(g)</u>	$k4 = 2.5 \times 10^{-10} \left(\frac{T}{298}\right)^{-0.57} \text{ cm}^3 \text{ molec}^{-1} \text{ s}^{-1}$
<u>BR5</u>	<u>Hg(0)(g)+BrO(g)→Hg(II)(g)</u>	$k5 = 1.0 \times 10^{-15} \text{ cm}^3 \text{ molec}^{-1} \text{ s}^{-1}$

Table S21. Long-term TGM/GEM measurements used for model evaluation (ng m^{-3}).

Site ^a	Years	Conc ^b	Reference
Alert, Canada (83N, 62W) [*]	1995-2002	1.55	Environment Canada (2003)
FortChipewyan, Canada (59N, 111W)	2000-2001	1.36	Temme et al. (2007)
Kuujuarapik, Canada (56N, 78W) [*]	1999-2000	1.82 [#]	Steffen et al. (2005)
Esther, Canada (52N, 110W)	1997-1999	1.65	Kellerhals et al. (2003)
Mingan, Canada (50N, 64W)	1997-1999	1.62	Kellerhals et al. (2003)
Bratts Lake, Canada (50N, 105W)	2001-2005	1.53	Temme et al. (2007)
Reifel Island, Canada (49N, 123W) [*]	1997-1999	1.67	Kellerhals et al. (2003)
Delta, Canada (49N, 123W)	1999-2001	1.73	Environment Canada (2003)
Burnt Island, Canada (46N, 83W)	1997-1999	1.58	Kellerhals et al. (2003)
St.Andrews, Canada (45N, 67W) [*]	1997-1999,2001	1.42	Environment Canada (2003)
St.Anicet, Canada (45N, 74W) [*]	1997-1999,2001	1.64	Kellerhals et al. (2003); Poissant et al. (2005)
Kejimkujik, Canada (44N, 65W) [*]	2001	1.45	Environment Canada (2003)
Egbert, Canada (44N, 80W)	1997-1999	1.67	Kellerhals et al. (2003)
Pt.Petre, Canada (44N, 77W)	1997-1999	1.78	Kellerhals et al. (2003)
Cheeka Peak, USA (48N, 125W) [*]	2001-2002	1.56	Weiss-Penzias et al. (2003)
NewcombNY, USA (43N, 74W) [*]	2006-2007	1.45	Choi et al. (2008)
PacMonadnock, USA (43N, 72W) [*]	2007	1.38 [#]	Sigler et al. (2009)
RenoDRI, USA (40N, 120W) [*]	2002-2005	2.10	Stamenkovic et al. (2007)
AthensOH, USA (39N, 82W) [*]	2004-2005	1.63 [#]	Yatavelli et al. (2006)
PensacolaOLF, USA (31N, 87W) [*]	2004-2006	1.34 [#]	Edgerton et al. (2006)
Pallas, Finland (68N, 24E) [*]	1998-2002	1.38	EMEP (2005)
Zingst, Germany (55N, 13E) [*]	2000	1.64	EMEP (2005)
Neuglobsow, Germany (53N, 13E) [*]	2004-2005	1.70	EMEP (2009)
Langenbruegge, Germany (53N, 11E) [*]	2002	1.98	EMEP (2005)
Mace Head, Ireland (54N, 10W) [*]	1995-2001	1.69	Ebinghaus et al. (2002)
SanLucido, Italy (39N, 16E)	2004-2005	1.80	EMEP (2009)
Zeppelin, Norway (79N, 12E) [*]	2000-2004	1.58	EMEP (2005)
Andoya, Norway (69N, 16E) [*]	2004	1.66	EMEP (2009)
Birkenes, Norway (58N, 8E) [*]	2005-2007	1.82	EMEP (2009)
Lista, Norway (58N, 7E) [*]	2000-2003	1.70	EMEP (2005)
Anderma, Russia (70N, 62E) [*]	2001-2003	1.66 [#]	Steffen et al. (2005)
CaboDeCreus, Spain (42N, 3E) [*]	2005	1.73	EMEP (2009)
Rao, Sweden (57N, 12E) [*]	2001	1.66	EMEP (2005)
Rorvik, Sweden (57N, 12E) [*]	2001-2002	1.66	EMEP (2005)
Cape Point, South Africa (34S, 19E) [*]	1998-2002, 2007-2008	1.22	Baker et al. (2002); Slemr et al. (2011)
Neumayer, Antarctica (70S, 8W) [*]	2000	1.06	Ebinghaus et al. (2002)

Changchun, China (44N, 125E)	1999-2000	15.10	Fang et al. (2004)
ChangbaiMt, China (42N, 129E)	2005-2006	3.15	Wan et al. (2009a)
Beijing, China (40N, 116E)	2005	6.60 [#]	Wang et al. (2007)
Chengshantou, China (37N, 123E)	2007-2009	2.17 [#]	Ci et al. (2011a)

Table S21. Continued.

Site ^a	Years	Conc ^b	Reference
Waliguan,China (36N, 101E)	2007-2008	1.98	Fu et al. (2012a)
Shanghai, China (31N, 121E)	2008-2010	7.79	Zhang et al. (2012)
GonggaMt, China (30N, 102E)	2005-2006	3.89	Fu et al. (2008a)
Chongqing, China (30N, 107E)	2006-2007	6.74 [#]	Yang et al. (2009)
Shangri-La, China (28N, 100E)	2009-2010	2.59	Zhang (2011)
Guiyang, China (27N, 107E)	2001-2002	6.95	Feng et al. (2004)
LeigongMt, China (26N, 108E) *	2008-2009	3.03 [#]	Fu et al. (2010c)
LulinMt, China (24N, 121E) *	2006-2007	1.62 [#]	Sheu et al. (2010)
Guangzhou, China (23N, 113E)	2010-2011	4.86	Liu et al. (2012)
Tokyo, Japan (36N, 140E)	2000-2001	2.70	Sakata and Marumoto (2002);
Chiba, Japan (36N, 140E)	1991-1996	11.90	Nakagawa and Hiromoto (1997)
Hayama, Japan (35N, 140E)	1991-1996	13.20	Nakagawa and Hiromoto (1997)
Chuncheon, Korea (38N, 127E) *	2006-2009	2.11	Holmes et al. (2010)
Seoul, Korea (37N, 127E)	1997-2002	4.42	Kim et al. (2005)
Kanghwa, Korea (37N, 126E)	2008-2009	1.92	Han et al. (2011)
An-Myun,Korea (37N, 126E)	2005	4.27	Nguyen et al. (2007)
Jeju Island, Korea (33N, 126E)	2006-2007	3.58	Nguyen et al. (2010)

^a Asterisk indicates that monthly mean observations are also available from the references.

^b Pound sign indicates GEM measurements.

Table S32. Mercury measurements from ship cruises used for model evaluation.

Cruise	Region	Date	Obs	Reference
Lamborg1999	South and equatorial Atlantic Ocean	May to Jun, 1996	TGM	Lamborg et al. (1999)
Temme2003	Atlantic Ocean	Feb 2001	TGM	Temme et al. (2003)
Laurier2003	North Pacific Ocean	May to Jun, 2002	TGM/RGM	Laurier et al. (2003)
Soerensen2010	North Atlantic, Indian Ocean, South Pacific	Aug 2006 to Apr 2007	GEM	Soerensen et al. (2010)
Fu2010	South China Sea	Aug 2008	GEM	Fu et al. (2010a)
Ci2011	Yellow Sea	Jul 2010	GEM	Ci et al. (2011b)

Table S43. Long-term RGM and TPM measurements used for model evaluation (pg m^{-3})^a.

Site	RGM	TPM	Total	Period	Reference
St.Anicet, Canada (45N, 74W)	3	26	29	2003	Poissant et al. (2005)
Barrow, USA (71N, 157W)	24	NA	24	1999-2001	Landis et al. (2002)
Potsdam, USA (45N, 75W)	4.2	NA	4.2	2002-2003	Han et al. (2005)
Sterling, USA (43N, 77W)	6	NA	6	2002-2003	Han et al. (2005)
Stockton, USA (42N, 79W)	5.7	NA	5.7	2002-2003	Han et al. (2005)
Durham, USA (36N, 79W)	16	NA	16	1999-2001	Landis et al. (2002)
Baltimore, USA (32N, 77W)	23	NA	23	1999-2001	Landis et al. (2002)
Everglades, USA (26N, 81W)	15	NA	15	1999-2001	Landis et al. (2002)
Zingst, Germany (55N, 13E)	25	22	47	1998-1999	Munthe et al. (2003)
Neuglobsow, Germany (53N, 13E)	18	25	43	1998-1999	Munthe et al. (2003)
Mace Head, Ireland (54N, 10W)	18	5	23	1998-1999	Munthe et al. (2003)
Avspretten, Sweden (58N, 17E)	8	9	17	1998-1999	Munthe et al. (2003)
Rorvik, Sweden (57N, 12E)	15	5	20	1998-1999	Munthe et al. (2003)
Changchun, China (44N, 125E)	NA	192.5	192.5	1999-2000	Fang et al. (2004)
ChangbaiMt, China (42N, 129E)	65	77	142	2005-2006	Wan et al. (2009b)
Beijing, China (40N, 116E)	NA	930	930	2003-2004	Wang et al. (2006)
Waliguan,China (36N, 101E)	7.4	19.4	26.8	2007-2008	Fu et al. (2012a)
Hefei, China (32N, 117E)	NA	330	330	2008-2009	Wang (2010)
Shanghai, China (31N, 121E)	NA	560	560	2004-2006	Xiu et al. (2009)
GonggaMt, China (30N, 102E)	6.2	30.7	36.9	2005-2006	Fu et al. (2008b)
Chongqing, China (30N, 107E)	NA	416	416	2005	Wu (2006)
Shangri-La, China (28N, 100E)	8.2	43.5	51.7	2009-2010	Zhang (2011)
Guiyang, China (27N, 107E)	35.7	368	403.7	2009	Fu et al. (2011)
LulinMt, China (24N, 121E)	12.1	2.3	14.4	2006-2007	Sheu et al. (2010)
Seoul, Korea (38N, 127E)	27.2	23.9	51.1	2005-2006	Kim et al. (2009)
Tokyo, Japan (36N, 140E)	NA	98	98	2000-2001	Sakata and Marumoto (2002)

^a The sum of RGM and TPM is defined as total oxidized mercury and compared to the sum of Hg(II)+Hg(P) in the model.

Table S54. Long-term dry and wet depositions measurements in East Asia used for model evaluation (Units for deposition and precipitation are $\mu\text{g m}^{-2} \text{yr}^{-1}$ and mm).

Site	Lat	Lon	Period	Dry	Wet	Prec	Reference
ChangbaiMt, China	42.4	128.5	2005-2006	16.5	8.4	613	Wan et al. (2009b)
Changchun, China	43.8	125.4	1999-2000	131.8	108.0	567	Fang et al. (2004)
Beijing, China	40.1	116.3	2003	338.3	NA	NA	Wang et al. (2006)
Shanghai, China	31.4	121.4	2008-2009	NA	250.5	947	Zhang et al. (2010)
Chongqin, China	29.6	104.7	2005-2006	256.0	77.6	1403	Wang et al. (2009)
GonggaMt, China	29.6	102.2	2005-2007	66.4	26.1	1818	Fu et al. (2010b)
Wujiang, China	26.5	106.1	2006	NA	34.7	963	Guo et al. (2008)
LeigongMt, China	26.4	108.2	2005-2006, 2008-2009	44.0	16.2	1437	Fu et al. (2010c) Wang et al. (2009)
Bekkai, Japan	43.4	145.1	2002-2003	4.4	5.8	1117	Sakata and Marumoto (2005)
Hayakita, Japan	42.7	141.6	2002-2003	5.2	7.1	882	Sakata and Marumoto (2005)
Akita, Japan	40.2	140.0	2002-2003	9.4	14.9	1576	Sakata and Marumoto (2005)
Fukushima, Japan	37.6	140.7	2002-2003	6.8	10.0	1599	Sakata and Marumoto (2005)
Ishikawa, Japan	37.2	136.9	2002-2003	6.6	14.2	2076	Sakata and Marumoto (2005)
Tokyo, Japan	35.6	139.6	2002-2003	NA	16.7	1912	Sakata and Marumoto (2005)
Aichi, Japan	35.0	137.5	2002-2003	13.2	13.1	1679	Sakata and Marumoto (2005)
Hyogo, Japan	34.8	134.8	2002-2003	8.2	14.0	1481	Sakata and Marumoto (2005)
Hiroshima, Japan	34.4	132.7	2002-2003	9.7	14.3	1624	Sakata and Marumoto (2005)
Nagasaki, Japan	33.3	129.7	2002-2003	8.3	17.7	2317	Sakata and Marumoto (2005)
Korea	35.9	127.8	2006-2008	NA	9.4	1068	Ahn et al. (2011)

Table S6. Hg budgets over East Asia (15-55°N, 75-145°E) in the global and nested simulations (Unit: Mg yr⁻¹).

	<u>global domain</u>	<u>nested domain</u>	<u>nested/global</u>
<u>Total Sources</u>	<u>1461</u>	<u>1461</u>	<u>1.00</u>
<u>anthropogenic</u>	<u>979</u>	<u>979</u>	<u>1.00</u>
<u>land</u>	<u>269</u>	<u>269</u>	<u>1.00</u>
<u>ocean</u>	<u>213</u>	<u>213</u>	<u>1.00</u>
<u>Total Sinks</u>	<u>824</u>	<u>843</u>	<u>1.02</u>
<u>Wet deposition</u>	<u>182</u>	<u>278</u>	<u>1.53</u>
<u>Dry deposition</u>	<u>642</u>	<u>565</u>	<u>0.88</u>
<u>TGM burden</u>	<u>548</u>	<u>512</u>	<u>0.93</u>

References

- Ahn, M. C., Yi, S. M., Holsen, T. M., and Han, Y. J.: Mercury wet deposition in rural Korea: concentrations and fluxes, *J. Environ. Monit.*, 13, 2748-2754, doi:10.1039/c1em10014a, 2011.
- [AMAP/UNEP: Technical Background Report to the Global Atmospheric Mercury Assessment, Tech. rep., Arctic Monitoring and Assessment Programme / UNEP Chemicals Branch, http://www.unep.org/hazardoussubstances/, 2008.](http://www.unep.org/hazardoussubstances/)
- Baker, P. G. L., Brunke, E. G., Slemr, F., and Crouch, A. M.: Atmospheric mercury measurements at Cape Point, South Africa, *Atmos. Environ.*, 36, 2459-2465, 2002.
- [Bullock, O. R., and Brehme, K. A.: Atmospheric mercury simulation using the CMAQ model: formulation description and analysis of wet deposition results, Atmos. Environ., 36, 2135-2146, doi:10.1016/s1352-2310\(02\)00220-0, 2002.](https://doi.org/10.1016/s1352-2310(02)00220-0)
- [CAMx: CAMx, user's guide, version 6.1, Environ International Corporation, California, 2014.](https://www.camx.com/)
- Choi, H. D., Holsen, T. M., and Hopke, P. K.: Atmospheric mercury (Hg) in the Adirondacks: Concentrations and sources, *Environ. Sci. Technol.*, 42, 5644-5653, doi:10.1021/es7028137, 2008.
- Ci, Z., Zhang, X., Wang, Z., and Niu, Z.: Atmospheric gaseous elemental mercury (GEM) over a coastal/rural site downwind of East China: Temporal variation and long-range transport, *Atmos. Environ.*, 45, 2480-2487, doi:10.1016/j.atmosenv.2011.02.043, 2011a.
- Ci, Z., Zhang, X., Wang, Z., Niu, Z., Diao, X., and Wang, S.: Distribution and air-sea exchange of mercury (Hg) in the Yellow Sea, *Atmos. Chem. Phys.*, 11, 2881-2892, doi:10.5194/acp-11-2881-2011, 2011b.
- [Clever, H. L., Johnson, S. A., and Derrick, M. E.: The solubility of mercury and some sparingly soluble mercury salts in water and aqueous-electrolyte solutions, J. Phys. Chem. Ref. Data, 14, 631-681, 1985.](https://doi.org/10.1063/1.471111)
- Ebinghaus, R., Kock, H. H., Temme, C., Einax, J. W., Lowe, A. G., Richter, A., Burrows, J. P., and Schroeder, W. H.: Antarctic springtime depletion of atmospheric mercury, *Environ. Sci. Technol.*, 36, 1238-1244, doi:10.1021/es015710z, 2002.
- Edgerton, E. S., Hartsell, B. E., and Jansen, J. J.: Mercury speciation in coal-fired power plant plumes observed at three surface sites in the southeastern US, *Environ. Sci. Technol.*, 40, 4563-4570, doi:10.1021/es0515607, 2006.
- Fang, F., Wang, Q., and Li, J.: Urban environmental mercury in Changchun, a metropolitan city in Northeastern China: source, cycle, and fate, *Sci. Total Environ.*, 330, 159-170, doi:10.1016/j.scitotenv.2004.04.006, 2004.
- Feng, X., Shang, L., Wang, S., Tang, S., and Zheng, W.: Temporal variation of total gaseous mercury in the air of Guiyang, China, *J. Geophys. Res.-Atmos.*, 109, D03303, doi:10.1029/2003jd004159, 2004.
- Fu, X., Feng, X., Zhu, W., Wang, S., and Lu, J.: Total gaseous mercury concentrations in ambient air in the eastern slope of Mt. Gongga, South-Eastern fringe of the Tibetan plateau, China, *Atmos. Environ.*, 42, 970-979, doi:10.1016/j.atmosenv.2007.10.018, 2008a.

- Fu, X., Feng, X., Zhu, W., Zheng, W., Wang, S., and Lu, J. Y.: Total particulate and reactive gaseous mercury in ambient air on the eastern slope of the Mt. Gongga area, China, *Appl. Geochem.*, 23, 408-418, doi:10.1016/j.apgeochem.2007.12.018, 2008b.
- Fu, X., Feng, X., Zhang, G., Xu, W., Li, X., Yao, H., Liang, P., Li, J., Sommar, J., Yin, R., and Liu, N.: Mercury in the marine boundary layer and seawater of the South China Sea: Concentrations, sea/air flux, and implication for land outflow, *J. Geophys. Res.-Atmos.*, 115, D06303, doi:10.1029/2009jd012958, 2010a.
- Fu, X., Feng, X., Zhu, W., Rothenberg, S., Yao, H., and Zhang, H.: Elevated atmospheric deposition and dynamics of mercury in a remote upland forest of southwestern China, *Environ. Pollut.*, 158, 2324-2333, doi:10.1016/j.envpol.2010.01.032, 2010b.
- Fu, X., Feng, X., Qiu, G., Shang, L., and Zhang, H.: Speciated atmospheric mercury and its potential source in Guiyang, China, *Atmos. Environ.*, 45, 4205-4212, doi:10.1016/j.atmosenv.2011.05.012, 2011.
- Fu, X., Feng, X., Dong, Z., Yin, R., Wang, J., Yang, Z., and Zhang, H.: Atmospheric gaseous elemental mercury (GEM) concentrations and mercury depositions at a high-altitude mountain peak in south China, *Atmos. Chem. Phys.*, 10, 2425-2437, 2010c.
- Fu, X., Feng, X., Liang, P., Deliger, Zhang, H., Ji, J., and Liu, P.: Temporal trend and sources of speciated atmospheric mercury at Waliguan GAW station, Northwestern China, *Atmos. Chem. Phys.*, 12, 1951-1964, doi:10.5194/acp-12-1951-2012, 2012a.
- [Fu, X. W., Feng, X., Shang, L. H., Wang, S. F. and Zhang, H.: Two years of measurements of atmospheric total gaseous mercury \(TGM\) at a remote site in Mt. Changbai area, Northeastern China, *Atmos. Chem. Phys.*, 12, 4215-4226, doi:10.5194/acp-12-4215-2012, 2012b.](#)
- Guo, Y., Feng, X., Li, Z., He, T., Yan, H., Meng, B., Zhang, J., and Qiu, G.: Distribution and wet deposition fluxes of total and methyl mercury in Wujiang River Basin, Guizhou, China, *Atmos. Environ.*, 42, 7096-7103, doi:10.1016/j.atmosenv.2008.06.006, 2008.
- Han, J. S., Choi, E. M., Seo, Y. S., Yi, S. M., Lee, J., and Chung, Y. C.: Contribution of total gaseous mercury (TGM) using TGM concentrations measured in urban and background areas, Korea, 10th International Conference on Mercury as a Global Pollutant, Halifax, Nova Scotia, Canada, 2011.
- Han, Y. J., Holsen, T. M., Hopke, P. K., and Yi, S. M.: Comparison between back-trajectory based modeling and Lagrangian backward dispersion Modeling for locating sources of reactive gaseous mercury, *Environ. Sci. Technol.*, 39, 1715-1723, doi:10.1021/es0498540, 2005.
- [Holmes, C. D., D. J. Jacob and X. Yang: Global lifetime of elemental mercury against oxidation by atomic bromine in the free troposphere. *Geophysical Research Letters* 33\(20\): L20808, 2006.](#)
- Holmes, C. D., Jacob, D. J., Corbitt, E. S., Mao, J., Yang, X., Talbot, R., and Slemr, F.: Global atmospheric model for mercury including oxidation by bromine atoms, *Atmos. Chem. Phys.*, 10, 12037-12057, doi:10.5194/acp-10-12037-2010, 2010.
- Kellerhals, M., Beauchamp, S., Belzer, W., Blanchard, P., Froude, F., Harvey, B., McDonald, K., Pilote, M., Poissant, L., Puckett, K., Schroeder, B., Steffen, A., and Tordon, R.: Temporal and spatial variability of total gaseous mercury in Canada: results from the Canadian Atmospheric Mercury Measurement Network (CAMNet), *Atmos. Environ.*, 37, 1003-1011, doi:10.1016/s1352-2310(02)00917-2, 2003.
- Kim, K. H., Ebinghaus, R., Schroeder, W. H., Blanchard, P., Kock, H. H., Steffen, A., Froude, F.

- A., Kim, M. Y., Hong, S. M., and Kim, J. H.: Atmospheric mercury concentrations from several observatory sites in the northern hemisphere, *J. Atmos. Chem.*, 50, 1-24, doi:10.1007/s10874-005-9222-0, 2005.
- Kim, S. H., Han, Y. J., Holsen, T. M., and Yi, S. M.: [Kim, S. H., Han, Y. J., Holsen, T. M., and Yi, S. M.: Characteristics of atmospheric speciated mercury concentrations \(TGM, Hg\(II\) and Hg\(p\)\) in Seoul, Korea, Atmos. Environ., 43, 3267-3274, doi:10.1016/j.atmosenv.2009.02.038, 2009.](#)
~~Characteristics of atmospheric speciated mercury concentrations (TGM, Hg(II) and Hg(p)) in Seoul, Korea, Atmos. Environ., 43, 3267-3274, doi:10.1016/j.atmosenv.2009.02.038, 2009.~~
- Lamborg, C. H., Rolfhus, K. R., Fitzgerald, W. F., and Kim, G.: The atmospheric cycling and air-sea exchange of mercury species in the South and equatorial Atlantic Ocean, *Deep-Sea Res. Pt. II.*, 46, 957-977, doi:10.1016/s0967-0645(99)00011-9, 1999.
- Landis, M. S., Stevens, R. K., Schaedlich, F., and Prestbo, E. M.: Development and characterization of an annular denuder methodology for the measurement of divalent inorganic reactive gaseous mercury in ambient air, *Environ. Sci. Technol.*, 36, 3000-3009, doi:10.1021/es015887t, 2002.
- Laurier, F. J. G., Mason, R. P., Whalin, L., and Kato, S.: Reactive gaseous mercury formation in the North Pacific Ocean's marine boundary layer: A potential role of halogen chemistry, *J. Geophys. Res.-Atmos.*, 108, 4529, doi:10.1029/2003jd003625, 2003.
- [Lin, C. J. and Pehkonen, S. O.: The chemistry of atmospheric mercury: a review, Atmos. Environ., 33, 2067-2079, doi:10.1016/s1352-2310\(98\)00387-2, 1999.](#)
- Liu, M., Chen, L., Tao, J., Xu, Z., Zhu, L., Qian, D., and Fan, R.: Seasonal and diurnal variation of total gaseous mercury in Guangzhou City (in Chinese), *China Environ. Sci.*, 32(9), 1554-1558, 2012.
- Munthe, J., Wangberg, I., Iverfeldt, A., Lindqvist, O., Stromberg, D., Sommar, J., Gardfeldt, K., Petersen, G., Ebinghaus, R., Prestbo, E., Larjava, K., and Siemens, V.: Distribution of atmospheric mercury species in Northern Europe: final results from the MOE project, *Atmos. Environ.*, 37, S9-S20, doi:10.1016/s1352-2310(03)00235-8, 2003.
- Nakagawa, R., and Hiromoto, M.: Geographical distribution and background levels of total mercury in air in Japan and neighbouring countries, *Chemosphere*, 34, 801-806, doi:10.1016/s0045-6535(97)00008-8, 1997.
- Nguyen, H. T., Kim, K. H., Kim, M. Y., Hong, S., Youn, Y. H., Shon, Z. H., and Lee, J. S.: Monitoring of atmospheric mercury at a global atmospheric watch (GAW) site on An-Myun Island, Korea, *Water Air Soil Pollut.*, 185, 149-164, doi:10.1007/s11270-007-9438-5, 2007.
- Nguyen, H. T., Kim, M. Y., and Kim, K. H.: The influence of long-range transport on atmospheric mercury on Jeju Island, Korea, *Sci. Total Environ.*, 408, 1295-1307, doi:10.1016/j.scitotenv.2009.10.029, 2010.
- [Pan, L., Carmichael, G. R., Adhikary, B., Tang, Y., Streets, D., Woo, J.-H., Friedli, H. R., and Radke, L. F.: A regional analysis of the fate and transport of mercury in East Asia and an assessment of major uncertainties, Atmos. Environ., 42, 1144-1159, doi:10.1016/j.atmosenv.2007.10.045, 2008.](#)
- Poissant, L., Pilote, M., Beauvais, C., Constant, P., and Zhang, H. H.: A year of continuous measurements of three atmospheric mercury species (GEM, RGM and Hg-p) in southern Quebec, Canada, *Atmos. Environ.*, 39, 1275-1287, doi:10.1016/j.atmosenv.2004.11.007, 2005.

- [Rutter, A. P., and Schauer, J. J.: The effect of temperature on the gas-particle partitioning of reactive mercury in atmospheric aerosols, *Atmos. Environ.*, 41, 8647-8657, 2007a.](#)
- [Rutter, A. P., and Schauer, J. J.: The impact of aerosol composition on the particle to gas partitioning of reactive mercury, *Environ. Sci. Technol.*, 41, 3934-3939, 2007b.](#)
- Sakata, M., and Marumoto, K.: Formation of atmospheric particulate mercury in the Tokyo metropolitan area, *Atmos. Environ.*, 36, 239-246, doi:10.1016/s1352-2310(01)00432-0, 2002.
- Sakata, M., and Marumoto, K.: Wet and dry deposition fluxes of mercury in Japan, *Atmos. Environ.*, 39, 3139-3146, doi:10.1016/j.atmosenv.2005.01.049, 2005.
- [Seigneur, C. and K. Lohman.: Effect of bromine chemistry on the atmospheric mercury cycle. *J. Geophys. Res.*, 113, D23309, doi:10.1029/2008JD010262, 2008.](#)
- [Seinfeld, C. P. and Pandis, S. N.: Atmospheric Chemistry and Physics, From Air Pollution to Climate Change. 1998.](#)
- Sheu, G. R., Lin, N. H., Wang, J. L., Lee, C. T., Yang, C. F. O., and Wang, S. H.: Temporal distribution and potential sources of atmospheric mercury measured at a high-elevation background station in Taiwan, *Atmos. Environ.*, 44, 2393-2400, doi:10.1016/j.atmosenv.2010.04.009, 2010.
- Sigler, J. M., Mao, H., and Talbot, R.: Gaseous elemental and reactive mercury in Southern New Hampshire, *Atmos. Chem. Phys.*, 9, 1929-1942, 2009.
- [Singh, H. B., Brune, W. H., Crawford, J. H., Flocke, F., and Jacob, D. J.: Chemistry and transport of pollution over the Gulf of Mexico and the Pacific: spring 2006 INTEX-B campaign overview and first results, *Atmos. Chem. Phys.*, 9, 2301-2318, doi:10.5194/acp-9-2301-2009, 2009.](#)
- Slemr, F., Brunke, E. G., Ebinghaus, R., and Kuss, J.: Worldwide trend of atmospheric mercury since 1995, *Atmos. Chem. Phys.*, 11, 4779-4787, doi:10.5194/acp-11-4779-2011, 2011.
- [Slinn, S.A. and W.G.N. Slinn. Predictions for particle deposition on natural waters. *Atmos. Environ.*, 24, 1013-1016, 1980.](#)
- Soerensen, A. L., Skov, H., Jacob, D. J., Soerensen, B. T., and Johnson, M. S.: Global concentrations of gaseous elemental mercury and reactive gaseous mercury in the marine boundary layer, *Environ. Sci. Technol.*, 44, 7425-7430, doi:10.1021/es903839n, 2010.
- Stamenkovic, J., Lyman, S., and Gustin, M. S.: Seasonal and diel variation of atmospheric mercury concentrations in the Reno (Nevada, USA) airshed, *Atmos. Environ.*, 41, 6662-6672, doi:10.1016/j.atmosenv.2007.04.015, 2007.
- Steffen, A., Schroeder, W., Macdonald, R., Poissant, L., and Konoplev, A.: Mercury in the Arctic atmosphere: An analysis of eight years of measurements of GEM at Alert (Canada) and a comparison with observations at Amderma (Russia) and Kuujuarapik (Canada), *Sci. Total Environ.*, 342, 185-198, doi:10.1016/j.scitotenv.2004.12.048, 2005.
- Temme, C., Slemr, F., Ebinghaus, R., and Einax, J. W.: Distribution of mercury over the Atlantic Ocean in 1996 and 1999-2001, *Atmos. Environ.*, 37, 1889-1897, doi:10.1016/s1352-2310(03)00069-4, 2003.
- Temme, C., Blanchard, P., Steffen, A., Banic, C., Beauchamp, S., Poissant, L., Tordon, R., and Wiens, B.: Trend, seasonal and multivariate analysis study of total gaseous mercury data from the Canadian atmospheric mercury measurement network (CAMNet), *Atmos. Environ.*, 41, 5423-5441, doi:10.1016/j.atmosenv.2007.02.021, 2007.
- Tilmes, S., Lamarque, J. F., Emmons, L. K., Conley, A., Schultz, M. G., Sauniois, M., Thouret, V., Thompson, A. M., Oltmans, S. J., Johnson, B., and Tarasick, D.: Technical Note: Ozonesonde

- climatology between 1995 and 2011: description, evaluation and applications, *Atmos. Chem. Phys.*, 12, 7475-7497, doi:10.5194/acp-12-7475-2012, 2012.
- [Vijayaraghavan, K., P. Karamchandani, C. Seigneur, R. Balmori, and S.-Y. Chen: Plume-in-grid modeling of atmospheric mercury, *J. Geophys. Res.*, 113, D24305, doi:10.1029/2008JD010580, 2008.](#)
- Wan, Q., Feng, X., Lu, J., Zheng, W., Song, X., Han, S., and Xu, H.: Atmospheric mercury in Changbai Mountain area, northeastern China I. The seasonal distribution pattern of total gaseous mercury and its potential sources, *Environ. Res.*, 109, 201-206, doi:10.1016/j.envres.2008.12.001, 2009a.
- Wan, Q., Feng, X., Lu, J., Zheng, W., Song, X., Li, P., Han, S., and Xu, H.: Atmospheric mercury in Changbai Mountain area, northeastern China II. The distribution of reactive gaseous mercury and particulate mercury and mercury deposition fluxes, *Environ. Res.*, 109, 721-727, doi:10.1016/j.envres.2009.05.006, 2009b.
- Wang, Y.: The speciation, levels and potential impacted factors of atmospheric mercury in Hefei, Central China (in Chinese), M.S. thesis, University of Science and Technology of China, China, 44 pp., 2010.
- Wang, Z., Chen, Z., Duan, N., and Zhang, X.: Gaseous elemental mercury concentration in atmosphere at urban and remote sites in China, *J. Environ. Sci.-China*, 19, 176-180, doi:10.1016/s1001-0742(07)60028-x, 2007.
- Wang, Z., Zhang, X., Xiao, J., Ci, Z., and Yu, P.: Mercury fluxes and pools in three subtropical forested catchments, southwest China, *Environ. Pollut.*, 157, 801-808, doi:10.1016/j.envpol.2008.11.018, 2009.
- Wang, Z., Zhang, X., Chen, Z., and Zhang, Y.: Mercury concentrations in size-fractionated airborne particles at urban and suburban sites in Beijing, China, *Atmos. Environ.*, 40, 2194-2201, doi:10.1016/j.atmosenv.2005.12.003, 2006.
- [Wangberg, I., Munthe, J., Berg, T., Ebinghaus, R., Kock, H. H., Temme, C., Bieber, E., Spain, T. G., and Stolk, A.: Trends in air concentration and deposition of mercury in the coastal environment of the North Sea Area, *Atmos. Environ.*, 41, 2612-2619, doi:10.1016/j.atmosenv.2006.11.024, 2007.](#)
- Weiss-Penzias, P., Jaffe, D. A., McClintick, A., Prestbo, E. M., and Landis, M. S.: Gaseous elemental mercury in the marine boundary layer: Evidence for rapid removal in anthropogenic pollution, *Environ. Sci. Technol.*, 37, 3755-3763, doi:10.1021/es0341081, 2003.
- [Wesely, M. L.: Parameterization of surface resistances to gaseous dry deposition in regional-scale numerical models, *Atmos. Environ.*, 23, 1293-1304, doi:http://dx.doi.org/10.1016/0004-6981\(89\)90153-4, 1989.](#)
- Wu, L.: Study on atmospheric mercury of Chongqing City (in Chinese), M.S. thesis, Southwest University, China, 74 pp., 2006.
- Xiu, G., Cai, J., Zhang, W., Zhang, D., Bueeler, A., Lee, S., Shen, Y., Xu, L., Huang, X., and Zhang, P.: Speciated mercury in size-fractionated particles in Shanghai ambient air, *Atmos. Environ.*, 43, 3145-3154, doi:10.1016/j.atmosenv.2008.07.044, 2009.
- Yang, Y., Chen, H., and Wang, D.: Spatial and temporal distribution of gaseous elemental mercury in Chongqing, China, *Environ. Monit. Assess.*, 156, 479-489, doi:10.1007/s10661-008-0499-8, 2009.
- Yatavelli, R. L. N., Fahrni, J. K., Kim, M., Crist, K. C., Vickers, C. D., Winter, S. E., and Connell,

- D. P.: Mercury, PM_{2.5} and gaseous co-pollutants in the Ohio River Valley region: Preliminary results from the Athens supersite, *Atmos. Environ.*, 40, 6650-6665, doi:10.1016/j.atmosenv.2006.05.072, 2006.
- Zhang, G., Zheng, X., Zhou, L., Huang, W., Qian, P., and Wang, Y.: Atmospheric mercury wet deposition and its ecological impacts in Shanghai City (in Chinese), *Environ. Chem.*, 29(1), 147-148, 2010.
- Zhang, H.: Concentrations of speciated atmospheric mercury at a high-altitude background station in the Shangri-La area of Tibetan Plateau, China, 10th International Conference on Mercury as a Global Pollutant, Halifax, Nova Scotia, Canada, 2011.
- Zhang, Y., Xiu, G., Zhang, D., Zhang, M., and Zhang, R.: Total gaseous mercury in ambient air of Shanghai: its seasonal variation in relation to meteorological condition (in Chinese), *Environ. Sci. Technol.*, 34(12), 155-158, 2012.